Spring 2019

Sustainable Polymers and Antimicrobial Biomaterials from Multicyclic Natural Products

Md Anisur Rahman

SUSTAINABLE POLYMERS AND ANTIMICROBIAL BIOMATERIALS FROM MULTICYCLIC NATURAL PRODUCTS

by

Md Anisur Rahman

Bachelor of Science
Jahangirnagar University, 2011

Master of Science
Tennessee State University, 2014

Submitted in Partial Fulfillment of the Requirements

For the Degree of Doctor of Philosophy in

Chemistry

College of Arts and Sciences

University of South Carolina

2019

Accepted by:

Chuanbing Tang, Major Professor

Brian C. Benicewicz, Committee Member

Mythreye Karthikeyan, Committee Member

Alan W. Decho, Committee Member

Cheryl L. Addy, Vice Provost and Dean of the Graduate School

DEDICATION

To my parents, for their love, support, lifelong sacrifices and guiding me to get the best education possible.

To Moumita Sharmin Jui, my loving wife, for her enormous love, care and support. None of my accomplishments would be possible without her support.

ACKNOWLEDGEMENTS

First and foremost, I would like to convey my sincere gratitude to my advisor, Dr. Chuanbing Tang, who gave me the opportunity to work in his research group and offered me tremendous support and guidance on my research projects throughout my Ph.D. journey. It has been a great honor and a privilege for me to work under such an enthusiastic and knowledgeable person. His passion and enthusiasm for polymer science has made an enormous impact on me and motivated me to develop as a polymer scientist. I sincerely thank his contributions to make my Ph.D. experience diverse, productive and stimulating. I want to appreciate him for being an excellent role model as a successful professor and a caring person that made a positive impact on my life.

Then I would like to thank my graduate committee members Dr. Brian Benicewicz, Dr. Alan W. Decho and Dr. Mythreye Karthikeyan for their advice, encouragement, and valuable suggestions on my research during graduate school. I also appreciate my committee chair Dr. Brian Benicewicz for being a great teacher in the introduction to polymer that creates the foundation of my polymer science knowledge. I want to thank Dr. Decho and his group members Dr. Yunpin Chen and Dr. Kristen Miller for their collaborations with our group. In addition, I want to mention Dr. Mitzi Nagarkatti and her group member Dr. Marpe Bam for his productive collaborations. Further, I would like to acknowledge Dr. Morgan Stefik and his students especially Nadee, Amrita and Zach for helping me to run SAXS and allowing me to use their SAXS instrument.

I am very appreciative of the experiences shared and friendships formed with other graduate students, post-docs and visiting scholars during the last 4.5 years at USC. I want to appreciate and mention the members of Tang Polymer Group. I thank Dr. Mitra Ganewatta and Dr. Liang Yuan for being my graduate mentor during the early stages of my graduate career. I had an opportunity to work and learn a lot of research techniques from some hard-working and motivating post-doctoral scientist such as Dr. Zhongkai, Dr. Jifu Wang, and Dr. Ye Sha, and I am thankful to them. It was a pleasant experience for me to work with Shichao Xu, Shaobo Tan, and Haijiao Kang. Thank you, Meghan E. Lamm, Tianyu Zhu, Yujin Cha and Pabel Kabir for being nice friends. Edgar Luat was excellent undergraduate students who worked with me. I also want to mention Dr. Perry Wilbon, Dr. Jeffery Hayat, Dr. Peng Yang, Dr. Hui Li, Nathen Trenor, Paras Pageni, Xinzhou Zhang, Ryan J. Miskin, Lin Fu, Jihyeon Hwang, Leman Kurnaz and many others. It is a great pleasure to work with all of you and learn from you. Thanks for all your help and suggestions. Besides the exciting research work, I feel thankful to get the chance to work with Dr. Brian Benicewicz while I served as the secretary of the ACS Poly/PMSE Student Chapter at USC. I want to mention Mitra, Julia, Andrew and Nadee for working with me to conduct many projects.

Further, I want to give my sincerest gratitude to my mother, my father, other family members and friends for their unconditional love and support. I also would like to thank my wife Moumita Sharmin Jui for her constant support, patience, and help throughout my graduate school career. Finally, I would like to acknowledge all the funding supports from the University of South Carolina, and the National Science Foundation (NSF).

ABSTRACT

In this dissertation, the development of sustainable polymers and antimicrobial biomaterials from multicyclic natural products is illustrated. In Chapter 1, an overall background and recent development of sustainable polymers from natural product-based renewable biomass, antimicrobial biomaterials, and polymerization methods are introduced. Afterward, the primary research objectives of my doctoral research work are illustrated.

In chapter 2, designing block copolymer architectures toward tough bioplastics from renewable natural rosin was described. One of the most abundant natural biomasses is resin acids, however, most of the polymers derived from resin acids are brittle because of their bulky hydrophenanthrene pendant group. To overcome the brittleness, rosin containing pentablock and triblock copolymers were synthesized through living sequential ring opening metathesis polymerization (ROMP). Their thermal and mechanical properties were investigated. The phase behaviors were also studied for the microphase-separated pentablock and triblock copolymers using small angle x-ray scattering (SAXS) and atomic force microscopy.

A new class of true facial amphiphilic cationic antimicrobial polymers was illustrated in chapter 3. Facially amphiphilic antimicrobial polymers were prepared from multicyclic natural products (e.g. bile acids) via reversible-addition fragmentation chain transfer (RAFT) polymerization. The antimicrobial activity against a range of bacteria and

hemolysis activity with mammalian cells is investigated. In addition, the antimicrobial mechanistic aspects of facially amphiphilic polymers were also illustrated. Chapter 4 is explained about the facial amphiphilicity-induced self-assembly (FAISA) of multicyclic natural product-based cationic copolymers. The detail self-assembly behavior of copolymers with different polyethylene glycol was explained. The self-assembly of these copolymers to form antimicrobial nanoparticles was investigated in Chapter 5. The nanoaggregates exhibited strong antimicrobial activity against Gram-negative bacteria and showed minimal toxicity against mammalian cell.

Finally, a summary and future directions of this dissertation research are provided in chapter 6. In future work, some suggestions about future directions involving renewable biomass for sustainable development are given.

TABLE OF CONTENTS

LIST OF TABLES

LIST OF FIGURES

List of Symbols

M_n	Number average molecular weight
$Đ$	Dispersity
M_e	Chain entanglement molecular weight
T_g	Glass transition temperature
D_h	Hydrodynamic diameter
T_d	Temperature at 10 % weight loss
ζ	Zeta potential
σ_{UTS}	Ultimate tensile stress

List of Abbreviation

AFM ..... Atomic Force Microscopy

AIBN .....Azobisisobutyronitrile

AMP ..... Antimicrobial Peptide

CDC .....Centers for Disease Control

CFU .....Colony Forming Unit

CLSM.....Confocal Laser Scanning Microscopy

CMC..... Critical Micellar Concentration

DCM .....Dichloromethane

DLS .....Dynamic Light Scattering

DMF ..... *N*,*N*-Dimethylformamide

DSC.....Differential Scanning Calorimetry

FTIR..... Fourier Transform Infrared Spectrometry

G3.....Grubbs' Third Generation Catalyst

GPC..... Gel Permeation Chromatography

HC .....Hemolytic Concentration

HG2.....Hoveyda-Grubbs' Second Generation Catalyst

HMW ..... High Molecular Weight

MIC .....Minimum Inhibitory Concentration

MRSA ..... Methicillin-resistant *Staphylococcus aureus*

MDR ..... Multiple Drug Resistance

NMR ..... Nuclear Magnetic Resonance

QAC .....Quaternary Ammonium Charge

RAFT ..... Radical Addition-Fragmentation Chain Transfer

ROMP .....Ring-Opening Metathesis Polymerization

SAXS .....Small-Angle X-ray Scattering

SD .....Standard Deviation

SEM .....Scanning Electron Microscopy

TEM ..... Transmission Electron Microscopy

TGA ..... Thermogravimetric Analysis

THF ..... Tetrahydrofuran

TSB ..... Tryptic Soy Broth

CHAPTER 1

GENERAL INTRODUCTION

1.1 Sustainable Polymers from Natural Product-Based Biomass

Petrochemical-based synthetic polymeric materials have benefited humankind in various ways. The outstanding properties of synthetic polymeric materials, such as their light weight, durability, degradability, and highly tunable malleability and conductivity, have made them ubiquitous in our daily life.[1] Due to the diverse properties and broad applications of plastic materials, plastic production has been increasing day by day, rising from 204 million tons in 2002 to about 299 million tons in 2013 globally. The production of synthetic polymers or plastic materials heavily relies on non-renewable fossil feedstocks, including natural gas or petroleum. Approximately 7% of fossil fuels are consumed for plastic production worldwide, and around 13% of fossil fuels produced in the USA goes into nonfuel chemical production.[2] The burning of fossil fuels associated with plastic production contributes to an enormous carbon footprint, greenhouse gas emission, air pollution, and global warming.

Plastics have suffered from a terrible reputation since the beginning of the 21st century. The inability to recycle, reprocess, or degrade plastic products has made them major contributors to environmental pollution. Plastic waste composes approximately 11% of the total waste generated by coastal 192 countries.[3] Oceanic pollution by plastic wastes also poses a significant threat to both marine organisms and our own environment.[3] Diminishing fossil fuel reserves, along with the production of environmental pollutants, have started to threaten not only the future of the polymer industry but also humanity. Growing concerns regarding these issues have inevitably driven academia and industry to explore sustainable and eco-friendly plastic materials from renewable resources in order to decrease our current dependence on fossil resources.[4] Renewable biomass has already

been recognized as one of the most promising and long-term alternatives for the production of sustainable polymers. Significant progress has been made to discover these polymers from renewable biomass, which is covered by recent books[5-6] and reviews.[2, 4, 7-9]

Sustainable polymers or green plastics derived from renewable biomass can be divided primarily into three categories. The first category consists of natural polymers or naturally occurring biopolymers including cellulose, hemicellulose, polysaccharides, chitosan, and lignin. Several approaches including the blending or surface modification of these preexisting biopolymers have been carried out to discover novel hybrid materials with improved properties. Most of these biopolymers additionally exhibit excellent biocompatibility and biodegradability. Fermentation products of sugars or lipids constitute the second class of renewable polymers, which includes polyhydroxy-alkanoates (PHAs) such as poly(hydroxybutyric acid).[10-11] PHA polymers are biodegradable, linear polyesters produced by bacterial fermentation.[12] These polymers are ideal candidates for replacing synthetic thermoplastics due to their structural diversity and similarities to plastics. The third class of renewable polymers is obtained from the polymerization of small molecular biomass (Figure 1). Various small molecular biomasses can be precisely engineered at a molecular level in order to prepare polymeric material with, particularly useful properties. These biomasses can also be organized into different subgroups according to their composition (carbon, oxygen, and hydrogen). Oxygen-rich biomass is one of these subgroups, including many products such as lactic acid, succinic acid, itaconic acid, levulinic acid, glycerol, dianhydroalditols, and furans produced by the fermentation of carbohydrates. One of the most promising commercialized renewable polymers is Polylactide or poly (lactic acid), which is used as thermoplastic polyester. Due to their

biodegradability, biocompatibility and sufficient mechanical properties, polylactide polymers have shown significant potential in replacing fossil oil-based thermoplastics. Another sub-class is hydrocarbon-rich biomass such as vegetable oils, fatty acids, terpenes, terpenoids, limonene, and resin acids, which is directly obtained from forestry and agricultural products. These are cheap and abundant, serving as promising candidates for sustainable polymer preparation. Soybean oil, olive oil, linseed oil, and sunflower oil are the most common vegetable oils. Most of these compounds are biodegradable and less toxic renewable feedstock for polymeric materials. Terpenes, terpenoids, and resin acids have also been studied extensively as starting materials for the synthesis of polymers.[2, 4, 13-15] Terpenes are the largest and most abundant class of natural hydrocarbons, and are particularly important for fine chemistry and the fragrance industry. Resin acids are another important terpenoid-based natural hydrocarbon produced by conifer trees and amount to more than 1 million tons annually. This cheap and widely available resource has quickly gained interest in the polymer industry.

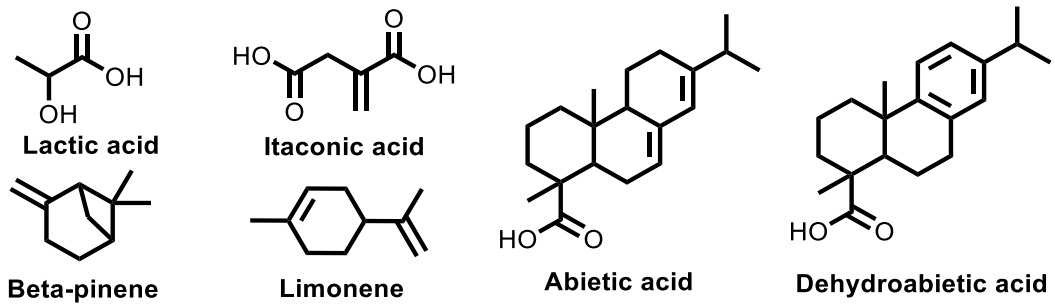

Figure 1.1 Examples of small molecular biomass used in sustainable polymers.

The increasing demand for green, sustainable materials from renewable biomass feedstock has resulted in a global spike in the popularity of renewable biomass chemicals or sustainable materials. Concern for the environment, the depletion of conventional fossil

fuels, and the instability of petroleum prices have encouraged the development of renewable monomers, polymers and sustainable materials that can outperform petroleum-derived materials. Sustainable polymers from natural biomass nonetheless require significant improvement to replace petrochemical-derived polymers in the future. Therefore, additional research is required to develop sustainable polymers capable of transforming our petrochemical-based polymer world to one that is sustainably bio-based.

1.2 Renewable Resin Acids

Rosin is an essential class of terpenoid-based natural biomass. The three major types of rosin include gum rosin, wood rosin, and tall oil rosin. Gum rosin is the nonvolatile component obtained from the exudate of pine trees, produced for the physical defense against herbivore and pathogen attacks.[16] Wood rosin is obtained from aged pine stumps, and tall oil rosin is obtained from tall crude oil and is a byproduct of wood pulp manufacturing.[1] Rosin is very cheap and abundant, every year more than one million metric tons of rosin produced globally. Rosin consists primarily of abietic and pimaric resin acids (Figure 1) and approximately 10% of other neutral materials. The most abundant resin acid is abietic acid with the empirical formula of $C_{20}H_{30}O_2$, and the other components are different isomers of abietic acid (Figure 1.2).

Resin acids consist of a cycloaliphatic or aromatic ring structure generally known as a hydrophenanthrene ring. The presence of hydrophenanthrene ring structures and functional groups such as carboxyl groups, conjugated double bonds, and other functionalities makes resin acids a unique small molecular biomass. These functional groups open avenues for the modification of resin acids to various derivatives with tunable properties and a wide range of applications.[4] The bulky hydrophenanthrene ring of resin acids provide rigidity

and both thermal and chemical stability to petroleum-based cycloaliphatic and aromatic compounds. Resin acids are also biocompatible FDA-approved food additives. These acids have exhibited a wide variety of biological traits including antimicrobial,[17] anti-inflammatory[18] and anticonvulsant[19] activity. Moreover, rosin is traditionally used as an ingredient in fine chemistry as an antifouling caulking agent, surface coating agent, paper sizing agent, and in inks, adhesives, cosmetics, varnishes, insulating materials, medicines, and chewing gums.[2] The biocompatibility and extensive functionality of rosin-derived esters make them ideal candidates as biomedically applicable polymeric materials.

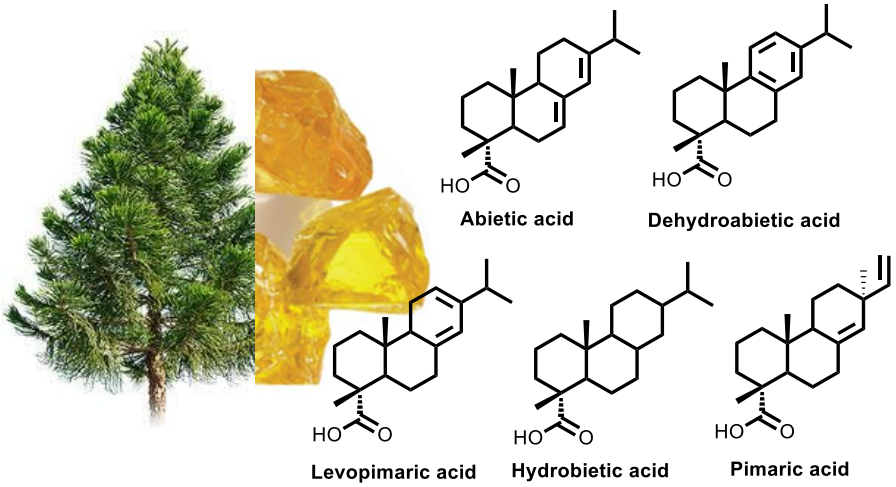

Figure 1.2 Chemical structures of representative resin acids.

Rosin-based main-chain and side-chain thermoplastic polymers were synthesized according to the position of the hydrophenanthrene structure. Main-chain rosin-based polymers were prepared by various condensation polymerization techniques. However, only low molecular weight polymers could be obtained by these techniques due to the steric hindrance, monomer impurities, and stoichiometric control.[20-24] To avoid this problem, side-chain rosin-based polymers were synthesized and controlled for molecular weight by free radical polymerization. Rosin constituents can be functionalized to yield a variety of

different monomers, such as Rosin-derived vinyl, acrylic, or allyl ester monomers, which are utilized to produce side-chain rosin-based polymers.[23] Our research group has also recently functionalized dehydroabietic acid (DA) and abietic acid to produce either methacrylate or acrylate monomers through esterification. However, the molecular weights were not high enough to exhibit chain entanglement. As a result, the polymers appeared as powders, making the production of mechanically robust materials nonviable. The bulky hydrophenanthrene moiety, when placed at the side group, significantly increases the M_e of rosin polymers and thus leads to brittle character. Subsequently, our group synthesized dehydroabietic acid containing polymers with high molecular weights. However, the polymerization was not under well enough control to obtain improved mechanical properties. Physical properties, especially the mechanical properties (such as tensile strength and Young's modulus) of polymers are mainly determined by molecular architectures. Incorporation of the bulky hydrophenanthrene moiety of rosin onto the side group of the polymers would undoubtedly have a significant impact on their mechanical properties. Rosin-based materials have already demonstrated enormous promise in the sustainable polymer field. Further investigation is required to prepare novel rosin-based polymers with enhanced mechanical properties and sophisticated chain architectural design.

1.3 Bile Acids

Bile acids are naturally occurring biological compounds that are obtained in the bile of mammals and other vertebrates. Bile acids are steroid acids produced from cholesterol in the liver and stored in the gallbladder. They are secreted into the duodenum to solubilize and emulsify nonpolar lipids into small droplets, enabling them to participate in metabolic digestion processes. Bile acids are reabsorbed into the liver from the bloodstream and made

available for a new cycle through a process called enterohepatic circulation.[25] Bile acids can be classified into two groups based on their order of formation within the human body. The primary bile acids, cholic acid, and chenodeoxycholic acid, are produced in human liver cells via cytochrome P-450 enzyme-mediated oxidation of cholesterol via a multi-step pathway.[26] In the intestine, microorganisms aid in their conversion into secondary bile acids such as deoxycholic acid and lithocholic acid.[27]

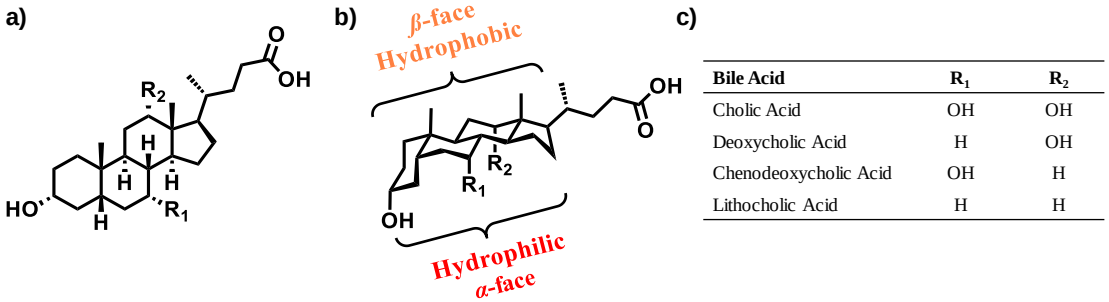

Bile Acid	R_1	R_2
Cholic Acid	OH	OH
Deoxycholic Acid	H	OH
Chenodeoxycholic Acid	OH	H
Lithocholic Acid	H	H

Figure 1.3 Chemical structures of bile acids a) planar form; b) chair form; c) Positions of hydroxyl groups in bile acid derivatives.

Bile acids possess a rigid steroidal backbone containing three six-membered rings and one five-membered ring. The two six-membered rings are connected in a cis configuration, providing the steroidal backbone with a curved geometry with both a convex and a concave side (Figure 1.3). Bile acids also contain polar functional groups, such as hydroxyl and carboxylic acid groups. Several hydroxyl groups converge on the concave side forming the hydrophilic α-face, while three methyl groups are directed towards opposite hydrophobic β-face. The four bile acids derivatives, cholic acid, chenodeoxycholic acid, deoxycholic acid, and lithocholic acid differ based on the number of hydroxyl groups (Figure 1.4). These acids have the unique ability to form a facially amphiphilic structure, with opposing hydrophilic and hydrophobic faces. Due to this inherent facial amphiphilicity, they are able to form mixed micelles with water-insoluble

compounds and serve as surfactants to solubilize dietary lipids and fats in the small intestine. This skeleton also provides diverse biological functions such as membrane fluidity regulation, signaling, and detergent activities.[25] The presence of a rigid steroidal skeleton, several chiral centers, and hydroxyl and carboxyl functional groups makes them attractive contenders for the construction of self-assembled nanostructures with a variety of applications. This skeleton also provides diverse biological functions such as membrane fluidity regulation, signaling, and detergent activities.[25]

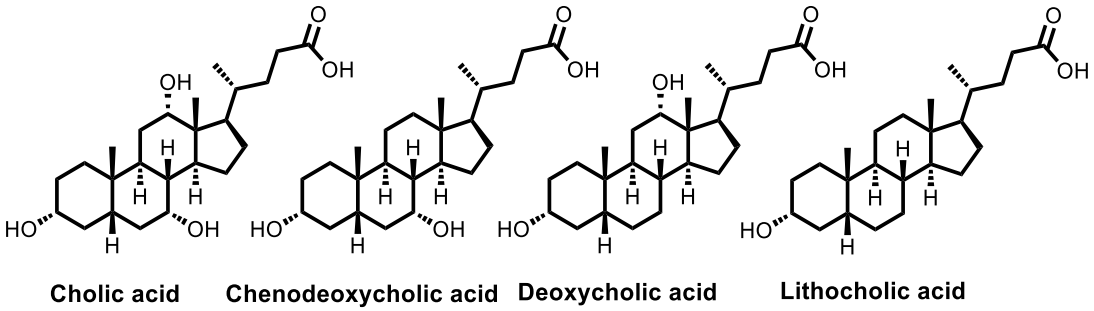

Figure 1.4 Chemical structures of bile acids derivatives.

Bile acids are low-cost, prolific and biocompatible as they are derived from natural biomass. These acids have been primarily used in biomedical applications such as drug delivery, prodrug formulation, and antimicrobial systems. Due to their unique structural features, these acids have been used for the development of different polymeric materials.[28] Recently, a broad variety of polymers have been established using bile acids as pendant groups along the polymer chain in block, statistical, and chain end-functional polymers.[29-30] These bile acid containing side-chain polymers have also been developed for a wide variety of applications such as drug delivery, self-healing materials, and sensing materials.[31-32] Though bile acid derived small cationic molecules were previously used for antimicrobial application; bile acid-based polymers were not studied.[33] Therefore, bile acids as antimicrobial biomaterials require more attention. The intrinsic facial

amphiphilicity and ease of functionalization of bile acids have directed the scientific community towards the development of novel antimicrobial agents and the investigation of the self-assembly behavior of bile acid derivatives.

1.4 Antimicrobial Polymers

Antibiotics and other antimicrobial agents have been consumed for the last 70 years to treat patients with infectious diseases, saving tens of millions of lives annually. However, pathogens are becoming increasingly resistant to most of the antibiotics, posing serious dangers to our health and well-being. Microbial contamination of food, drinking water, medical devices, drugs, health care, and hygienic applications, dental surgery equipment, textiles, food packaging, and food storage has posed a significant threat to public health and in some cases can lead to epidemics. Molecular targets of pathogens such as the cell wall, 60S ribosomes, cell membranes, genetic materials and biosynthetic pathways which are either absent or significantly different from human cells, are utilized in designing effective antimicrobial agents. The development of resistance to a microbial agent largely depends on target specificity.[34] Bacteria are capable of acquiring resistance against antibiotics through different mechanisms such as efflux pumps, chemical modification (phosphorylation, acetylation or hydrolysis that alters target and reprogramming biosynthesis), genetic mutation, and gene transfer.[35-36] Bacterial infections have now evolved into a global healthcare crisis due to epidemic bacterial resistance. Two million patients suffer from hospital-acquired infections in the United States, claiming 100,000 in deaths and adding 45 billion dollars to healthcare costs. The ever-increasing level of bacterial resistance to traditional antibiotics is a puzzling issue in battling infectious diseases. For example, β-lactam antibiotics (e.g. penicillin), once life-saving drugs, are

becoming futile due to the production of inactivating enzyme β-lactamase that causes hydrolysis of the lactam ring of penicillin. Several well-known drug-resistant bacterial pathogens, e.g. methicillin-resistant *Staphylococcus aureus* (MRSA), have employed this major defense mechanism. Therefore, it is a crucial need to continuously develop antibiotics with novel modes of action to face this evolving resistance that can successfully treat bacterial infections.[37]

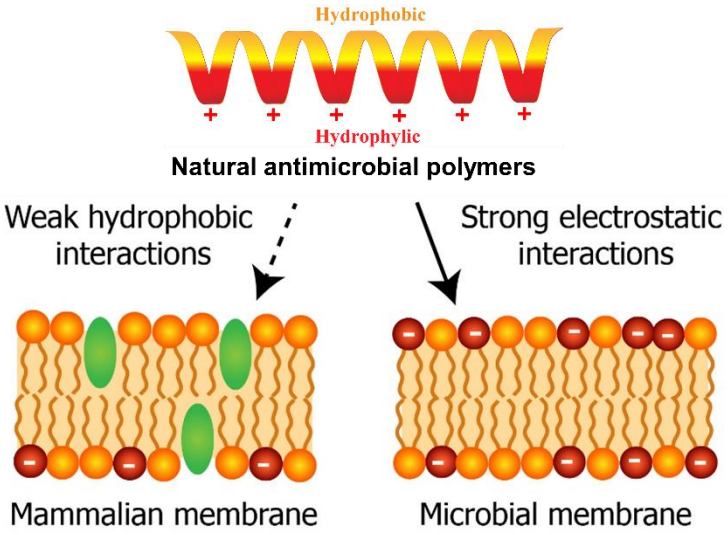

Figure 1.5 Selective interactions between cell membranes and cationic antimicrobial polymers.

In an effort to develop such antimicrobial agents, one strategy can be examined in nature. Host-defense antimicrobial peptides (AMPs) are broad-spectrum antimicrobials that act as the first line of defense against bacterial pathogens. AMPs are obtained in multicellular organisms as a part of an innate immune system for the clearance of bacterial pathogens.[38] Natural antimicrobial peptides (AMPs) are amphiphilic, combining cationic charges and hydrophobic components, and are able to preferentially bind to anionic bacterial membranes or other anionic targets selectively over zwitterionic human cell membranes (Figure 1.5). Upon contact with bacterial membranes, AMPs form an α-helix

structure with positive charges arrayed on one side and lipophilic groups aligned along the other side.[39-41] The global segregation of cationic and lipophilic side chains of these AMPs is also referred to as facial amphiphilicity (i.e., separate hydrophilic and hydrophobic faces).[41-42] These special structural features of AMPs allows them to efficiently insert themselves into bacterial membranes via the barrel-stave pore, toroidal pore, disordered toroidal pore, and carpet mechanisms, leading to cytoplasmic leakage, membrane depolarization, lysis, and eventual cell death.[36, 43] Since AMPs exhibit a low propensity for resistance development in bacteria and they are effective at killing cells via non-specific disruption of microbial membranes, AMP-mimicking synthetic derivatives have arisen as a class of promising antimicrobials.[38] Over the last two decades, natural AMP-mimicking peptide derivatives such as β-peptides and peptoids have been developed with potent antimicrobial activity.[44-47] However, the clinical implementation of AMPs is minimal due to their low bioavailability, low stability, high manufacturing cost, as well as in many cases nonspecific toxicity to mammalian cells.[38, 43, 48-49] To overcome these issues, synthetic polymers with cationic charges, which mimic natural AMPs, have been investigated widely as a promising solution to combat bacteria. These antimicrobial polymers include several classes of materials such as cationic polymers, biocide-releasing polymers, and antibiotic-conjugated polymers. These macromolecules typically have cationic functionality such as quaternary ammonium groups along with hydrophobic alkyl moieties. These polymers offer a broad spectrum of antimicrobial activity, a membrane disruption mechanism as well as a low propensity for developing resistance.[36, 38, 50-51] In addition, cationic charge-containing polymers can be obtained in large quantities at a much lower cost. Many antimicrobial polymers are highly effective in killing traditional strains

and are particularly effective against Gram-positive bacteria. In Gram-positive bacteria, teichoic acids, linked to either the peptidoglycan cell wall or the underlying cell membrane, resulting in net negative charges because of the presence of phosphate moieties in their structure. On the other hand, Gram-negative bacteria have an additional outer membrane bearing phospholipids and lipopolysaccharides.[36] The presence of this double cell membrane in Gram-negative bacteria inherently provides chemical resistance to traditional antimicrobials.

Most antimicrobial polymers do not comprise true facial amphiphilicity, suffer poor selectivity and high cytotoxicity against mammalian cells and are also ineffective against MDR Gram-negative bacteria. Therefore, the development of strongly antimicrobial, biocompatible polymers is essential to controlling multidrug-resistant Gram-positive and gram-negative bacteria.

1.5 Self-assembly of Amphiphilic Polymers

Self-assembly is critical for establishing complex structures in nature and has been studied for over 100 years. The essential characteristic of nature's building blocks is amphiphilicity. Biological systems transport molecules throughout the body by self-assembling amphiphilic building blocks. Micelles with a wide variety of shapes and sizes can be made from amphiphilic block copolymer species and serve as transporters. The self-assembly of polymeric materials at the nanoscale has already shown promising potential in the field of nanotechnology, nanodevices and drug delivery. Amphiphilic copolymers comprising hydrophilic and hydrophobic segments can self-assemble in water to form a wide variety of morphologies or nanoaggregates, where the hydrophobic portions form the core to reduce contacts with water and the hydrophilic segments form the corona to

stabilize the micelles or aggregates.[52] Various amphiphilic copolymers with different monomer sequences and architectures, such as amphiphilic block,[53-55] random,[56-58] gradient[59-61] and alternating[62] have been developed for desired morphologies. Extensive research has been focused on the self-assembly behavior of amphiphilic block copolymers due to their precisely controlled and well-defined morphologies.[63-65] Most amphiphilic block copolymers are capable of forming nanoscale structures with different morphologies such as spheres, micelles, worms-like micelles, rods, cylinders, and vesicles.[53-55] However, the self-assembly behavior of homopolymers and random copolymers is uncommon. Moreover, the self-assembly of block copolymers sometimes suffers from contamination by homopolymers due to a lack of precise control on desired composition and monomer sequence. Therefore, the study of the self-assembly behavior of pure amphiphilic homopolymers and random copolymers is appealing.

1.6 Polymerization Techniques

Ring-Opening Metathesis Polymerization (ROMP). ROMP is a type of olefin metathesis allows for the synthesis of linear polymers with high molecular weight. The cyclic olefins undergo chain-growth polymerization with releasing of the ring strain energy. The release of ring strain is the main driving force for the ROMP.[66-67] A variety of transition metals were used to prepare the catalysts. Tungsten and molybdenum catalysts (Schrock catalysts) typically have rapid initiation rates to produce well-defined polymers with control. However, Grubbs' ruthenium-based catalysts are well-known for their stability, functional group tolerance and ease of use for polymerization under mild conditions. Three different generations of Grubbs' catalysts are given in Figure 1.6.

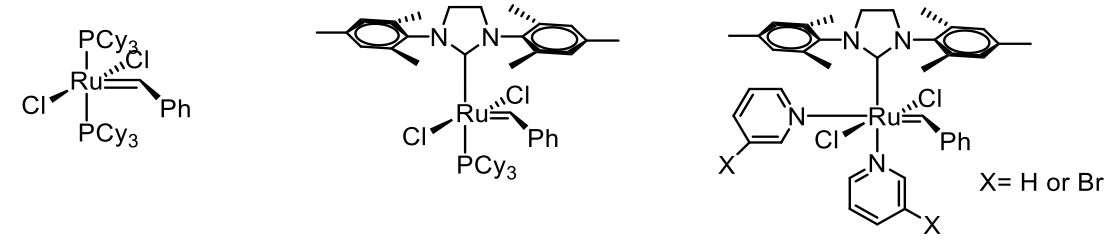

Grubbs' I catalyst | Grubbs' II catalyst | Grubbs' III catalyst

Figure 1.6 Grubbs' catalyst structures.

ROMP undergoes a chain-growth olefin metathesis of the monomers as illustrated in the mechanism (Figure 1.7). The overall mechanism of ROMP is a catalyst-mediated carbon-carbon double bond exchange. The alkylidene catalyst coordinates with the cyclic olefin and a new olefin that is generated coordinates with the catalyst as the polymer chain grows. The metathesize of the unstrained olefinic bonds in the growing polymer chain known as backbiting and chain transfer can increase the dispersity of the polymers.

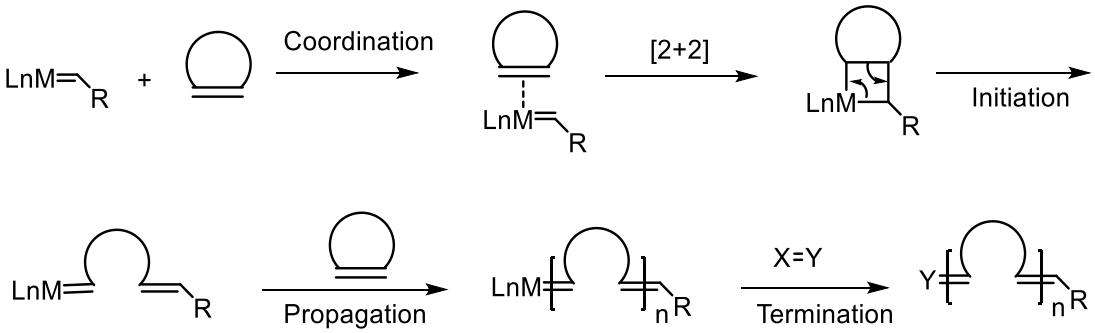

Figure 1.7 Schematic illustration of ROMP mechanism.

There are some excellent monomers used for ROMP such as norbornenes, cyclopentenes, and cyclooctenes.[68] Though the monomer for ROMP is relatively limited, linear polymers with unique functionalities can be prepared from substituted cyclic olefins. Besides, sequential monomer additions provide a path for the preparation of block copolymers.[69] ROMP provides a useful platform for synthesizing polymeric materials with diverse functionalities and architectures.

Reversible Addition-Fragmentation Chain Transfer Polymerization (RAFT).[70-72] RAFT polymerization is one of the common controlled radical polymerization techniques used to obtain predetermined molecular weight and narrow molecular weight distribution. This can tolerate a wide range of monomers and reaction conditions to provide controlled molecular weight polymers with very narrow dispersity. RAFT was first reported by a group of Australian scientists in 1998.[71] The RAFT agent promotes chain transfer between the active and dormant species (Figure 1.8). Specifically, the R groups are those that can leave as a free-radical leaving group and also reinitiate the polymerization. Since RAFT is a radical process, the stability of the radical intermediate and its ability to fragment largely depends on the R group. Cumyl and cyanoalkyl groups are the common R groups used in the RAFT agent. On the other hand, Z groups favor the stability of the RAFT agent and influence the rate of radical addition/fragmentation. Phenyl rings are the most common Z groups used in the RAFT. Polymers of various architectures, including homopolymers, diblock, triblock copolymers, grafted polymers, and star polymers can be prepared using RAFT polymerization.

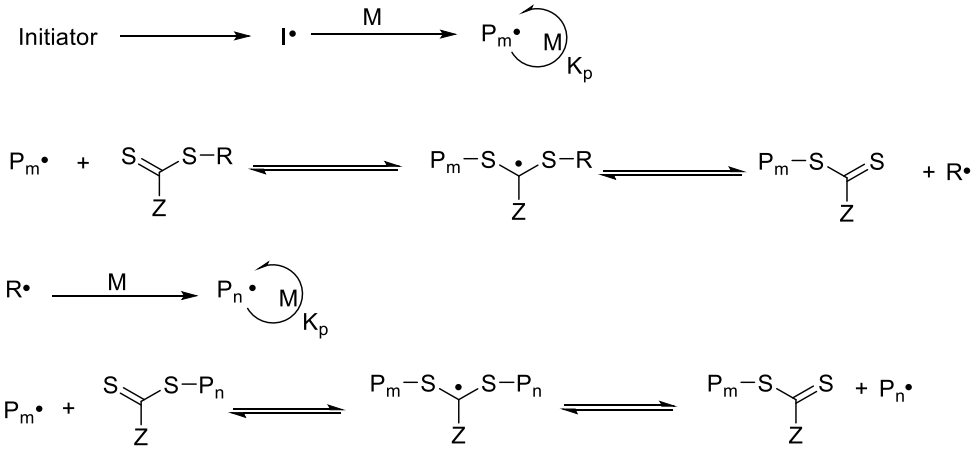

Figure 1.8 Overall mechanism of RAFT polymerization.

1.7 Research Objectives

Development of sustainable polymers and biomaterials from multi-cyclic natural product/biomass is widely expected to diminish the carbon footprint as well as our dependence on fossil oil resources. In addition, to address the current emergence of drug-resistant bacteria, the development of new antimicrobial agents with the potent ability to kill the MDR bacteria is another significant demand of our society. The objectives of this dissertation are based upon these two areas of research.

First, mechanically robust rosin containing A–B–A type triblock and A–B–A–B–A type pentablock copolymers were synthesized by ring-opening metathesis polymerization (ROMP) with one-pot sequential monomer addition of a rosin-based monomer and norbornene. The effect of chain architecture and microphase separation on mechanical properties of both types of block copolymers was investigated. Block copolymer architectures enhanced chain entanglement and improved toughness of bulky rosin-based side chain polymers. This study helps to understand the fundamental structure-property relationship and opens up an avenue to make mechanically robust polymers using bulky hydrocarbon-rich biomass.

Second, true facial amphiphilic polymers were developed from bile acid derivatives for antimicrobial application, where hydrophilic and hydrophobic components are interfaced in a single system. The hydrophilic moieties include oxygen-rich groups and cationic charges such as a quaternary ammonium group. A new class of cationic antimicrobial polymers was designed and synthesized that cluster local facial amphiphilicity from repeating units and therefore enhance interactions with bacterial membranes. This system does not require a globally conformational arrangement

associated with highly unfavorable entropic loss. These cationic materials have been demonstrated to be active antimicrobial agents against Gram-negative bacteria with low toxicity to mammalian cells.

Third, the self-assembly behavior of multicyclic natural product-based cationic copolymers has been explored. The relative amount of hydrophilic and hydrophobic segments in amphiphilic copolymers can determine their self-assembly behavior in water, allowing for the production of spherical, lenticular and rod-like nanostructures via supramolecular interactions. These nanoaggregates exhibited excellent antimicrobial activity against Gram-negative bacteria with significantly low toxicity.

1.8 References

1. Isikgor, F. H.; Becer, C. R., Lignocellulosic biomass: a sustainable platform for the production of bio-based chemicals and polymers. *Polym. Chem.* **2015,** *6*, 4497-4559.
2. Yao, K.; Tang, C., Controlled Polymerization of Next-Generation Renewable Monomers and Beyond. *Macromolecules* **2013,** *46* (5), 1689-1712.
3. Jambeck, J. R.; Geyer, R.; Wilcox, C.; Siegler, T. R.; Perryman, M.; Andrady, A.; Narayan, R.; Law, K. L., Plastic waste inputs from land into the ocean. *Science* **2015,** *347* (6223), 768-771.
4. Wilbon, P. A.; Chu, F.; Tang, C., Progress in Renewable Polymers from Natural Terpenes, Terpenoids, and Rosin. *Macromol. Rapid Commun.* **2013,** *34* (1), 8-37.
5. Belgacem, M. N.; Gandini, A., *Monomers, polymers and composites from renewable resources*. Elsevier: 2011.
6. Azapagic, A.; Emsley, A.; Hamerton, I., *Polymers: the environment and sustainable*

development. John Wiley & Sons: 2003.

7. Babu, R.; O'Connor, K.; Seeram, R., Current progress on bio-based polymers and their future trends. *Progress in Biomaterials* **2013,** *2* (8).
8. Gandini, A., The Irruption of Polymers from Renewable Resources on the Scene of Macromolecular Science and Technology. *Green Chem.* **2011,** *13* (5), 1061-1083.
9. Holmberg, A. L.; Reno, K. H.; Wool, R. P.; Epps III, T. H., Biobased Building Blocks for the Rational Design of Renewable Block Polymers. *Soft Matter* **2014,** *10* (38), 7405-7424.
10. Chen, G.-Q., A microbial polyhydroxyalkanoates (PHA) based bio- and materials industry. *Chem. Soc. Rev.* **2009,** *38* (8), 2434-2446.
11. Chen, G.-Q.; Patel, M. K., Plastics Derived from Biological Sources: Present and Future: A Technical and Environmental Review. *Chem. Rev.* **2012,** *112* (4), 2082-2099.
12. Reddy, C. S. K.; Ghai, R.; Rashmi; Kalia, V. C., Polyhydroxyalkanoates: an overview. *Bioresour. Technol.* **2003,** *87* (2), 137-146.
13. Quirino, R. L.; Garrison, T. F.; Kessler, M. R., Matrices from vegetable oils, cashew nut shell liquid, and other relevant systems for biocomposite applications. *Green Chem.* **2014,** *16* (4), 1700-1715.
14. Holmberg, A. L.; Reno, K. H.; Wool, R. P.; Epps, I. I. I. T. H., Biobased building blocks for the rational design of renewable block polymers. *Soft Matter* **2014,** *10* (38), 7405-7424.
15. Gandini, A.; Lacerda, T. M.; Carvalho, A. J. F.; Trovatti, E., Progress of Polymers from Renewable Resources: Furans, Vegetable Oils, and Polysaccharides. *Chem. Rev.* **2015**.
16. Bohlmann, J.; Keeling, C. I., Terpenoid Biomaterials. *The Plant Journal* **2008,** *54* (4),

656-669.

17. Smith, E.; Williamson, E.; Zloh, M.; Gibbons, S., Isopimaric acid from Pinus nigra shows activity against multidrug-resistant and EMRSA strains of Staphylococcus aureus. *Phytother. Res.* **2005,** *19* (6), 538-542.
18. Fernandez, M. A.; Tornos, M. P.; Garcia, M. D.; de las Heras, B.; Villar, A. M.; Saenz, M. T., Anti-inflammatory activity of abietic acid, a diterpene isolated from *Pimenta racemosa var. grissea*. *J. Pharm. Pharmacol.* **2001,** *53* (6), 867-72.
19. Talevi, A.; Cravero, M. S.; Castro, E. A.; Bruno-Blanch, L. E., Discovery of anticonvulsant activity of abietic acid through application of linear discriminant analysis. *Biorg. Med. Chem. Lett.* **2007,** *17* (6), 1684-1690.
20. Maiti, S., ; Ray, S.; Kundu, A., Rosin: A renewable resource for polymers and polymer chemicals. *Prog. Polym. Sci.* **1989,** *14*, 297-338.
21. Bicu, I., ; Mustata, F., Polymers from a Levopimaric Acid-Acrylic Acid Diels-Alder Adduct: Synthesis and Characterization. *Journal of Polymer Science: Part A: Polymer Chemistry* **2007,** *45*, 5979-5990.
22. DSilvestre, A., ; Gandini, A., *In Monomers, Polymers and Composites from Renewable Resources*. Elsevier: Amsterdam, 2008; p 67-88.
23. Wang, J.; Yao, K.; Wilbon, P.; Wang, P.; Chu, F.; Tang, C., Rosin-Derived Polymers and Their Progress in Controlled Polymerization. In *Rosin-based Chemicals and Polymers*, Zhang, J., Ed. ISmithers: Shawbury, UK, 2012; pp 85-127.
24. Wilbon, P.; Gulledge, A.; Benicewicz, B.; Tang, C., Renewable rosin fatty acid polyesters: the effect of backbone structure on thermal properties. *Green Mater.* **2013,** *1* (2), 96-104.

25. di Gregorio, M. C.; Travaglini, L.; Del Giudice, A.; Cautela, J.; Pavel, N. V.; Galantini, L., Bile Salts: Natural Surfactants and Precursors of a Broad Family of Complex Amphiphiles. *Langmuir* **2018**.

26. Russell, D. W.; Setchell, K. D. R., Bile acid biosynthesis. *Biochemistry* **1992,** *31* (20), 4737-4749.

27. Björkhem, I., Chapter 9 Mechanism of bile acid biosynthesis in mammalian liver. *New Compr. Biochem.* **1985,** *12*, 231-278.

28. Denike, J. K.; Zhu, X. X., Preparation of new polymers from bile acid derivatives. *Macromol. Rapid Commun.* **1994,** *15* (6), 459-465.

29. Cunningham, A. J.; Zhu, X. X., Polymers made of bile acids: from soft to hard biomaterials. *Can. J. Chem.* **2016,** *94* (8), 659-666.

30. Zhu, X.-X.; Nichifor, M., Polymeric Materials Containing Bile Acids. *Acc. Chem. Res.* **2002,** *35* (7), 539-546.

31. Hao, J.; Li, H.; Zhu, X. X., Preparation of a Comb-Shaped Cholic Acid-Containing Polymer by Atom Transfer Radical Polymerization. *Biomacromolecules* **2006,** *7* (3), 995-998.

32. Jia, Y.-G.; Zhu, X. X., Self-Healing Supramolecular Hydrogel Made of Polymers Bearing Cholic Acid and β-Cyclodextrin Pendants. *Chem. Mater.* **2015,** *27* (1), 387-393.

33. Ye, W.; Li, Y.; Zhou, Z.; Wang, X.; Yao, J.; Liu, J.; Wang, C., Synthesis and antibacterial activity of new long-chain-alkyl bile acid-based amphiphiles. *Bioorg. Chem.* **2013,** *51*, 1-7.

34.Poole, K., Mechanisms of bacterial biocide and antibiotic resistance. *J. Appl. Microbiol.*

2002, *92*, 55S-64S.

35. Gillings, M. R., Evolutionary consequences of antibiotic use for the resistome, mobilome and microbial pangenome. *Frontiers in Microbiology* **2013,** *4*.
36. Ganewatta, M. S.; Tang, C., Controlling macromolecular structures towards effective antimicrobial polymers. *Polymer* **2015,** *63*, A1-A29.
37. Boucher, H. W.; Talbot, G. H.; Bradley, J. S.; Edwards, J. E.; Gilbert, D.; Rice, L. B.; Scheld, M.; Spellberg, B.; Bartlett, J., Bad Bugs, No Drugs: No ESKAPE! An Update from the Infectious Diseases Society of America. *Clin. Infect. Dis.* **2009,** *48* (1), 1-12.
38. Takahashi, H.; Caputo, G. A.; Vemparala, S.; Kuroda, K., Synthetic Random Copolymers as a Molecular Platform To Mimic Host-Defense Antimicrobial Peptides. *Bioconj. Chem.* **2017,** *28* (5), 1340-1350.
39. Xiong, M.; Han, Z.; Song, Z.; Yu, J.; Ying, H.; Yin, L.; Cheng, J., Bacteria-Assisted Activation of Antimicrobial Polypeptides by a Random-Coil to Helix Transition. *Angew. Chem. Int. Ed.* **2017,** *56* (36), 10826-10829.
40. Zasloff, M., Antimicrobial peptides of multicellular organisms. *Nature* **2002,** *415*, 389-395.
41. Mowery, B. P.; Lindner, A. H.; Weisblum, B.; Stahl, S. S.; Gellman, S. H., Structure−activity Relationships among Random Nylon-3 Copolymers That Mimic Antibacterial Host-Defense Peptides. *J. Am. Chem. Soc.* **2009,** *131* (28), 9735-9745.
42. Lienkamp, K.; Madkour, A. E.; Musante, A.; Nelson, C. F.; Nüsslein, K.; Tew, G. N., Antimicrobial Polymers Prepared by ROMP with Unprecedented Selectivity: A Molecular Construction Kit Approach. *J. Am. Chem. Soc.* **2008,** *130* (30), 9836-9843.
43. Ong, Z. Y.; Wiradharma, N.; Yang, Y. Y., Strategies employed in the design and

optimization of synthetic antimicrobial peptide amphiphiles with enhanced therapeutic potentials. *Adv. Drug Del. Rev.* **2014,** *78*, 28-45.

44. Porter, E. A.; Wang, X.; Lee, H.-S.; Weisblum, B.; Gellman, S. H., Non-haemolytic β-amino-acid oligomers. *Nature* **2000,** *404*, 565.
45. Porter, E. A.; Weisblum, B.; Gellman, S. H., Mimicry of Host-Defense Peptides by Unnatural Oligomers: Antimicrobial β-Peptides. *J. Am. Chem. Soc.* **2002,** *124* (25), 7324-7330.
46. Chongsiriwatana, N. P.; Patch, J. A.; Czyzewski, A. M.; Dohm, M. T.; Ivankin, A.; Gidalevitz, D.; Zuckermann, R. N.; Barron, A. E., Peptoids that mimic the structure, function, and mechanism of helical antimicrobial peptides. *Proc. Natl. Acad. Sci. U.S.A.* **2008,** *105* (8), 2794-2799.
47. Reuther, J. F.; Goodrich, A. C.; Escamilla, P. R.; Lu, T. A.; Del Rio, V.; Davies, B. W.; Anslyn, E. V., A Versatile Approach to Noncanonical, Dynamic Covalent Single- and Multi-Loop Peptide Macrocycles for Enhancing Antimicrobial Activity. *J. Am. Chem. Soc.* **2018,** *140* (10), 3768-3774.
48. Ilker, M. F.; Nüsslein, K.; Tew, G. N.; Coughlin, E. B., Tuning the Hemolytic and Antibacterial Activities of Amphiphilic Polynorbornene Derivatives. *J. Am. Chem. Soc.* **2004,** *126* (48), 15870-15875.
49. Nederberg, F.; Zhang, Y.; Tan, J. P. K.; Xu, K.; Wang, H.; Yang, C.; Gao, S.; Guo, X. D.; Fukushima, K.; Li, L.; Hedrick, J. L.; Yang, Y.-Y., Biodegradable nanostructures with selective lysis of microbial membranes. *Nat. Chem.* **2011,** *3*, 409-414.
50. Geng, Z.; Finn, M. G., Thiabicyclononane-Based Antimicrobial Polycations. *J. Am. Chem. Soc.* **2017,** *139* (43), 15401-15406.

51. Ergene, C.; Yasuhara, K.; Palermo, E. F., Biomimetic antimicrobial polymers: recent advances in molecular design. *Polym. Chem.* **2018,** *9* (18), 2407-2427.

52. Mai, Y.; Eisenberg, A., Self-assembly of block copolymers. *Chem. Soc. Rev.* **2012,** *41* (18), 5969-5985.

53. Bhargava, P.; Zheng, J. X.; Li, P.; Quirk, R. P.; Harris, F. W.; Cheng, S. Z. D., Self-Assembled Polystyrene-block-Poly(ethylene Oxide) Micelle Morphologies in Solution. *Macromolecules* **2006,** *39*, 4880.

54. Jain, S.; Bates, F. S., On the Origins of Morphological Complexity in Block Copolymer Surfactants. *Science* **2003,** *300*, 460.

55. Discher, D. E.; Eisenberg, A., Polymer Vesicles. *Science* **2002,** *297*, 967.

56. Li, L.; Raghupathi, K.; Song, C.; Prasad, P.; Thayumanavan, S., Self-Assembly of Random Copolymers. *Chem. Commun.* **2014,** *50*, 13417.

57. Mavila, S.; Eivgi, O.; Berkovich, I.; Lemcoff, N. G., Intramolecular Cross-Linking Methodologies for the Synthesis of Polymer Nanoparticles. *Chem. Rev.* **2016,** *116*, 878.

58. Terashima, T.; Sugita, T.; Fukae, K.; Sawamoto, M., Synthesis and Single-Chain Folding of Amphiphilic Random Copolymers in Water. *Macromolecules* **2014,** *47*, 589.

59. Ogura, Y.; Artar, M.; Palmans, A. R. A.; Sawamoto, M.; Meijer, E. W.; Terashima, T., Self-Assembly of Hydrogen-Bonding Gradient Copolymers: Sequence Control via Tandem Living Radical Polymerization with Transesterification. *Macromolecules* **2017,** *50*, 3215.

60. Ogura, Y.; Terashima, T.; Sawamoto, M., Amphiphilic PEG-Functionalized Gradient Copolymers via Tandem Catalysis of Living Radical Polymerization and Transesterification. *Macromolecules* **2017,** *50*, 822.

61. Hattori, G.; Hirai, Y.; Sawamoto, M.; Terashima, T., Self-Assembly of PEG/dodecyl-Graft Amphiphilic Copolymers in Water: Consequences of the Monomer Sequence and Chain Flexibility on Uniform Micelles. *Polym. Chem.* **2017,** *8*, 7248.

62. Ueda, M.; Hashidzume, A.; Sato, T., Unicore–Multicore Transition of the Micelle Formed by an Amphiphilic Alternating Copolymer in Aqueous Media by Changing Molecular Weight. *Macromolecules* **2011,** *44*, 2970.

63. Jain, S.; Bates, F. S., On the Origins of Morphological Complexity in Block Copolymer Surfactants. *Science* **2003,** *300* (5618), 460-464.

64. Discher, D. E.; Eisenberg, A., Polymer Vesicles. *Science* **2002,** *297* (5583), 967-973.

65. Cui, H.; Chen, Z.; Zhong, S.; Wooley, K. L.; Pochan, D. J., Block Copolymer Assembly via Kinetic Control. *Science* **2007,** *317* (5838), 647-650.

66. Bielawski, C. W.; Grubbs, R. H., Highly efficient ring-opening metathesis polymerization (ROMP) using new ruthenium catalysts containing N-heterocyclic carbene ligands. *Angew. Chem. Int. Ed.* **2000,** *39* (16), 2903-2906.

67. Bielawski, C. W.; Grubbs, R. H., Living ring-opening metathesis polymerization. *Prog. Polym. Sci.* **2007,** *32* (1), 1-29.

68. Sutthasupa, S.; Shiotsuki, M.; Sanda, F., Recent Advances in Ring-Opening Metathesis Polymerization, and Application to Synthesis of Functional Materials. *Polym. J.* **2010,** *42* (12), 905-915.

69. Ganewatta, M. S.; Ding, W.; Rahman, M. A.; Yuan, L.; Wang, Z.; Hamidi, N.; Robertson, M. L.; Tang, C., Biobased Plastics and Elastomers from Renewable Rosin via "Living" Ring-Opening Metathesis Polymerization. *Macromolecules* **2016,** *49*, 7155-7164.

70. Barner-Kowollik, C., *Handbook of RAFT Polymerization*. Wiley: 2008.

71. Chiefari, J.; Chong, Y. K.; Ercole, F.; Krstina, J.; Jeffery, J.; Le, T. P. T.; Mayadunne, R. T. A.; Meijs, G. F.; Moad, C. L.; Moad, G.; Rizzardo, E.; Thang, S. H., Living Free-Radical Polymerization by Reversible Addition−Fragmentation Chain Transfer: The RAFT Process. *Macromolecules* **1998,** *31* (16), 5559-5562.

72. Chiefari, J.; Mayadunne, R. T. A.; Moad, C. L.; Moad, G.; Rizzardo, E.; Postma, A.; Thang, S. H., Thiocarbonylthio Compounds (SC(Z)S−R) in Free Radical Polymerization with Reversible Addition-Fragmentation Chain Transfer (RAFT Polymerization). Effect of the Activating Group Z. *Macromolecules* **2003,** *36* (7), 2273-2283.

CHAPTER 2

DESIGNING BLOCK COPOLYMER ARCHITECTURES TOWARD TOUGH BIOPLASTICS FROM NATURAL ROSIN[1]

[1] Rahman Md. A.; Lokupitia H.; Ganewatta M.; Yuan L; Morgan S; Tang, C. Designing Block Copolymer Architectures toward Tough Bioplastics from Natural Rosin Macromolecules, **2017**, *50* (5), 2069–2077. Reprinted here with permission. Copyright (2017) American Chemical Society.

2.1 Abstract

Resin acids (or natural rosin) are a class of abundant, renewable natural biomass. Most low molecular weight resin acid-containing polymers are very brittle due to their low chain entanglement associated with the pendant, intrinsically bulky hydrophenanthrene group. The use of block copolymer architectures can enhance chain entanglement and thus improve toughness. A–B–A type triblock and A–B–A–B–A type pentablock copolymers were synthesized by ring-opening metathesis polymerization (ROMP) with one-pot sequential monomer addition of a rosin-based monomer and norbornene. We investigated the effect of chain architecture and microphase separation on mechanical properties of both types of block copolymers. Pentablock copolymers exhibited higher strength and toughness as compared to both the triblock copolymers and the corresponding homopolymers. The greater toughness of pentablock copolymers is due to the presence of the rosin-based midblock chains that act as bridging chains between two polynorbornene domains. SAXS and AFM data were consistent with short-range phase separation of microdomains in all tri- and pentablock copolymers.

2.2 Introduction

The development of bioplastics fully or partially from renewable biomass is gaining momentum in both industry and academia.[1] Limited fossil oil resources and growing concerns on environmental changes have led to renewed interest in partially replacing and/or complementing unsustainable petrochemical-based plastics.[1-4] However, the production and utilization of bio-based plastics in daily life is still minor compared to petroleum-based counterparts.[5-7] Therefore, the search of plastics with better properties from nonedible and low cost natural biomass is a focus of scientific communities.(8)

Especially, the forestry-based natural resources such as cellulose,[9, 10] lignin,[11-13] and rosin[14] are economical due to their high abundance and can be utilized toward novel sustainable polymeric materials.[15] Resin acids (abietic, dehydroabietic, pimaric, levepimaric acids, etc.) are the main components of rosin obtained from the exudate of pine and conifer trees.[14] Resin acids are hydrocarbon-rich small molecular biomass with characteristic bulky hydrophenanthrene ring structures that make them unique from other natural biomass. This moiety can increase the hydrophobicity and thermal properties of polymers. Especially, the bulkiness of rosin structures has a significant impact on thermomechanical properties (e.g., glass transition temperature and toughness) of polymers associated with.[5, 14]

Rosin-based side-chain and main-chain polymeric materials have been prepared by us and a few other groups over the past few years.[5, 16] Main-chain rosin-based polymers were prepared by various condensation polymerization techniques.[14] Tang and co-workers reported rosin-based side-chain polymers via controlled polymerization techniques such as ATRP, RAFT, and ROP.[17-23] However, almost all rosin-containing polymers are very brittle and powdery and could not produce mechanically robust free-standing films. The major reason for brittleness is the low molecular weight of polymers associated with various polymerization techniques.

The chain entanglement molecular weight (M_e) is a fundamental property of a polymer that is closely related with mechanical properties (e.g., ductility). It typically increases with the bulkiness of side chain/pendant group of a polymer.[24, 25] The Me of rosin polymers is very high with bulky hydrophenanthrene moieties as side groups. A polymer with high M_e tends to form crazes that breakdown readily to generate cracks; meanwhile, a low M_e polymer inclines to form shear deformation zones rather than crazes.[26, 27]

Block copolymers are an important class of materials because of their superior ability to tune the morphology and properties by changing the molecular weight, composition, and block sequences.[28, 29] Chain architecture and morphology of block copolymers have a tremendous effect on the mechanical properties. Brittle homopolymers can be strengthened by copolymerizing with elastomeric (low T_g) chain.[30] One of the important toughening methods is to make linear triblock copolymers where a rubbery midblock is anchored by two glassy hard blocks. Such polymers can demonstrate either plastic or elastomeric properties based on the choice polymeric compositions forming a microphase-separated morphology.[31-36] There are several other strategies to toughen brittle polymers (such as PLA) including plasticization,[37] melt blending,[38] reactive blending,[39, 40] and graft block copolymers.[41]

The ductility of glassy polymers with bulky side chains can be improved by raising network density (entanglements and cross-links), which can be made either by very high molecular weight polymers far above M_e or by copolymerizing with rubbery domains.[42] On the other hand, Kramer et al. investigated the effects of chain architectures on deformation and fracture mechanism of homopolymers, tri- and pentablock copolymers, with highly entangled polyethylene dispersed in an untangled poly(vinylcyclohexane) or poly(cyclohexylethylene) (PCHE) matrix.[42, 43] They found that the pentablock copolymers exhibited a brittle-to-ductile transition, whereas triblock and homopolymers still showed brittle behaviors. The reason for the ductility was that pentablock copolymers could increase the network density that disfavors both craze formation and premature craze breakdown. In addition, the PCHE midblock chains in pentablock copolymers can form bridging chains between highly entangled domains of PE, which can transfer stress from

one entangled domain to its neighbors and prevent crack propagation. This early seminal work was primarily based on thin film analysis. Recently, the Register group extended further and synthesized pentablock copolymers as thermoplastic elastomers to enhance the mechanical properties by incorporating crystalline and amorphous blocks.[44, 45] Specifically pentablock copolymers with the block sequence crystalline–glassy–rubbery–glassy–crystalline achieved physical cross-linking via crystallization of the end crystalline blocks followed by vitrification of the adjacent glassy blocks. Other multiblock copolymers were also developed to enhance the mechanical properties of brittle and glassy polymers particularly in plastic limit by bridging between multiple nanoscale domains.[46-50]

We recently reported a method to synthesize ultrahigh molecular weight rosin-containing homopolymers (up to half million daltons) through ring-opening metathesis polymerization (ROMP) where we determined the Me of side-chain rosin-containing homopolymers about 86 000 g/mol.[51] For the first time mechanically robust free-standing films were achieved from rosin-based homopolymers. However, these homopolymers require very high molecular weight to form sufficient chain entanglement for good mechanical properties. In addition, at this high molecular weight the dispersity of homopolymers is high and difficult to control.

Inspired by the above pioneer work, herein we report the preparation and characterization of rosin-based A–B–A triblock and A–B–A–B–A pentablock copolymers to enhance mechanical properties where the B block is polynorbornene with low Me and the A block is a rosin-containing segment. The mechanical properties are dependent on molecular weight, compositions, morphology, and chain architectures of block copolymers. We investigated how the chain architecture improved the mechanical properties of an

untangled matrix. As we changed from triblock to pentablock, a brittle-to-ductile transition was observed. Rosin-based pentablock copolymers exhibit significant improvement of mechanical properties in bulk phase compared to homopolymers and triblock copolymers. We also explored how microphase-separated morphology influenced the mechanical properties of block copolymers.

2.3 Results and Discussion

Synthesis of Polymers. Dehydroabietic acid-derived norbornene monomer (**M**) and homopolymers were synthesized by following our recently reported method.[51] ROMP was conducted to prepare homopolymers with different molecular weight in the presence of Grubbs III catalyst (G3) and the reaction scheme is shown in Figure 2.1 and characterized by ^{1}H NMR (Figure 2.9). Two homopolymers with ratios of monomer to catalyst at 148 : 1 and 250 : 1 were prepared and denoted as **H1** and **H2**. The molecular weight (M_n) of 60 kg/mol and 100 kg/mol with dispersity ($Đ$) of 1.07 and 1.17 was respectively obtained, as characterized by gel permeation chromatography (GPC). A series of tri and pentablock copolymers with different feed ratios were prepared using one-pot ROMP through sequential addition of monomers using G3 as a catalyst. Block copolymers were prepared using rosin-based monomer **M** and norbornene. Norbornene was chosen as an auxiliary monomer due to lower M_e of its polymer. Triblock copolymers, as shown in the Figure 2.2, were made where the two outer blocks are rosin-containing segments, and the middle block is polynorbornene. At first, the monomer **M** was polymerized with controlled feed ratios of monomer to catalyst (131 : 1, 116 : 1, and 108 : 1), and complete conversions were achieved within one hour as confirmed by the disappearance of ^{1}H NMR peak at 6.10 ppm of double bond protons of norbornene in **M**. Norbornene and **M** were

then added sequentially to the same reaction mixture after the complete conversion of each monomer. Triblock copolymers with an overall M_n of 134 kg/mol with 80, 70, and 65 wt% of rosin-containing polymers were synthesized and designated as **T1**, **T2**, and **T3** respectively. Similarly, pentablock copolymers, as shown in Figure 2.2, were prepared where the first, third and fifth blocks were made of rosin monomer, and the second and fourth blocks were norbornene. The molecular weight of rosin based blocks was kept consistent in pentablock copolymers with corresponding triblock copolymers for a better comparison. The overall M_n of each pentablock copolymer were 200 kg/mol and 80, 70, and 65 wt% of rosin containing polymer were synthesized and depicted as **P1**, **P2**, and **P3** respectively. The progress of the reaction was monitored by the ^{1}H NMR on the peak intensity difference in the aromatic protons (Peaks at 6.8 - 7.2 ppm) of rosin and backbone double bond protons (peaks at 5.0 – 5.5 ppm), which are shown in Figures 2.10 and 2.11. The GPC traces also remained monomodal with narrow molecular weight distribution after each polymerization step. The weight percentage (wt %) of rosin-containing block in the tri and pentablock was calculated by ^{1}H NMR (Figure 2.12) and shown in Table 2.1. The GPC traces after each polymerization step are shown in Figure 2.3A for triblock and Figure 2.3B for pentablock copolymers. The GPC traces in each step shifted to high molecular weight indicating the successful chain extension. It should be noted that the molecular weight distribution is narrow for tri and pentablock copolymers ($Đ < 1.3$ in triblock and $Đ < 1.4$ in pentablock) compared to high dispersity in ultrahigh molecular weight homopolymers that we recently reported.[51] These results suggested the sequential block copolymerization was well controlled with good yield (> 99%) and low dispersity. The characterization data of all homopolymers, tri- and pentablock are provided in Table 2. 1.

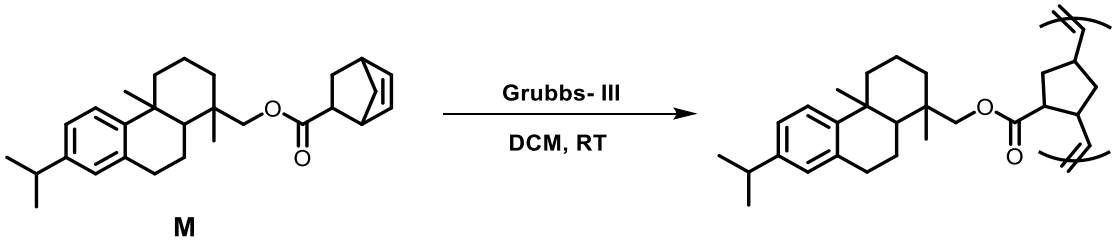

Figure 2.1 Synthesis of homopolymer by ROMP.

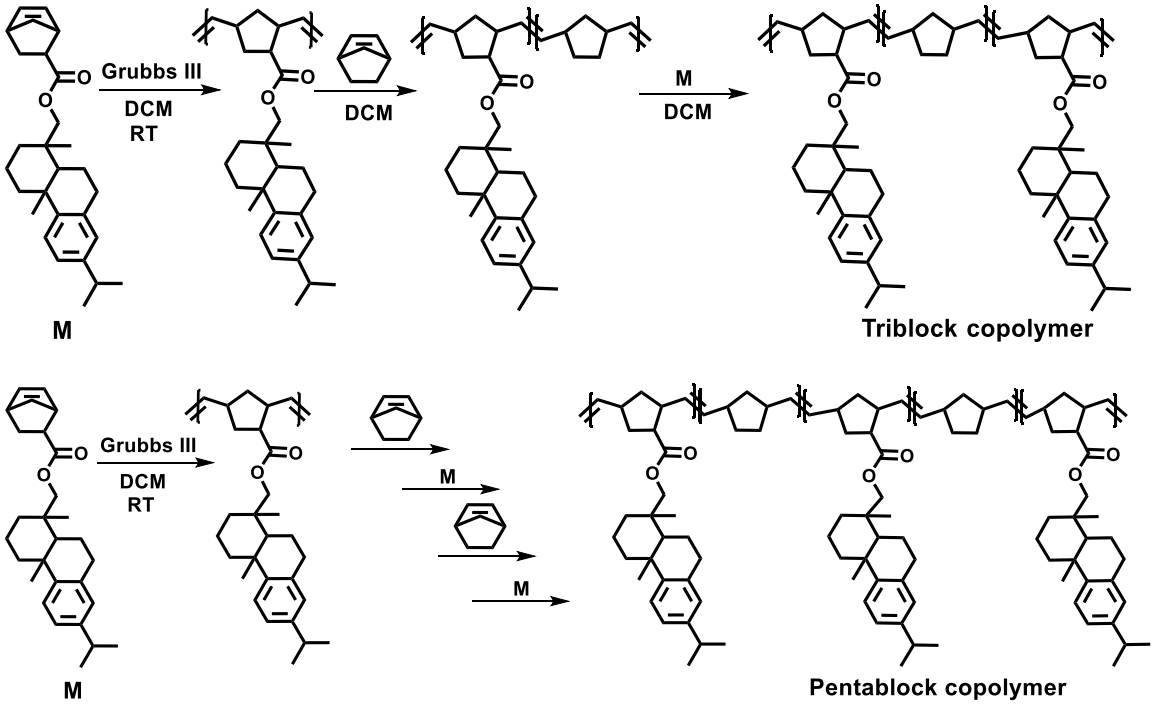

Figure 2.2 Synthesis of triblock and pentablock copolymers by one-pot ROMP through sequential addition of monomers.

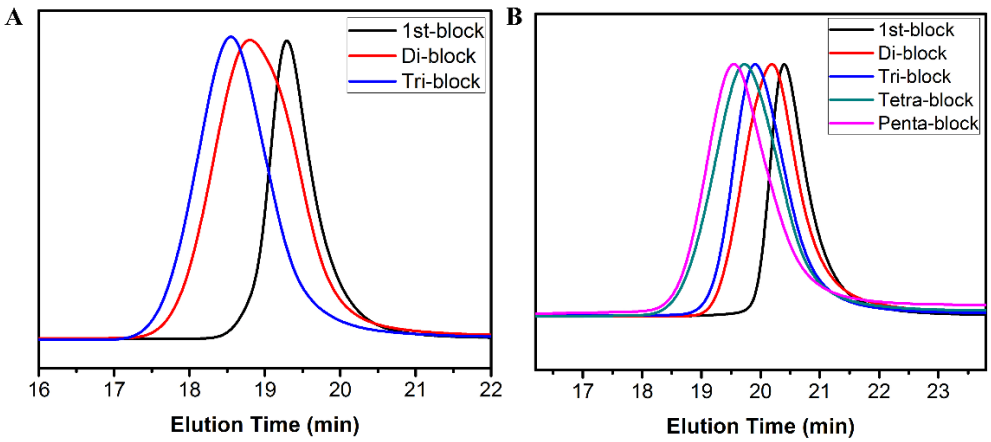

Figure 2.3 GPC traces after each polymerization step in the ROMP synthesis of (A) Triblock copolymers; (B) Pentablock copolymers.

Table 2.1 Molecular characterization data for homopolymers, tri and pentablock copolymers.

Polymer	Polymer Chain Architecture With M_n of Each Block (kg/mol)	M_n (kg/mol) (Theo)	M_n [a] (kg/mol) (GPC)	$Đ$ [a]	f_{Rosin} (Theo, wt %)	f_{Rosin} (^{1}H NMR, wt %)	T_g [b] (**M** block, °C)	T_g [b] (Nb block, °C)	T_d [c] (°C)
H1	60	60	62	1.07			110		400
H2	100	100	117	1.17			110		420
T1	53+28+53	134	120	1.26	80	80	85	44	425
T2	47+40+47	134	114	1.30	70	68	99	44	424
T3	44+46+44	134	132	1.50	65	62	101	50	413
P1	53+20+53+20+53	200	187	1.30	80	80	104	53	376
P2	47+30+47+30+47	200	175	1.41	70	70	100	51	383
P3	44+35+44+35+44	200	168	1.55	65	62	98	49	394

[a]Relative molecular weight measured by GPC with refractive index detector and calibrated with polystyrene standards.
[b]Measured by DSC.
[c]Decomposition temperature at 10 wt % loss determined by TGA.

Thermal Properties. Thermal properties of tri and pentablock copolymers were measured by differential scanning calorimetry (DSC). The DSC curves of all copolymers, as shown in Figure 2.4, indicated two distinct glass transition temperature (T_g). All homopolymers, tri and pentablock copolymers are amorphous without visible melting temperature. The two T_gs appear at 44-54 ^oC and 98-105 ^oC corresponding to the polynorbornene block and rosin-containing block respectively in both tri and pentablock copolymers. All T_gs of block copolymers and homopolymers are listed in Table 2. 1. The T_gs at $\sim$ 45 ^oC and 110 ^oC are reported in the literature respectively for polynorbornene and rosin-based homopolymer.[51] However, the observed T_gs of polynorbornene and rosin-containing segments in tri and pentablock copolymers are slightly higher and lower respectively than their homopolymers. These results indicated that both tri and pentablock copolymers are microphase separated, but with the possibility of partial mixing of the two segments (polynorbornene and rosin-based polynorbornene).

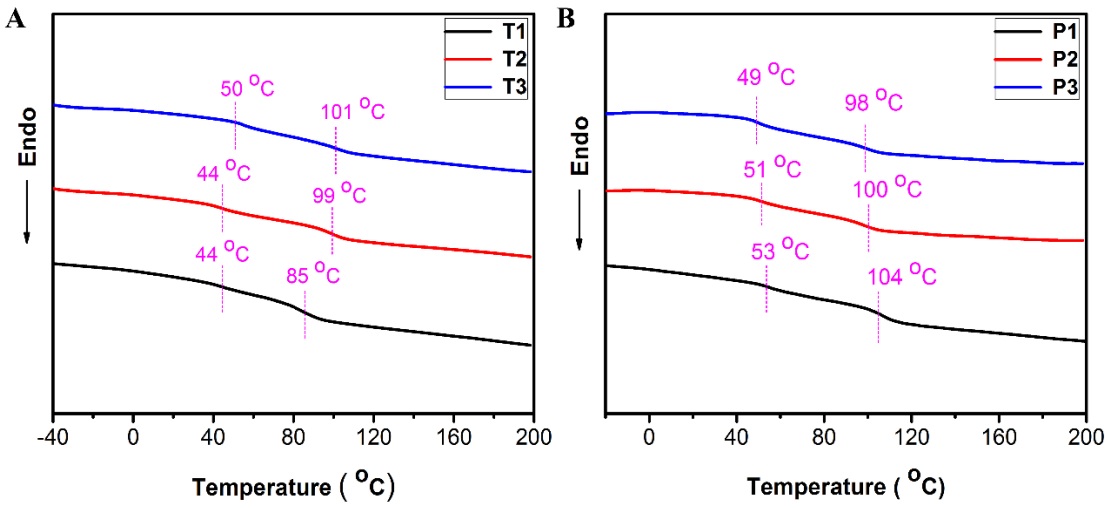

Figure 2.4 DSC curves of (A) Triblock copolymers **T1**, **T2**, and **T3**; and (B) Pentablock copolymers **P1**, **P2**, and **P3**.

Phase Behaviors. The tri and pentablock copolymers are expected to show microphase separation due to immiscibility of the rosin matrix and polynorbornene domains, as observed in the DSC analysis. The morphologies of all tri and pentablock copolymers were investigated using small-angle X-ray scattering (SAXS) and atomic force microscopy (AFM). The SAXS patterns were collected for solution-cast films with and without thermal annealing, as shown in Figure 2.5 (all the scattering peaks of tri and pentablock copolymers are summarized in Table 2.3). Almost all block copolymers showed a strong principle scattering peak (q^*) and a broad shoulder peak, indicating the presence of microphase separation. Triblock copolymers **T1**, **T2**, and **T3** exhibited primary peaks at $q^* = 0.15$, 0.14, and 0.13 nm^{-1} respectively with their corresponding domain spacing ($D = 2\pi/q^*$) about 42, 45 and 48 nm. The **P1**, **P2**, **P3** pentablock copolymers also showed strong primary peaks at $q^* = 0.11$, 0.11, 0.09 nm^{-1} with the domain spacing of 57, 57, 70 nm respectively. The presence of only a primary scattering peak with a broad shoulder in all SAXS patterns made structural identification rather equivocal. The observed scattering pattern is consistent with the short-range correlations expected from random packing that generate multiple peaks due to the radial distribution function.[52, 53] The weak ordering observed in bulk films could be attributed to fairly high molecular weight of tri and pentablock copolymer and the bulky rosin moiety that could hinder the diffusion of polymer chains, and/or partial mixing of polynorbornene and rosin-containing blocks. Indeed, designing the block copolymer architecture to enhance chain entanglement is expected to inhibit the formation of long-range order.

The morphology was examined in real-space using atomic force microscopy (AFM). We sought to investigate surface morphology and hope it could help shed light on

the bulk morphology, though we understood the difference between each other. Thin films (thickness ~ 100 nm) were prepared by spin-coating a 2 wt % solution of polymers in toluene onto silicon wafer. Since the high T_g could impair the formation of long-range ordered morphology by thermal annealing, solvent vapor annealing was conducted for the thin films. The solvent allows plasticization for fast chain rearrangement.[54] The characteristic AFM height images were taken after the spin-coating (shown in Figure 2.14) and after 24h solvent vapor annealing in tetrahydrofuan (THF) (shown in Figure 2.6). The AFM images before and after solvent annealing exhibited microphase separated morphology where the rosin-containing matrix is brighter, and polynorbornene domains are darker because the tip of AFM can penetrate further into the relatively softer regions. Solvent annealing improved the ordering of the films, as evidenced by Fast Fourier Transform (FFT) shown in the inset of the AFM images, however the FFT images did not exhibit long rang order either. For polymers **P1** and **P2** where f_{Rosin} = 0.78 and 0.67 respectively, the surface morphology has predominant round domains with a spacing of 60-65 nm and 62-67 nm, appearing to be weakly ordered spheres or perpendicular cylinders dispersed in a matrix. Such features were also observed on the thin films of **T1** and **T2**, although their domain spacing is decreased (around 45-48 nm) probably associated with their chain architecture and lower molecular weight. The worm-like textures were observed on the surface of **P3** and **T3** where f_{Rosin} = 0.60 with domain spacing 68-73 nm and 52-57 nm respectively, in a relatively good agreement with those determined by SAXS. These features could be interpreted as cylinders, or defect-rich edge-on lamellae or a mixture of both. The top surface observations by AFM suggest a continuous matrix of the majority rosin component with discrete localized clusters polynorbornene of the minority

component. Again, the dispersed soft polynorbornene domains appeared much darker than the continuous rosin-contain matrix.

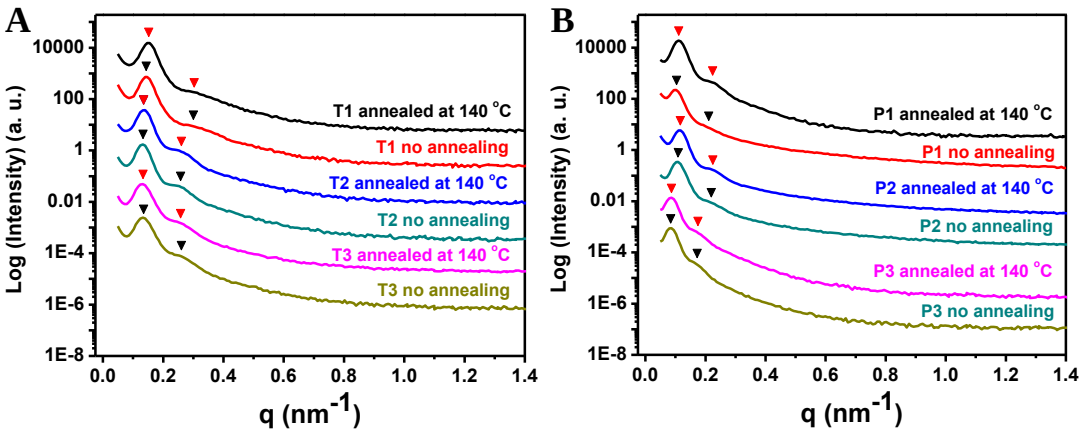

Figure 2.5. SAXS patterns of bulk films with and without thermal annealing at 140 ºC: (A) Triblock copolymers; (B) Pentablock copolymers.

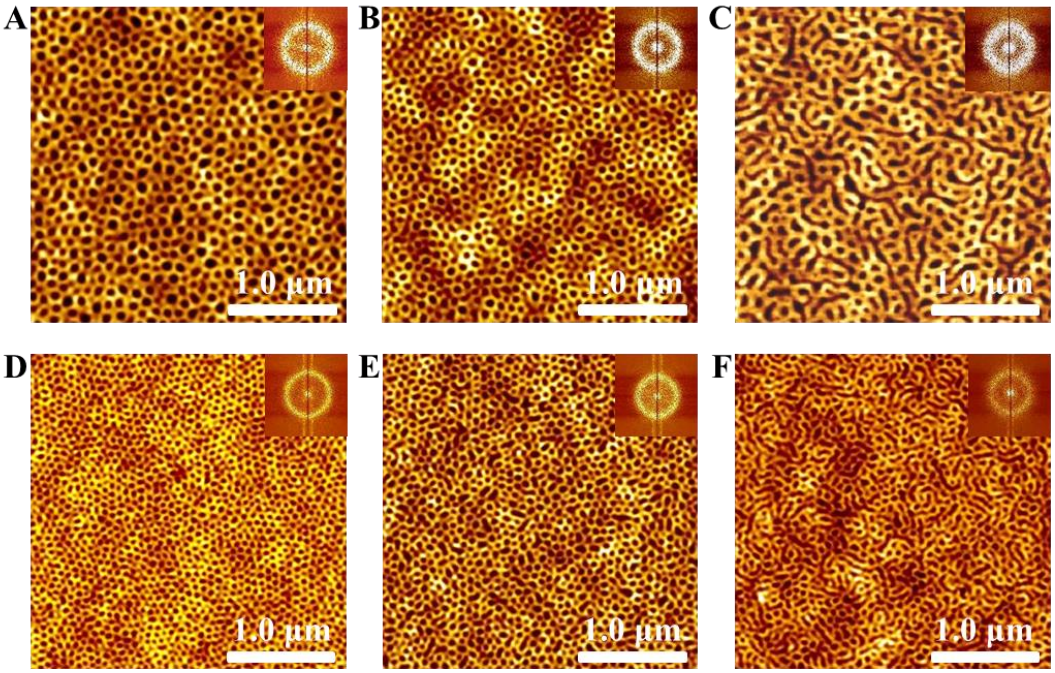

Figure 2.6 AFM height images of (A) **P1**, (B) **P2**, (C) **P3**, (D) **T1**, (E) **T2**, and (F) **T3** after 24h solvent annealing in THF.

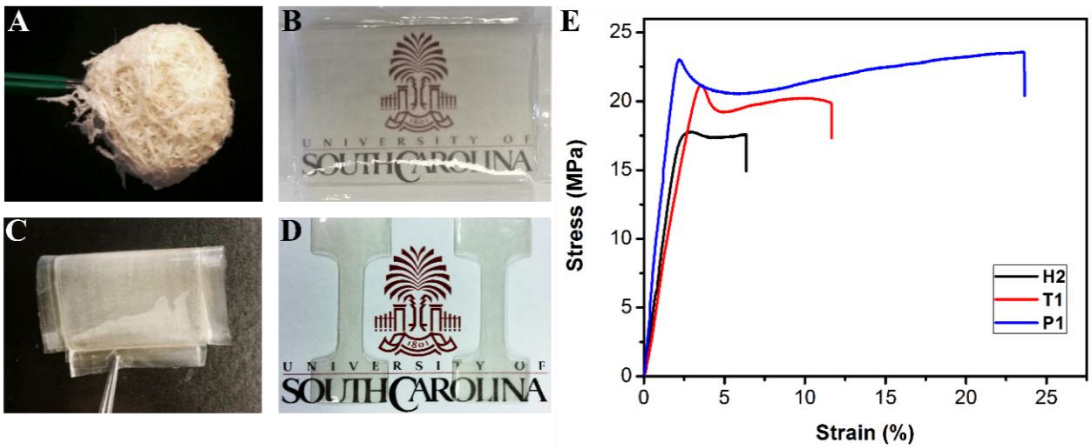

Figure 2.7 Polymer films and mechanical properties; (A) Fiber-like pentablock copolymer **P1**; (B) Free-standing film of **P1**; (C) Flexibility of **P1**; (D) Dog-bone sample of **P1**; (E) Representative uniaxial tensile stress-strain curves of **H2**, **T1**, and **P1**.

Mechanical Properties. The mechanical properties of homopolymers, tri and pentablock copolymers were characterized by uniaxial tensile tests using dog-bone specimens that were cut from solvent-cast dry films. Rosin-containing homopolymers with lower M_n are brittle and cannot form free-standing films (Figure 2.15**),** as we observed in the case of **H1** (M_n = 60 kg/mol). On the other hand, **H2** with the higher molecular weight (M_n = 100 kg/mol) could produce free-standing films, however, the polymer film is not flexible, with poor mechanical properties such as lower tensile strain and stress. The M_e of rosin based homopolymers is 86 kg/mol, as determined recently,[51] indicating M_n at 100 kg/mol is still not enough to have sufficient chain entanglements. We then assessed the mechanical properties of rosin-containing tri and pentablock copolymers. All copolymers showed a clear yield point, necking, and significantly greater toughness compared to homopolymers with comparable molecular weight of rosin blocks. Representative stress-strain curves of **H2**, **T1** and **P1** are illustrated in Figure 2.7, with all others shown in Figure 2.16. Mechanical properties are summarized for all samples in Table 2.2**,** including Young's modulus (E), yield stress (σ_{yield}), ultimate tensile stress (σ_{UTS}), tensile strain at break (ε), and

toughness. In the case of tri and pentablock copolymers, the dispersion of polynorbornene domains into a rosin matrix led to slight decrease in modulus compared to homopolymers. As shown in Figure 2.7, **P1** (with 80 wt % of rosin-containing block) has strain at break at near 24 %, which is almost double to that of **T1** triblock copolymers. The ultimate tensile strength of **P1** was found to be at 23.6 MPa and the ultimate tensile stress at break 23.2 MPa, which were also higher than those of **T1**. Though the molecular weight of each rosin-containing chains in **P1** is much below the M_e, the **P1** showed greater toughness than the **T1** and homopolymers. All tri and pentablock copolymers exhibited similar yield strength because the length of rosin based blocks was kept consistent in pentablock copolymers with corresponding triblock. All other pentablock copolymers also displayed higher strength, larger strain at break and greater toughness properties compared to triblock and homopolymers. The promising toughening properties of pentablock copolymers are most likely due to the existence of the rosin-containing middle block chains, which can act as bridging chains between the neighboring polynorbornene domains, and thus increases the energy needed for crack propagation through the rosin-containing matrix (Figure 2.8). The larger strain hardening in **P1** suggested that the bridging chains may act as crosslinks sufficiently to tolerate the stress. Not surprisingly, the mechanical properties of pentablock copolymers were affected by decreasing the amount of f_{Rosin}, which may be due to the decreased length of bridging chains and the increased glassy polynorbornene domains. For example, **P3** shows strain at break near 14 % while **P2** shows at near 16 %, suggesting that the bridging chain fractions are not sufficient to sustain the stress associated with the alignment of chains and microphase-separated domains.

Table 2.2 Summary of mechanical properties of all polymers.

Polymer	f_{Rosin} [wt %]	σ yield [MPa]	E [GPa][a]	σ_{UTS} [MPa]	$\mathcal{E}$ [%]	Toughness [MJ m^{-3}]
H2	100	17.1 ± 0.6	0.96 ± 0.02	17.2 ± 0.4	6.2 ± 0.2	0.91 ±0.01
P1	80	23.2 ± 0.2	1.24 ± 0.01	23.6 ± 0.1	23.6 ± 0.2	5.02 ±0.10
P2	70	21.4 ± 0.1	0.95 ± 0.05	19.6 ± 0.8	15.7 ± 0.1	3.32 ±0.02
P3	62	21.5 ± 0.3	1.22 ± 0.02	21.6 ± 0.2	13.3 ± 0.3	2.53 ±0.06
T1	80	21.1 ± 0.2	0.87 ± 0.01	19.8 ± 0.1	11.9 ± 0.2	2.02 ±0.04
T2	70	21.0 ± 0.2	0.80 ± 0.02	19.7 ± 0.2	11.3 ± 0.2	2.01 ±0.02
T3	62	21.8 ± 0.3	1.10 ± 0.01	20.6 ± 1.5	5.1 ± 0.4	0.86 ±0.01

[a]Young's modulus (E) calculated for the linear response until 2 % elongation.

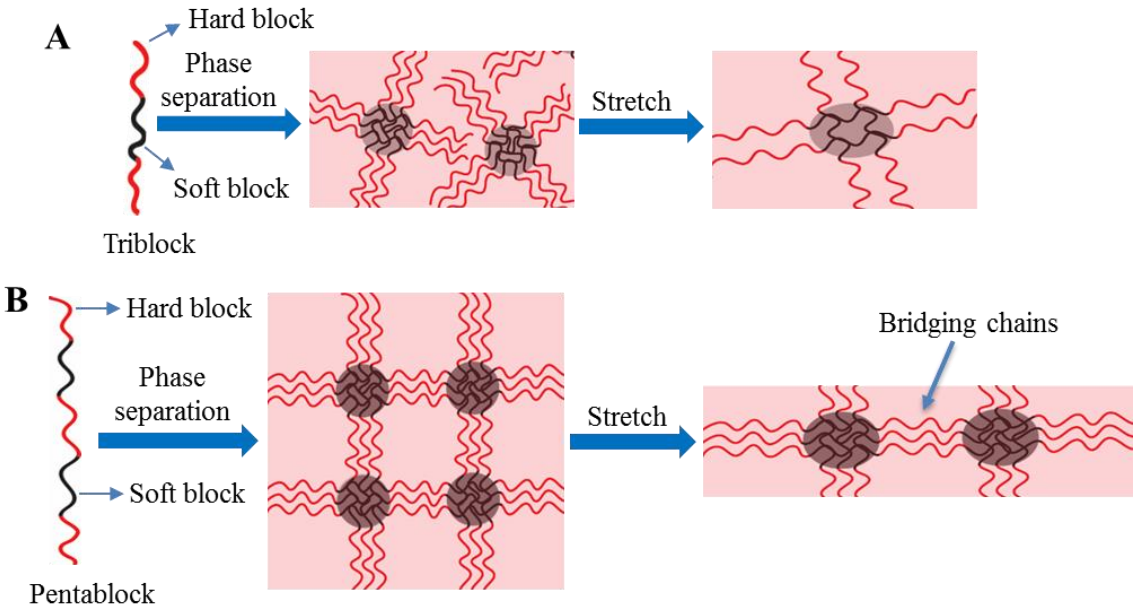

Figure 2.8 Schematic illustration of microphase separation and chain entanglement in (A) triblock and (B) pentablock copolymers.

Block Copolymer Architectures. In general, the pentablock copolymers are tougher bioplastics than the corresponding triblock with equivalent segment length of each block, and the toughness increases with the higher number of bridging chains. It is well established that the microphase separated polymeric architecture plays an important role in mechanical properties. In the case of pentablock copolymers, when a film is stretched as illustrated in Figure 2.8, the stress can be transferred by the bridging chains from one polynorbornene domain to its neighbors and prevent the crack propagation entirely within the rosin-based matrix. In contrast, there is no rosin based bridging chain in triblock copolymers to transfer the stress, leading to break at lower strain. The stress transfer seems to be easier in ordered morphology, for example, **P1** and **P2** shows the better mechanical properties where stress transferred from microphase separated polynorbornene domains through the bridging rosin-based matrix. On the other hand, **T1** and **T2** show poorly ordered morphology, where polynorbornene domain is surrounded by glassy rosin matrix, making them less tough thermoplastics.

2.4 Conclusions

In summary, our study demonstrated that bulky rosin-containing tri- and pentablock copolymers with low dispersity can be prepared by ROMP with one-pot sequential monomer addition. Pentablock copolymers were compared against homopolymers and triblock copolymers with comparable rosin content. Rosin-based homopolymers below the chain entanglement molecular weight are brittle, whereas the tri- and pentablock copolymers are tough thermoplastic, even though their rosin-containing block has much lower molecular weight than M_e. Pentablock copolymers showed remarkable toughening properties compared to the tri- and homopolymers, primarily because the presence of the

rosin-based middle block bridges between its neighbors of minority polynorbornene domains, thus preventing the easy crack propagation in the rosin-based matrix. This study provides a strategy to innovate biomass-containing sustainable polymers with superior performance via control of macromolecular architectures.

2.5 Experimental Section

Materials. Dehydroabietic acid (DHAA, ~90%) was obtained from Wuzhou Chemicals, China. Lithium aluminum hydride (95%, Acros-Organic), exo-5-norbornenecarboxylic acid (97%, Aldrich), trimethylacetic anhydride (99%, Aldrich), 4-dimethylaminopyridine (DMAP, 99%, Aldrich), and Grubbs-II catalyst ((1,3-Bis(2,4,6-trimethylphenyl)-2-imidazolidinylidene) dichloro(phenylmethylene)(tricyclohexyl phosphine) ruthenium) (97%, Aldrich) were used as received. Norbornene (99%, Aldrich) was purified by distillation before used. Tetrahydrofuran (THF) and dichloromethane (DCM) were dried over drying columns. Grubbs III catalyst (Dichloro[1,3-bis(2,4,6-trimethylphenyl)-2-imidazolidinylidene](benzylidene)bis-pyridine ruthenium(II)) was synthesized from Grubbs II catalyst following a procedure in literature and purified by recrystallization.[55] Rosin-containing norbornene monomer (**M**) was prepared according to our previously reported method.[51]

Molecular Characterization. The purity of monomer (Figure 2.9), polymer conversion and the block copolymer compositions were monitored by proton nuclear magnetic resonance (^{1}H NMR) spectroscopy using Bruker Avance III HD 300 spectrometer. Spectra were recorded in deuterated chloroform (99.96 atom % D) solvent in ppm (δ) relative to tetramethylsilane as an internal standard. Molecular weight and Molecular weight distribution of polymers were measured by gel permeation chromatography (GPC) in THF

equipped with a Waters 1525 Binary Pump, three Styragel columns and a Waters 2414 Refractive Index (RI) detector. HPLC grade THF solvent was used as eluent at 35 °C with a flow rate of 1.0 mL/min. A series of narrow dispersed polystyrene standards obtained from Polymer Laboratories were used to calibrate the GPC system. GPC samples were prepared by dissolving the polymer in HPLC grade THF at a concentration of 2-5 mg/mL and filtered by PTFE micro-filters with an average pore size of 0.2 μm.

Thermal Properties Characterization. The thermal transition temperature of polymer samples was determined by using TA Q2000 Differential scanning calorimetry (DSC) instrument. Samples with a mass of 5-10 mg were loaded into hermetically sealed aluminum DSC pans, first heated to 200 ^{o}C, cooled it down to -50 ^{o}C, then reheated to 200 ^{o}C at a rate of 10 ^{o}C/min with a nitrogen gas flow rate of 50 mL/min. The glass transition temperature (T_g) of samples was obtained from the midpoint of the transitions in the third heating cycle. The thermal degradation properties (Figure 2.13) were measured by thermogravimetric analysis (TGA) using TA Instruments Q5000 TGA system. The samples with a mass of 6-10 mg was used for this measurement. The sample was heated from room temperature to 150 °C at a rate of 10 °C/min under nitrogen and kept at 150 °C for 5 min then cooled it back to room temperature and reheated to 800 °C at the same rate.

Mechanical Properties Characterization. Tensile stress and strain of polymer samples was conducted using an Instron 5543A testing instrument. The films were prepared by solution casting method, dissolving 750 mg of polymer in dry HPLC grade THF, centrifugation at 5000 rpm to remove any particles and casting the solution of the polymer in a PTFE mold. After the slow evaporation of solvent in THF solvent chamber, the film was dried under vacuum for 18 hours at room temperature, 12 hours at 50 °C under nitrogen

and 12 hours at 50 °C under vacuum. A punch was used to cut the dog bone shape films with a width of 5 mm and a length of 22 mm were tested at room temperature. The dried samples were tested with the crosshead speed of 5 mm/min for plastics. Young's modulus was measured from the linear portion of the stress-strain curve. Toughness was calculated from the area under the stress-strain curve. The average and standard deviation of at least three specimens for each sample was reported here.

Morphological Characterization. The bulk films with and without thermal annealing were used for SAXS measurement. The films were annealed at 140 ^{o}C under nitrogen atmosphere for 3-6 h. The polymer films are still soluble, and the molecular weight distribution is not changed significantly when it is annealed for shorter time however for longer time annealing it might be crosslinked.

Small-Angle-X-ray Scattering (SAXS). The transmission experiments of free-standing, bulk films (thickness ~ 0.20-0.28 mm) were conducted using a SAXSLab Ganesha at the South Carolina SAXS Collaborative. A Xenocs GeniX3D microfocus source and a Cu target were used to generate a monochromic beam with a 0.154 nm wavelength. A Pilatus 300 K detector (Dectris) was used to collect the two-dimensional (2D) scattering patterns. 2D images were azimuthaly integrated to one-dimensional (1D) data of intensity (I) versus q (momentum transfer) where $q = 4\pi\lambda^{-1} \sin\theta$ with a total scattering angle of 2θ. The instrument was calibrated using National Institute of Standards and Technology (NIST) reference material, 640c silicon powder with the peak position at $2\theta=28.44^{\circ}$ where 2θ is the total scattering angle. The data were collected for 1 hr with an incident X-ray flux of ~1.5 M photons/s and a 1,050 mm sample-to-detector distance.

Preparation of Thin Films. Thin films were prepared by spin coating from a 2 wt% toluene solution of block copolymers onto oxidized silicon wafer (100 nm thick thermal oxide) at 2000 rpm. The silicon wafers were cleaned using acetone water mixture then isopropyl alcohol or ethanol and dried in oven, before spin coating the silicon wafer were further cleaned by plasma cleaning. The thin films were annealed at room temperature for 24 hours under THF solvent chamber.

Atomic force microscopy (AFM). AFM was accomplished using a Multimode Nanoscope V system (Bruker, Santa Barbara, CA). Tapping mode AFM was used to map the topography by tapping the surface using an oscillating tip. The measurements were achieved using commercial Si cantilevers with a nominal spring constant and resonance frequency at 20–80 N m^{-1} and 230–410 kHz, respectively (TESP, Bruker AFM Probes, Santa Barbara, CA). The spacing was calculated from the power spectral density using the Bruker software.

Synthesis of Homopolymers. Homopolymers were synthesized by following the previously reported procedure.[51] Homopolymers (**H2**) was synthesized with a ratio of monomer to G3 catalyst at 250:1. Grubbs III catalyst (2.15 mg, 2.96 μmol, 1 equiv) was dissolved in 2.0 mL of anhydrous DCM in a round-bottom flask under nitrogen. The monomer **M** (300 mg, 0.74 mmol, 250 equiv) was dissolved in 6 mL of anhydrous DCM. The monomer was transferred to the catalyst solution via cannula under vigorous stirring. The reaction was allowed to stir at room temperature (usually 1 h) until the polymerization was complete. After confirming the complete conversion using ^{1}H NMR, the reaction was quenched with 1 mL of ethyl vinyl ether (EVE). The product mixture was concentrated

using rotavap and precipitated into methanol twice. The white color product was vacuum-dried to obtain the pure polymer.

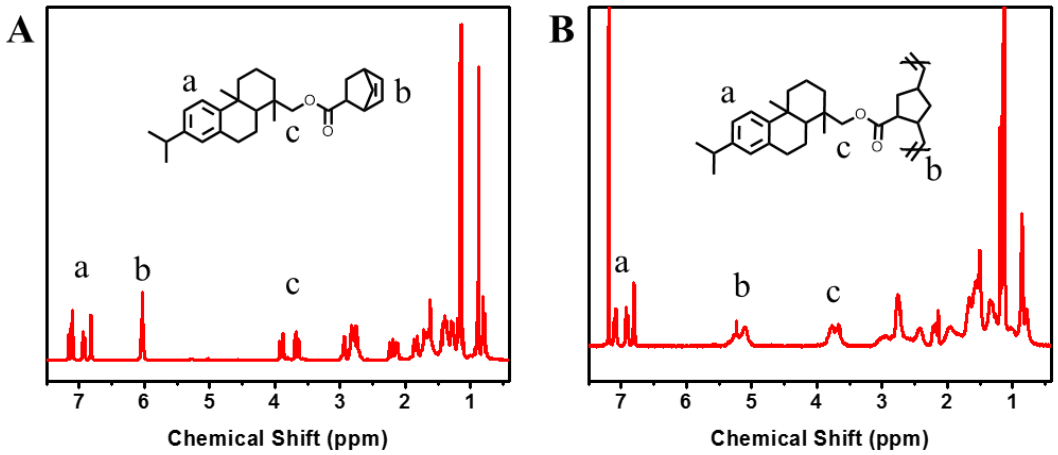

Figure 2.9 ^{1}H NMR spectra of (A) Monomer (**M**); (B) Homopolymer.

Synthesis of Triblock Copolymers. Triblock copolymers were synthesized by one pot sequential monomer addition. First block was made by following the same procedure to homopolymers except quenching. Sequential monomer addition was used before quenching the reaction. In the case of **T1**, Grubbs III catalyst (4.10 mg, 5.64 µmol, 1 equiv) was dissolved in dry DCM under nitrogen. Then monomer **M** (300 mg, 0.74 mmol, 131 equiv) in dry DCM (6 mL) was transferred to the catalyst very quickly and stirred at room temperature until the reaction was fully completed. After one hour, an aliquot sample was taken for GPC and ^{1}H NMR analysis. Then the second monomer (Norbornene, 152.83 mg) was dissolved in 3 mL dry DCM and added into the reaction flask via syringe. The reaction was allowed to continue for chain extension until the second monomer was fully polymerized. To monitor the progress of polymerization, another aliquot of sample was taken for GPC and ^{1}H NMR analysis (Figure 2.10). Similarly, the third block was also made using **M** (300 mg). When the polymerization was complete, the reaction was

quenched with 2 mL of ethyl vinyl ether and stirred for another 10 min. For GPC analysis, an aliquot of sample was taken. The crude product was precipitated in cold methanol twice and white color product was dried under high vacuum. Following the same procedure, a series of different molecular weight triblock copolymers were synthesized.

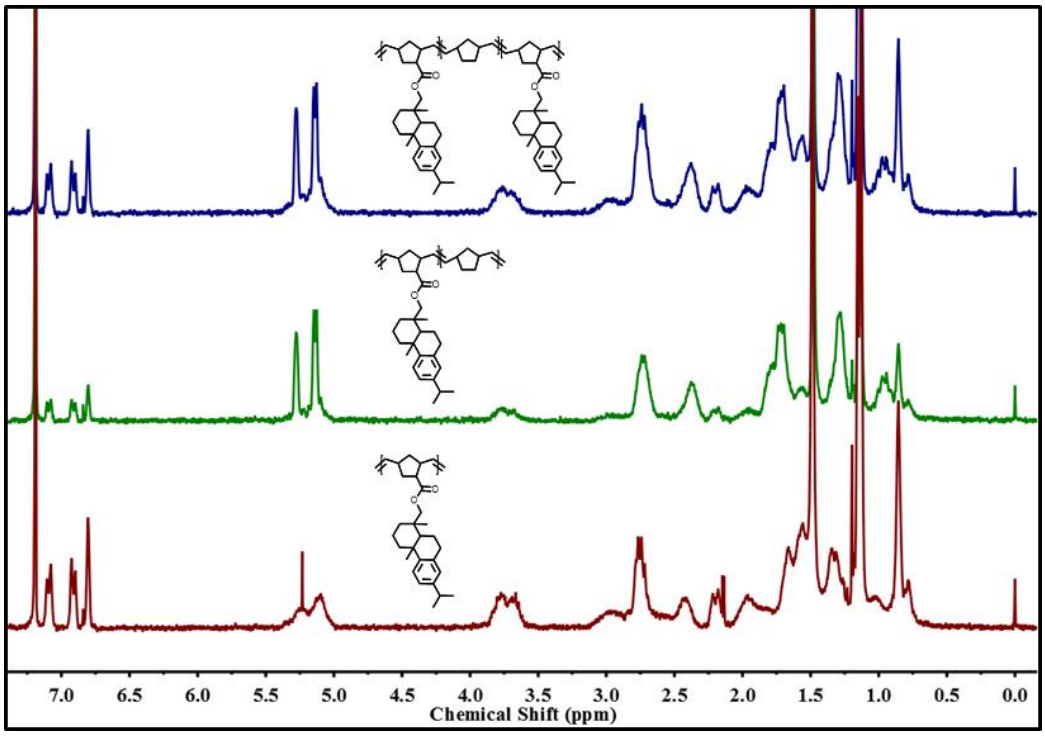

Figure 2.10 ^{1}H NMR spectra of polymers from each step in synthesis of triblock copolymers.

Synthesis of Pentablock Copolymers. Following the same procedure of ROMP to triblock preparation, pentablock copolymers were synthesized by sequential addition of monomers. Reaction was continued after the addition of third block, and desired amount of fourth monomer (Norbornene) was added into the reaction mixture. In the case of **P1**, Grubbs III catalyst (4.10 mg, 5.64 μmol, 1 equiv) was dissolved in dry DCM under nitrogen. Then monomer **M** (300 mg, 0.74 mmol, 131 equiv) in dry DCM (6 mL) was transferred to the catalyst very quickly and stirred at room temperature until the reaction was fully completed. After one hour, an aliquot sample was taken for GPC and ^{1}H NMR analysis.

Then the second monomer (Norbornene, 113.21 mg) was dissolved in 2 mL dry DCM and added into the reaction flask via syringe. The reaction was allowed to continue for chain extension until the second monomer was fully polymerized. To measure the progress of polymerization, another aliquot of sample was taken for GPC and ^{1}H NMR analysis. Similarly, the sequential addition of **M**, Norbornene and **M** respectively produced pentablock copolymers. An aliquot of sample was taken after completion of every steps and measured the molecular weight by GPC. When the polymerization was complete, the reaction was quenched with 3 mL of ethyl vinyl ether and stirred another 20 min. The crude reaction mixture was precipitated in cold methanol twice and white color product was dried under high vacuum. Following the same procedure, a series of different molecular weight pentablock copolymers were synthesized.

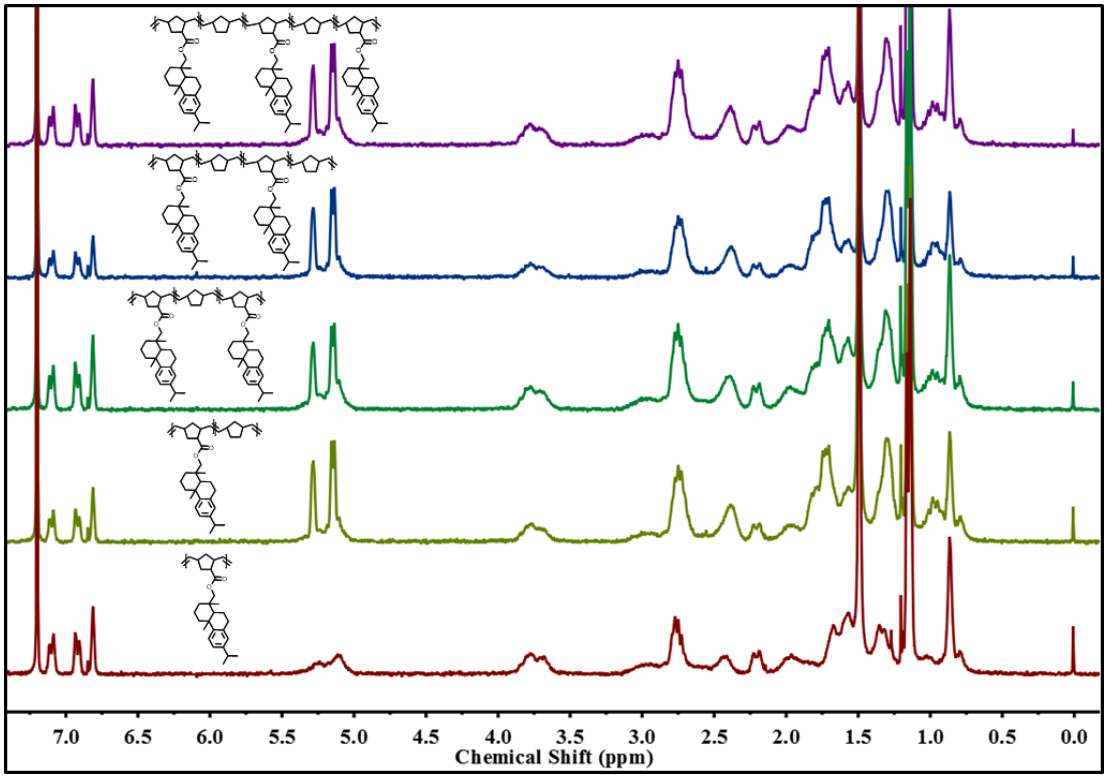

Figure 2.11 ^{1}H NMR spectra of polymers from each step in synthesis of pentablock copolymers.

Additional Figures and Tables

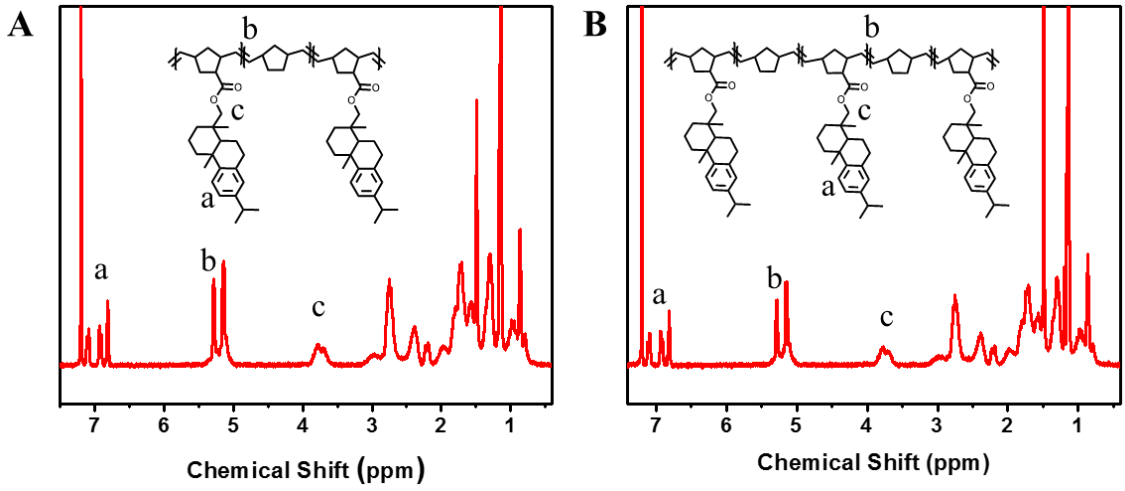

Figure 2.12 ^{1}H NMR spectra of (A) Triblock copolymer; (B) Pentablock copolymers.

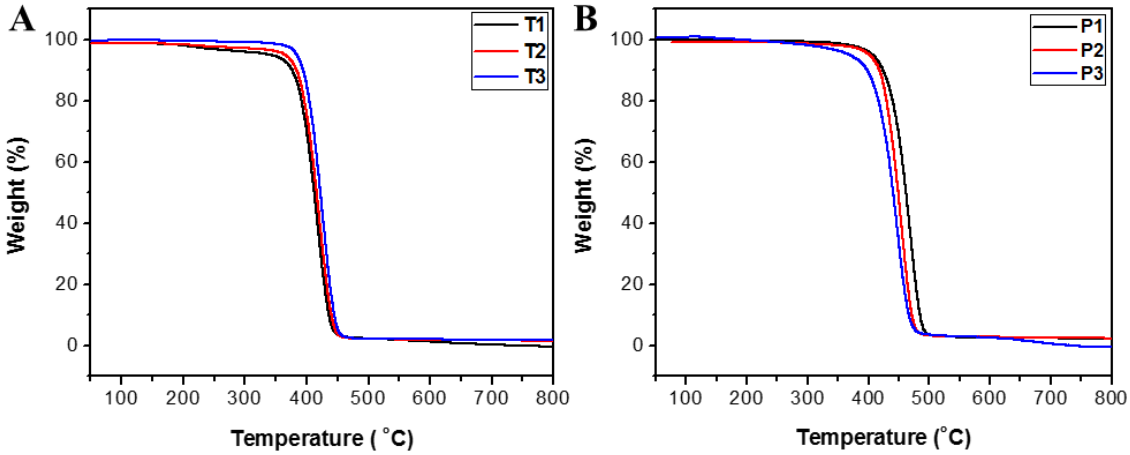

Figure 1.13 TGA curves of (A) Triblock copolymers **T1**, **T2**, and **T3**; and (B) Pentablock copolymers **P1**, **P2**, and **P3**.

Table 2.3 SAXS results of all tri and pentablock copolymers.

Polymer	f_{Rosin} (Theo)	q^* (nm^{-1})	D ($2\pi/q^*$) (nm)	q_1 (nm^{-1})	q / q^*
T1	0.78	0.15	42	0.30	1, 2
T2	0.68	0.14	45	0.28	1, 2
T3	0.63	0.13	48	0.26	1, 2
P1	0.78	0.11	57	0.22	1, 2
P2	0.68	0.11	57	0.22	1, 2
P3	0.63	0.09	70	0.17	1, 2

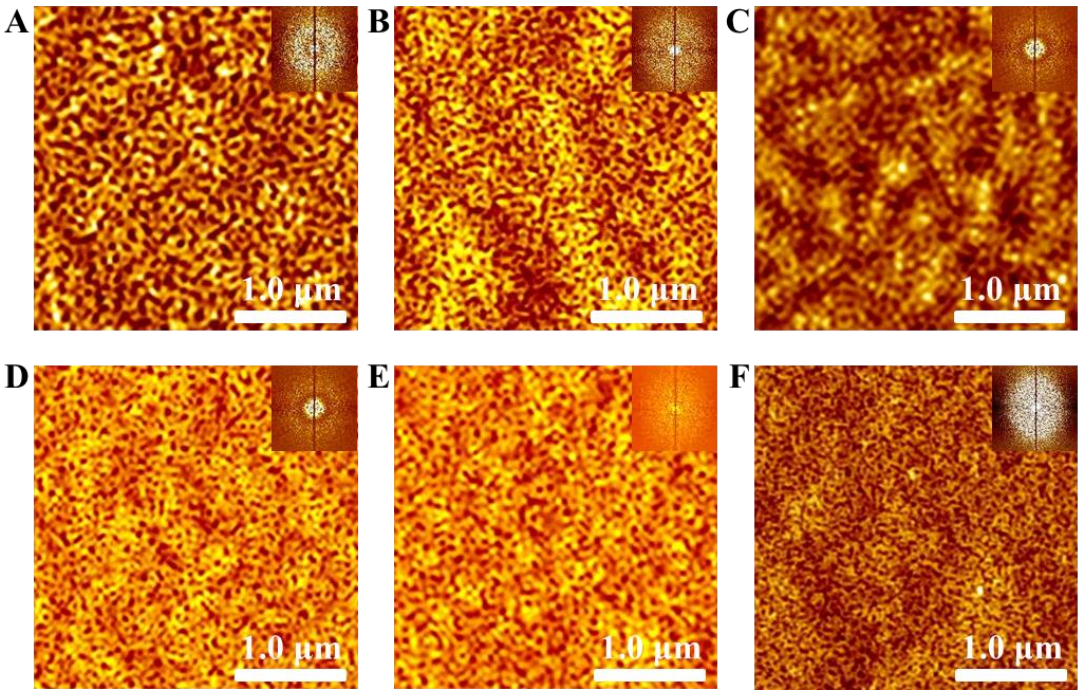

Figure 2.14 AFM height images of thin films of (A) **P1;** (B) **P2;** (C) **P3;** (D) **T1;** (E) **T2;** (F) **T3** prepared immediately after spin coating. FFTs of each image are shown in the insets.

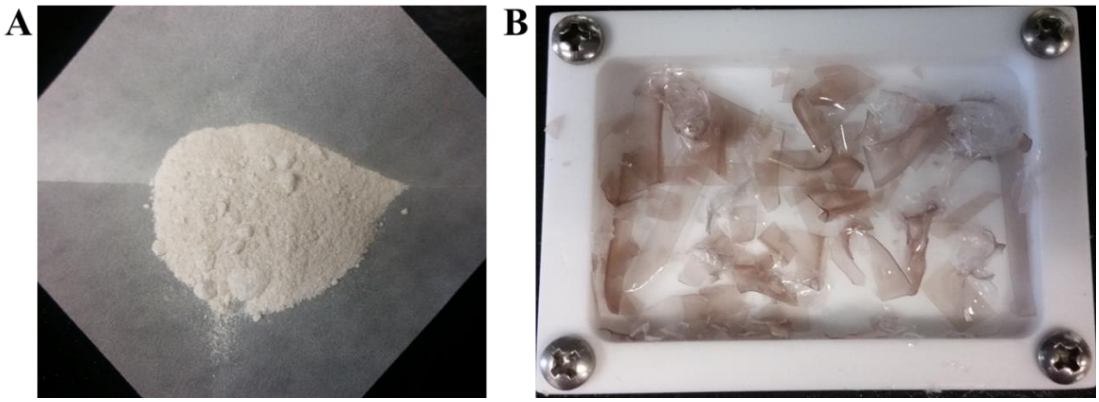

Figure 2.15 Images of H1 polymer: (A) powder and (B) brittle films.

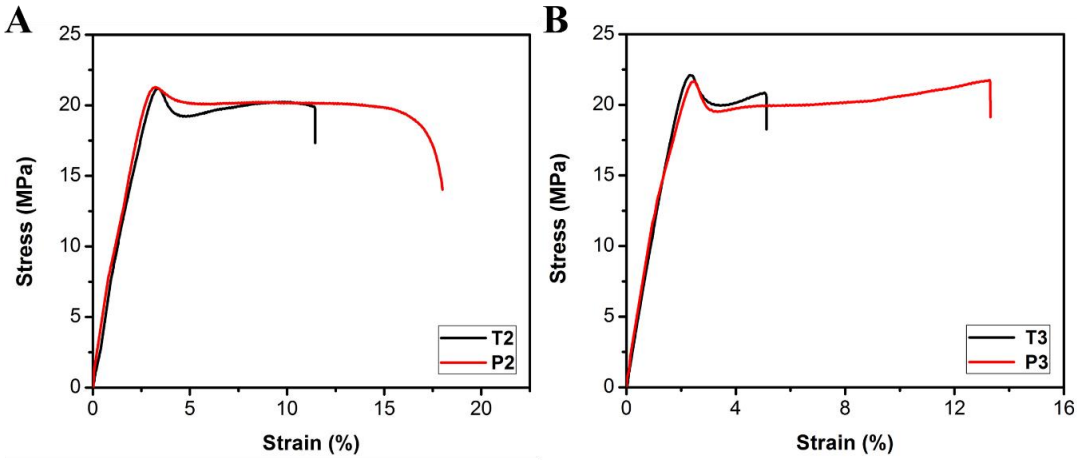

Figure 2.16 Uniaxial stress-strain curves for the (A) **T2** and **P2;** (B) **T3** and **P3**.

2.6 References

1. Gandini, A.; Lacerda, T. M.; Carvalho, A. J. F.; Trovatti, E. Progress of Polymers from Renewable Resources: Furans, Vegetable Oils, and Polysaccharides. *Chemical Reviews* **2016,** *116*, 1637-1669.
2. Zhu, Y.; Romain, C.; Williams, C. K. Sustainable polymers from renewable resources. Nature 2016, 540, 354-362.
3. Miller, S. A. Sustainable polymers: replacing polymers derived from fossil fuels. *Polymer Chemistry* **2014,** *5*, 3117-3118.

4. Biermann, U.; Bornscheuer, U.; Meier, M. A. R.; Metzger, J. O.; Schäfer, H. J. Oils and Fats as Renewable Raw Materials in Chemistry. Angew. Chem. Int. Ed. 2011, 50, 3854-3871.
5. Yao, K.; Tang, C. Controlled Polymerization of Next-Generation Renewable Monomers and Beyond. *Macromolecules* **2013,** *46*, 1689-1712.
6. Mathers, R. T. How well can renewable resources mimic commodity monomers and polymers? *Journal of Polymer Science Part A: Polymer Chemistry* **2012,** *50*, 1-15.
7. Mülhaupt, R. Green Polymer Chemistry and Bio-based Plastics: Dreams and Reality. *Macromolecular Chemistry and Physics* **2013,** *214*, 159-174.
8. Tuck, C. O.; Pérez, E.; Horváth, I. T.; Sheldon, R. A.; Poliakoff, M. Valorization of Biomass: Deriving More Value from Waste. *Science* **2012,** *337*, 695.
9. Moon, R. J.; Martini, A.; Nairn, J.; Simonsen, J.; Youngblood, J. Cellulose nanomaterials review: structure, properties and nanocomposites. *Chemical Society Reviews* **2011,** *40*, 3941-3994.
10. Habibi, Y.; Lucia, L. A.; Rojas, O. J. Cellulose Nanocrystals: Chemistry, Self-Assembly, and Applications. *Chem. Rev.* **2010,** *110*, 3479.
11. Chung, H.; Washburn, N. R. Chemistry of Lignin-based Materials. *Green Mater.* **2013,** *1*, 137.
12. Wang, J.; Yao, K.; Korich, A. L.; Li, S.; Ma, S.; Ploehn, H. J.; Iovine, P. M.; Wang, C.; Chu, F.; Tang, C. Combining Renewable Gum Rosin And Lignin: Towards Hydrophobic Polymer Composites by Controlled Polymerization. *J. Polym. Sci., Part A: Polym. Chem.* **2011,** *49*, 3728.
13. Isikgor, F. H.; Becer, C. R. Lignocellulosic biomass: a sustainable platform for the production of bio-based chemicals and polymers. *Polymer Chemistry* **2015,** *6*, 4497-4559.
14. Wilbon, P. A.; Chu, F.; Tang, C. Progress in Renewable Polymers from Natural Terpenes, Terpenoids, and Rosin. *Macromol. Rapid Commun.* **2013,** *34*, 8-37.
15. Ding, C.; Matharu, A. S. Recent Developments on Biobased Curing Agents: A Review of Their Preparation and Use. *ACS Sustainable Chemistry & Engineering* **2014,** *2*, 2217-2236.
16. Winnacker, M.; Rieger, B. Recent Progress in Sustainable Polymers Obtained from

Cyclic Terpenes: Synthesis, Properties, and Application Potential. *ChemSusChem* **2015,** *8*, 2455-2471.

17. Zheng, Y.; Yao, K.; Lee, J.; Chandler, D.; Wang, J.; Wang, C.; Chu, F.; Tang, C. Well-Defined Renewable Polymers Derived from Gum Rosin. *Macromolecules* **2010,** *43*, 5922-5924.
18. Wang, J.; Yu, J.; Liu, Y.; Chen, Y.; Wang, C.; Tang, C.; Chu, F. Synthesis and characterization of a novel rosin-based monomer: free-radical polymerization and epoxy curing. *Green Materials* **2013,** *1*, 105-113.
19. Wang, J.; Yuan, L.; Wang, Z.; Rahman, M. A.; Huang, Y.; Zhu, T.; Wang, R.; Cheng, J.; Wang, C.; Chu, F.; Tang, C. Photoinduced Metal-Free Atom Transfer Radical Polymerization of Biomass-Based Monomers. *Macromolecules* **2016,** *49*, 7709-7717.
20. Wilbon, P. A.; Zheng, Y.; Yao, K.; Tang, C. Renewable Rosin Acid-Degradable Caprolactone Block Copolymers by Atom Transfer Radical Polymerization and Ring-Opening Polymerization. *Macromolecules* **2010,** *43*, 8747-8754.
21. Yu, J.; Liu, Y.; Liu, X.; Wang, C.; Wang, J.; Chu, F.; Tang, C. Integration of renewable cellulose and rosin towards sustainable copolymers by "grafting from" ATRP. *Green Chemistry* **2014,** *16*, 1854-1864.
22. Yao, K.; Wang, J.; Zhang, W.; Lee, J. S.; Wang, C.; Chu, F.; He, X.; Tang, C. Degradable Rosin-Ester–Caprolactone Graft Copolymers. *Biomacromolecules* **2011,** *12*, 2171-2177.
23. Wilbon, P.; Gulledge, A. L.; Benicewicz, B. C.; Tang, C. Renewable Rosin Fatty Acid Polyesters: The Effect of Backbone Structure on Thermal Properties. *Green Mater.* **2013,** *1*, 96.
24. Fetters, L. J.; Lohse, D. J.; Richter, D.; Witten, T. A.; Zirkel, A. Connection between Polymer Molecular Weight, Density, Chain Dimensions, and Melt Viscoelastic Properties. *Macromolecules* **1994,** *27*, 4639-4647.
25. Fetters, L. J.; Lohse, D. J.; Milner, S. T.; Graessley, W. W. Packing Length Influence in Linear Polymer Melts on the Entanglement, Critical, and Reptation Molecular Weights. *Macromolecules* **1999,** *32*, 6847-6851.
26. Creton, C.; Brown, H. R.; Deline, V. R. Influence of Chain Entanglement on the Failure Modes in Block Copolymer Toughened Interfaces. *Macromolecules* **1994,** *27*, 1774-

1780.

27. Kramer, E. J.; Berger, L. L., Fundamental processes of craze growth and fracture. In *Crazing in Polymers Vol. 2*, Kausch, H. H., Ed. Springer Berlin Heidelberg: Berlin, Heidelberg, **1990**; pp 1-68.
28. Ruzette, A.-V.; Leibler, L. Block copolymers in tomorrow's plastics. *Nat Mater* **2005,** *4*, 19-31.
29. Bates, F. S.; Hillmyer, M. A.; Lodge, T. P.; Bates, C. M.; Delaney, K. T.; Fredrickson, G. H. Multiblock Polymers: Panacea or Pandora's Box? *Science* **2012,** *336*, 434-440.
30. Holmberg, A. L.; Reno, K. H.; Wool, R. P.; Epps, I. I. I. T. H. Biobased building blocks for the rational design of renewable block polymers. *Soft Matter* **2014,** *10*, 7405-7424.
31. Koo, C. M.; Wu, L.; Lim, L. S.; Mahanthappa, M. K.; Hillmyer, M. A.; Bates, F. S. Microstructure and Mechanical Properties of Semicrystalline−Rubbery−Semicrystalline Triblock Copolymers. *Macromolecules* **2005,** *38*, 6090-6098.
32. Xiong, M.; Schneiderman, D. K.; Bates, F. S.; Hillmyer, M. A.; Zhang, K. Scalable production of mechanically tunable block polymers from sugar. *Proceedings of the National Academy of Sciences* **2014,** *111*, 8357-8362.
33. Wang, S.; Vajjala Kesava, S.; Gomez, E. D.; Robertson, M. L. Sustainable Thermoplastic Elastomers Derived from Fatty Acids. *Macromolecules* **2013,** *46*, 7202-7212.
34. Hillmyer, M. A.; Tolman, W. B. Aliphatic Polyester Block Polymers: Renewable, Degradable, and Sustainable. *Accounts of Chemical Research* **2014,** *47*, 2390-2396.
35. Shin, J.; Martello, M. T.; Shrestha, M.; Wissinger, J. E.; Tolman, W. B.; Hillmyer, M. A. Pressure-Sensitive Adhesives from Renewable Triblock Copolymers. *Macromolecules* **2011,** *44*, 87-94.
36. Shin, J.; Lee, Y.; Tolman, W. B.; Hillmyer, M. A. Thermoplastic Elastomers Derived from Menthide and Tulipalin A. *Biomacromolecules* **2012,** *13*, 3833-3840.
37. Jacobsen, S.; Fritz, H. G. Plasticizing polylactide—the effect of different plasticizers on the mechanical properties. *Polymer Engineering & Science* **1999,** *39*, 1303-1310.
38. Anderson, K. S.; Lim, S. H.; Hillmyer, M. A. Toughening of polylactide by melt blending with linear low-density polyethylene. *J. Appl. Polym. Sci.* **2003,** *89*, 3757.

39. Thurber, C. M.; Xu, Y.; Myers, J. C.; Lodge, T. P.; Macosko, C. W. Accelerating Reactive Compatibilization of PE/PLA Blends by an Interfacially Localized Catalyst. *ACS Macro Lett.* **2015,** *4*, 30.
40. Xu, Y.; Loi, J.; Delgado, P.; Topolkaraev, V.; McEneany, R. J.; Macosko, C. W.; Hillmyer, M. A. Reactive Compatibilization of Polylactide/Polypropylene Blends. *Ind. Eng. Chem. Res.* **2015,** *54*, 6108.
41. Zhang, J.; Li, T.; Mannion, A. M.; Schneiderman, D. K.; Hillmyer, M. A.; Bates, F. S. Tough and Sustainable Graft Block Copolymer Thermoplastics. *ACS Macro Letters* **2016,** *5*, 407-412.
42. Ryu, C. Y.; Ruokolainen, J.; Fredrickson, G. H.; Kramer, E. J.; Hahn, S. F. Chain Architecture Effects on Deformation and Fracture of Block Copolymers with Unentangled Matrices. *Macromolecules* **2002,** *35*, 2157-2166.
43. Khanna, V.; Ruokolainen, J.; Kramer, E. J.; Hahn, S. F. Deformation and Fracture of Lamellar and Cylindrical Block Copolymers with Unentangled Glassy Matrices: Effect of Chain Architecture and Microdomain Orientation. *Macromolecules* **2006,** *39*, 4480-4492.
44. Bishop, J. P.; Register, R. A. Thermoplastic Elastomers with Composite Crystalline−Glassy Hard Domains and Single-Phase Melts. *Macromolecules* **2010,** *43*, 4954-4960.
45. Burns, A. B.; Register, R. A. Thermoplastic Elastomers via Combined Crystallization and Vitrification from Homogeneous Melts. *Macromolecules* **2016,** *49*, 269-279.
46. Mannion, A. M.; Bates, F. S.; Macosko, C. W. Synthesis and Rheology of Branched Multiblock Polymers Based on Polylactide. *Macromolecules* **2016,** *49*, 4587-4598.
47. Panthani, T. R.; Bates, F. S. Crystallization and Mechanical Properties of Poly(l-lactide)-Based Rubbery/Semicrystalline Multiblock Copolymers. *Macromolecules* **2015,** *48*, 4529-4540.
48. Lin, J.-O.; Chen, W.; Shen, Z.; Ling, J. Homo- and Block Copolymerizations of ε-Decalactone with l-Lactide Catalyzed by Lanthanum Compounds. *Macromolecules* **2013,** *46*, 7769-7776.
49. Lee, I.; Panthani, T. R.; Bates, F. S. Sustainable Poly(lactide-b-butadiene) Multiblock Copolymers with Enhanced Mechanical Properties. *Macromolecules* **2013,** *46*, 7387-

7398.

50. Matsumiya, Y.; Watanabe, H.; Takano, A.; Takahashi, Y. Uniaxial Extensional Behavior of (SIS)p-Type Multiblock Copolymer Systems: Structural Origin of High Extensibility. *Macromolecules* **2013,** *46*, 2681-2695.
51. Ganewatta, M. S.; Ding, W.; Rahman, M. A.; Yuan, L.; Wang, Z.; Hamidi, N.; Robertson, M. L.; Tang, C. Biobased Plastics and Elastomers from Renewable Rosin via "Living" Ring-Opening Metathesis Polymerization. *Macromolecules* **2016,** *49*, 7155-7164.
52. Wang, X.; Dormidontova, E. E.; Lodge, T. P. The Order−Disorder Transition and the Disordered Micelle Regime for Poly(ethylenepropylene-b-dimethylsiloxane) Spheres. *Macromolecules* **2002,** *35*, 9687-9697.
53. Lokupitiya, H. N.; Jones, A.; Reid, B.; Guldin, S.; Stefik, M. Ordered Mesoporous to Macroporous Oxides with Tunable Isomorphic Architectures: Solution Criteria for Persistent Micelle Templates. *Chemistry of Materials* **2016,** *28*, 1653-1667.
54. Ye, C.; Takigawa, T.; Burtovvy, O.; Langsdorf, L.; Jablonski, D.; Bell, A.; Vogt, B. D. Impact of Nanostructure on Mechanical Properties of Norbornene-based Block Copolymers under Simulated Operating Conditions for Biobutanol Membranes. *ACS Applied Materials & Interfaces* **2015,** *7*, 11765-11774.
55. Sanford, M. S.; Love, J. A.; Grubbs, R. H. A Versatile Precursor for the Synthesis of New Ruthenium Olefin Metathesis Catalysts. *Organometallics* **2001,** *20*, 5314-5318.

CHAPTER 3

MACROMOLECULAR-CLUSTERED FACIAL AMPHIPHILIC ANTIMICROBIALS[2]

[2] Rahman, M. A.; Bam, M.; Luat, E.; Jui, M. S.; Ganewatta, M. S.; Shokfai, T.; Nagarkatti, M.; Decho, A. W.; Tang, C., Macromolecular-clustered facial amphiphilic antimicrobials. *Nature Communications* **2018**, *9* (1), 5231. Reprinted here with permission. Copyright (2018) Springer Nature.

3.1 Abstract

Bacterial infections and antibiotic resistance, particularly by Gram-negative pathogens, have become a global healthcare crisis. We report the design of a class of cationic antimicrobial polymers that cluster local facial amphiphilicity from repeating units to enhance interactions with bacterial membranes without requiring a globally conformational arrangement associated with highly unfavorable entropic loss. This concept of macromolecular architectures is demonstrated with a series of multicyclic natural product-based cationic polymers. We have shown that cholic acid derivatives with three charged head groups are more potent and selective than lithocholic and deoxycholic counterparts, particularly against Gram-negative bacteria. This is ascribed to the formation of true facial amphiphilicity with hydrophilic ion groups oriented on one face and hydrophobic multicyclic hydrocarbon structures on the opposite face. Such local facial amphiphilicity is clustered via a flexible macromolecular backbone in a concerted way when in contact with bacterial membranes.

3.2 Introduction

Antimicrobial resistance is an ever-increasing threat to public health, and is projected to be accountable for more deaths than cancer and AIDS combined by 2050.[1, 2] The effective treatments for bacterial infections are becoming radically diminished as bacteria develop resistance against most available antibiotics.[3] Among these multidrug-resistant (MDR) pathogens, Gram-negative bacteria pose more perilous threats to human life.[4] Most infections caused by Gram-negative MDR bacteria are essentially untreatable, and may lead to severe illness or even death.[4, 5] Despite this fact, the development of new

antimicrobial therapies has been primarily focused on Gram-positive bacteria.[6, 7] The presence of dual membranes in Gram-negative bacteria acts as an impermeable barrier to most antibiotics. As a result, there arises an urgent need for new-generation antimicrobials with potent therapeutic activity, novel modes of action, and without driving the current increase of antimicrobial resistance, especially to combat the growing epidemic of infections caused by MDR pathogens.

Natural antimicrobial peptides (AMPs) are amphiphilic, combining cationic charges and hydrophobic components, and able to electrostatically bind to anionic bacterial membranes or other anionic targets.[8, 9, 10, 11, 12, 13] It is well known that in many cases, AMPs form an α-helix structure with positive charges arrayed on one side and lipophilic groups aligned along the other side in contact with bacterial membranes (Figure 3.1a).[14, 15, 16] The common structural features of these AMPs with a global segregation of cationic and lipophilic side chains are also referred to as facial amphiphilicity (i.e. separate hydrophilic and hydrophobic faces).[16, 17] Facial amphiphilicity allows AMPs to efficiently insert into bacterial membranes via the barrel-stave pore, toroidal pore, disordered toroidal pore and/or carpet mechanisms, leading to cytoplasmic leakage, membrane depolarization, lysis, and cell death.[18, 19] Over the last two decades, natural AMP-mimicking peptide derivatives such as β-peptides and peptoids have been developed with potent antimicrobial activity.[20, 21, 22, 23] However, the clinical applications of AMPs are very limited due to their low bioavailability, low stability, high manufacturing cost, as well as in many cases nonspecific toxicity to mammalian cells.[7, 13, 19, 24] To address these issues, synthetic polymers with cationic charges, which mimic natural AMPs and selectively attack negative bacterial cell membranes over zwitterionic mammalian cell membranes, have been studied widely

as a promising solution to combat bacteria. These polymers offer a broad spectrum of antimicrobial activity, a membrane disruption mechanism as well as a low propensity for developing resistance.[13, 18, 25, 26] In addition, cationic charge-containing polymers can be obtained in large quantities at much lower cost. Many antimicrobial polymers are highly effective in killing traditional strains. We have developed several antimicrobial macromolecules utilizing bulky hydrophobic structures containing natural resin acids and antibiotic-metal bioconjugates that exhibit excellent activities against bacteria, particularly against Gram-positive bacteria such as methicillin-resistant *Staphylococcus aureus* (MRSA), while simultaneously exhibiting low hemolysis against red blood cells and minimal *in vitro* and *in vivo* cytotoxicity.[27, 28, 29, 30, 31, 32, 33, 34, 35]

However, most antimicrobial polymers with AMP-mimicking designs are based on the adoption of a conformation that is globally amphiphilic, which requires control on the sequence of hydrophobic and hydrophilic subunits. Gellman and coworkers stated that the facial amphiphilicity could be achieved from random copolymerization of hydrophobic and hydrophilic monomers that did not require control of subunit sequences.[16, 36, 37] Their copolymers contained both cationic and lipophilic groups as well as sufficiently flexible backbones that could form a globally amphiphilic, but conformationally irregular helical structure induced by negatively charged bacterial membranes (Figure 3.1b). DeGrado, Kuroda and coworkers also synthesized methacrylate-based copolymers consisting of flexible backbones and amphiphilic compositions with low toxicity and good antimicrobial activity.[38, 39] Tew et al. synthesized amphiphilic cationic polymers that also exhibited good antimicrobial activity, where they used amphiphilic monomers (i.e., containing both a hydrophilic ammonium and a hydrophobic norbornene on the same polymerizable unit).[40,

[41] However, most of these approaches rely on uncontrolled polymeric self-aggregation to achieve global facial amphiphilicity, which is difficult to manipulate. From the perspective of free energy change upon the contact with bacterial cell membranes, the fact of adopting a facial amphiphilic conformation without the helical structures from random coil structures of synthetic polymers would suffer a very high entropic penalty from a whole macromolecule (Figure 3.1b).

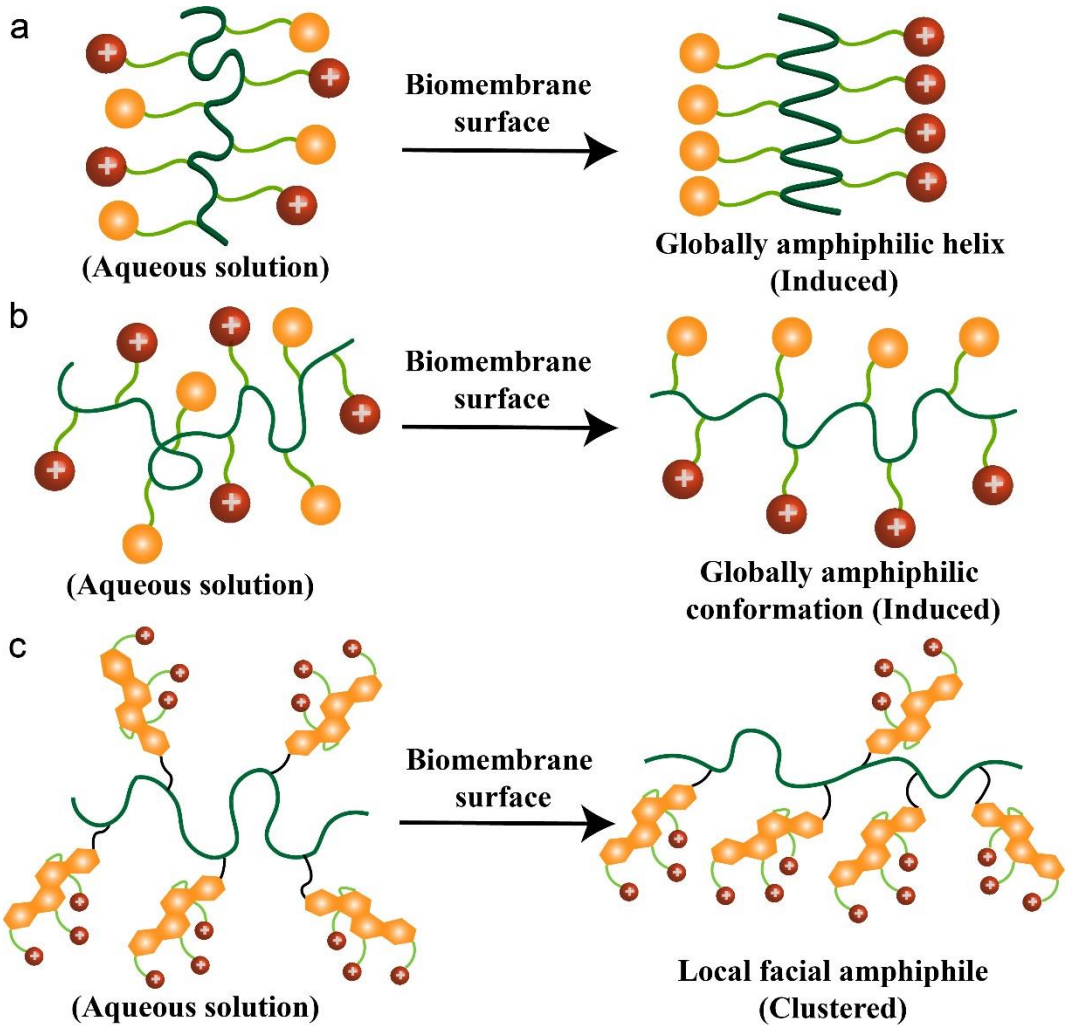

Figure 3.1 Modes of action adopt upon approaching to a biomembrane surface; **a** Host-defense peptides adopting a globally amphiphilic helical conformation;[36] **b** Synthetic antimicrobial polymers adopting a globally amphiphilic conformation; and **c** A flexible macromolecular chain clustering intrinsic local facial amphiphiles (this work). Red color: Cationic/hydrophilic groups, yellow color: hydrophobic groups.

In fact, most antimicrobial polymers do not comprise truly facial amphiphilicity and suffer poor selectivity and high cytotoxicity against mammalian cells and are also ineffective against MDR Gram-negative bacteria. We hypothesized that a flexible macromolecule carrying intrinsic facial amphiphilic units with a large cross-sectional area would offer a novel type of antimicrobial polymer, in which each local unit could exert an insertable handle upon contact with bacterial membranes. The polymeric backbone not only avoids adopting a highly energetic, global amphiphilicity, but also assembles the intrinsic local facial amphiphilic structures on cell membranes. The macromolecular structures would significantly increase the density of local facial amphiphilicity and thus enhance the overall interactions with bacterial cells. To test this hypothesis, we chose multicyclic natural products, e.g. steroid acids or terpenoids, as a functionalized building block to possess local facial amphiphilicity.

Bile acids are cholesterol-derived amphiphilic steroid acids produced in mammals and other vertebrates. They have been utilized in many areas including drug delivery, sensors, polymeric gels, antimicrobials and other biological applications.[35, 42, 43, 44] There are four different derivatives of bile acids, which vary by the number of hydroxyl groups, such as cholic acid (CA), deoxycholic acid (DCA), chenodeoxycholic acid and lithocholic acid (LCA) (Figure 3.9a**)**. Hydroxyl groups of bile acid molecules are positioned in the concave α-face while the multicyclic hydrocarbon structure is constituted as the convex β-face, thereby providing the potential to achieve true facial amphiphilicity (Figure 3.2). The steroidal nucleus with four fused rings provides a hydrophobic core with a significantly larger cross-sectional area compared to linear alkyl chains. The facial amphiphilicity,

biocompatibility, and hydrophobicity of bile acid derivatives are considered highly favorable for interactions with bacterial cell membranes.

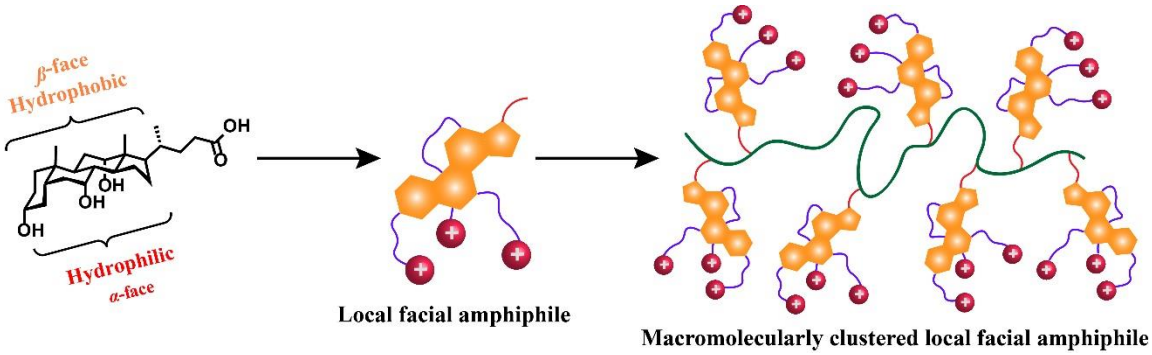

Figure 3.2 Design principle of cationic polymers with an intrinsic facial amphiphilic structure at repeat units. The key building block should have a multicyclic structure with the possibility for derivatization to possess one face hydrophilic and the other face hydrophobic. Cholic acid is illustrated as an example here.

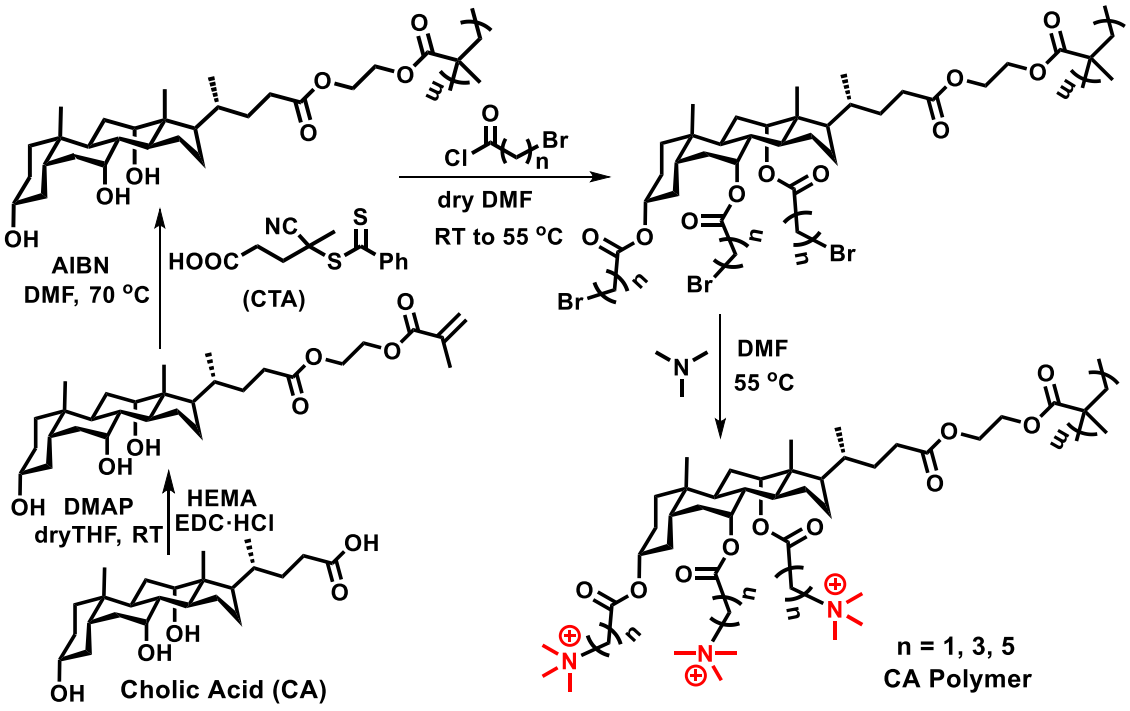

Figure 3.3 Synthesis of cholic acid-containing polymers.

Herein we report the synthesis of cationic bile acid-based polymers that possess intrinsic local facial amphiphilicity clustered together via a flexible macromolecular chain (Figure 3.2). The presence of hydroxyl groups from the α-face allows the installation of cationic quaternary ammonium charges (QAC) as hydrophilic components. The carboxylic acid at the edge of this particular structure offers chemical functionalization for attachment as a pendant monomeric unit integrated into a flexible macromolecular skeleton. Three different bile acid derivatives, lithocholic, deoxycholic, and cholic acid are constructed with one, two, and three QAC respectively, as cationic head groups via the hydroxyl functionality. This provides a unique avenue for tuning amphiphilicity and testing the level of facial amphiphilicity.

3.3 Results and Discussion

Synthesis of Cationic Multicyclic Natural Product-Derived Polymers.

A class of cationic polymers was synthesized from bile acid derivatives in four steps. Methacrylate monomers of cholic acid, (2-methacryloyloxy)ethyl cholate (MAECA), deoxycholic acid, (2-methacryloyloxy)ethyl deoxycholate (MAEDA), and lithocholic acid, (2-methacryloyloxy)ethyl lithocholate (MAELA) were synthesized by simple esterification coupling reactions of respective bile acid and hydroxyethyl methacrylate (HEMA) at room temperature.[45] The reaction scheme in Figure 2.3 illustrates the synthesis using cholic acid as an example. Each monomer of MAECA, MAEDA, and MAELA was then polymerized via reversible addition fragmentation transfer (RAFT) polymerization utilizing 4-cyano-4-(thiobenzylthio)pentanoic acid as a chain transfer agent. Molecular weight of all three bile acid-containing polymers was controlled with low dispersity as determined by Gel Permeation Chromatography (GPC). Hydroxyl groups of these

homopolymers were further modified through an esterification reaction with bromoalkanoyl chloride. After post modification, the peaks next to the alcohol group in ^{1}H NMR at ~ 3.2 to 3.8 ppm shifted to 4.7 to 5.2 ppm (Figure 3.10a). The methylene group next to the bromine group appears at ~ 3.4 to 3.6 ppm, indicating the formation of an ester linkage. The disappearance of a broad peak at 3500-3600 cm^{-1} corresponding to hydroxyl groups and appearance of a higher intensity peak at 1720 cm^{-1} in FTIR spectra (Figure 3.10b) for the ester group further confirmed the post-polymerization modification of hydroxyl groups in homopolymers. Evidence of successful post-polymerization modification was also established by the slight shift of GPC traces of polymers before and after modification (Figure 3.10c). Finally, the bromine groups were substituted by trimethylamine to offer quaternary ammonium-containing polymers. The appearance of an intense peak at ~ 3.0 ppm for three methyl and one methylene group in ^{1}H NMR spectra confirmed the formation of quaternary ammonium-containing polymers (Figure 3.10a). Finally, cationic homopolymers with single, double, and triple QAC head groups were obtained from lithocholic acid, deoxycholic acid, and cholic acid respectively (Figure 3.4).

Cholic acid-based cationic polymers having a series of molecular weight were further prepared to study the effect of molecular weight on antimicrobial activity (Table 3.2). The spacer length of methylene (one, three and five) between QAC and the ester group was also investigated in order to examine its effect on antimicrobial efficacy, for which polymers with similar molecular weight were used for post-polymerization modification. Polymers were denoted according to their respective derivative resource, molecular weight and spacer unit (i. e. CA_19k_5 is a cholic acid polymer with molecular weight of 19, 000 g mol^{-1} and a spacer of five methylene). To compare the antimicrobial activity with

polymers, a three QAC-containing cholic acid-based monomer (labeled as CA_Monomer) was also prepared, shown in Figure 3.9b. The experimental details are given in the supplementary information.

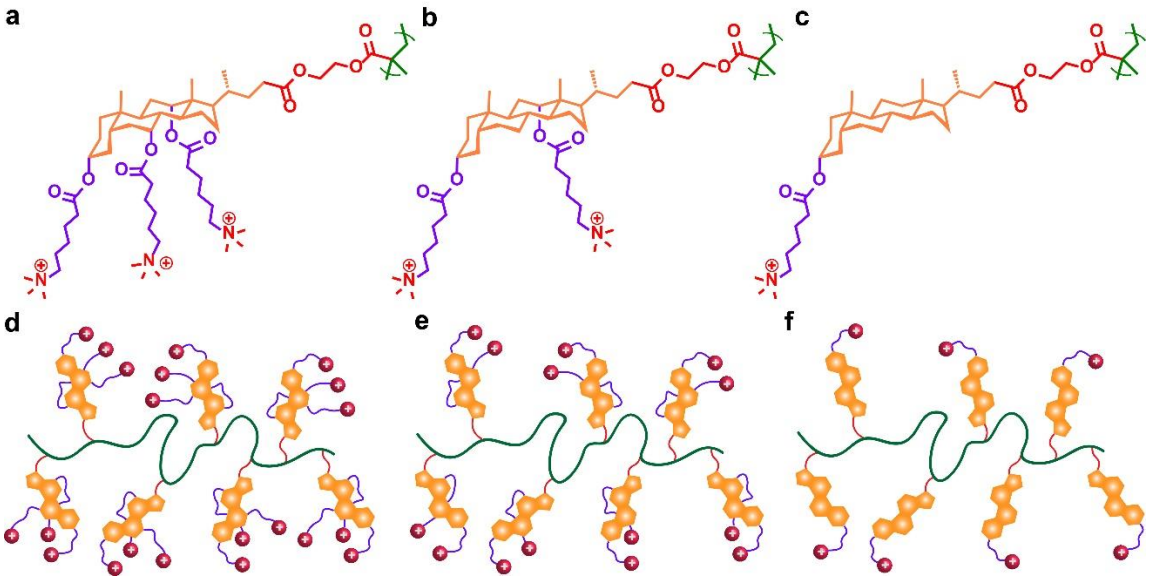

Figure 3.4 Multicyclic natural product-based cationic polymer structures and their illustration; **a** and **d** CA polymer, **b** and **e** DCA polymer, **c** and **f** LCA polymer.

Antimicrobial Activities.

The antimicrobial activities of multicyclic natural product-based cationic polymers were evaluated against clinically-relevant Gram-positive bacteria *S. aureus* and Gram-negative bacteria *E. coli* and *P. aeruginosa*. Initially, the antimicrobial activity of three different bile acid polymers with a spacer of five methylene and molecular weight ~ 19,000 g mol^{-1} was evaluated by standard agar disc diffusion assay. The observation of clear inhibition zones indicated that all three polymers have potent activity against both Gram-negative and Gram-positive bacteria at different levels. Among them cholic acid polymers are most effective, and lithocholic acid ones are the least (Figure 3.16). Interestingly, the

initial studies also revealed that all these polymers had higher efficacies towards Gram-negative bacteria than Gram-positive pathogens.

We then determined the minimum inhibitory concentration (MIC) of polymers by a broth microdilution method and compared the killing efficiency of each bile acid polymer. The MIC results (Table 3.1) demonstrated that the cholic acid-based polymer (CA_19k_5) exhibited more potent antimicrobial activity, with significantly lower MICs in comparison to deoxycholic acid (DCA_19k_5) and lithocholic acid (LCA_20k_5) based polymers. A delicate balance of hydrophobicity and hydrophilicity is one of the essential factors for selective interactions with bacterial membranes. Since all bile acid-based cationic polymers contain the same hydrophobic four fused rings in each repeating unit, the change in hydrophilicity is critical for the antimicrobial activities. The cholic acid-based polymer contains three QAC groups in each repeating unit, making it more hydrophilic with higher charge densities, whereas deoxycholic acid and lithocholic acid are less hydrophilic because of fewer charged groups. Consequently, deoxycholic acid-containing polymer DCA_19k_5 exhibited moderate sensitivity towards bacteria while LCA_20k_5 is least effective towards bacteria. Our results demonstrated that the higher charge densities of a polymer could lead to more significant interactions with bacterial membranes, similar to observations made by Yang and colleagues.[46, 47] Though all polymers can inhibit bacterial growth, they again exhibited enhanced potency towards Gram-negative bacteria. For example, the MICs of CA_19k_5 are 11.2 and 3.1 μg mL^{-1} against *E. coli* and *P. aeruginosa* respectively, whereas about 19.1 μg mL^{-1} against *S. aureus*. This is significant as there are few antibiotics available for the treatment of infections by Gram-negative bacteria, in particular, pathogenic *P. aeruginosa.*

Table 3.1 Antimicrobial activity of different multicyclic natural product-based cationic polymers by a broth microdilution method.

Polymers	Minimum Inhibitory Concentration (MIC)[a] (μg mL^{-1})				HC_{50} (μg mL^{-1})	Selectivity of *E. coli* (ATCC-11775) (HC_{50}/MIC)	Selectivity of *P. aeruginosa* (ATCC-10145) (HC_{50}/MIC)	Selectivity of *E. coli* (ATCC-BAA-197) (HC_{50}/MIC)
	E. coli (ATCC-11775)	*P. aeruginosa* (ATCC-10145)	*E. coli* (ATCC-BAA-197)	*S. aureus* (ATCC-33591)				
CA_19k_5	11.2	3.1	11.5	19.1	>306	>27	>98	>26
DCA_19k_5	11.5	6.4	20.4	24.6	>37	>3	>5	1
LCA_20k_5	11.4	3.4	20.5	56.8	NT	NT	NT	NT
Effect of the spacer length on antimicrobial activity of cholic acid-based cationic polymers								
CA_19k_5	11.2	3.1	11.5	19.1	>306	>27	>98	>26
CA_19k_3	12.5	10.4	12.4	19.6	>31	>2	3	2
CA_19k_1	25.6	22.2	37.7	45.6	>8	NT	NT	NT
Effect of molecular weight on antimicrobial activity of cholic acid-based cationic polymers								
CA_10k_5	6.4	3.0	6.8	15.3	>110	>17	>37	>16
CA_19k_5	11.2	3.1	11.5	19.1	>306	>27	>98	>26
CA_25k_5	11.4	10.5	11.9	19.1	>315	>28	>30	>26
CA_32k_5	12.2	19.4	14.5	27.4	>1886	>154	>97	130
CA_Monomer	22.3	12.8	22.5	25.6	NT	NT	NT	NT

NT = Not tested. [a]MIC is the lowest polymer concentration that completely inhibits bacterial growth.

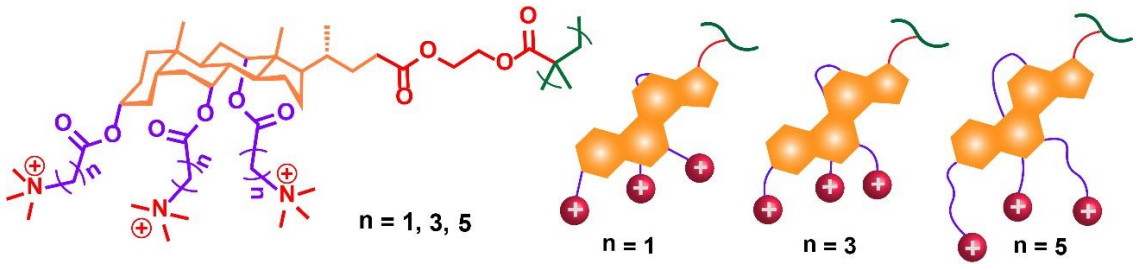

Figure 3.5 Cholic acid-based cationic polymers with different spacers.

We further studied the effect of methylene spacers in cholic acid-based polymers on antimicrobial activity (Figure 3.5). We observed that polymers containing a longer spacer showed more potent killing efficacy compared to those with shorter spacers. As shown in Table 3.1, CA_19k_5 polymer (5 methylene units separated from the cationic charge) exhibited higher antimicrobial activity against both Gram-positive and Gram-negative bacteria than CA_19k_3 and CA_19k_1. According to the snorkeling effect in peptides,[48, 49, 50] a longer spacer unit could provide increased hydrophobicity, and the additional distance between the QAC groups and the hydrophobic multicyclic ring attached to the polymer backbone would facilitate a deeper insertion of the polymer chain into the bacterial membrane. In contrast, a shorter spacer has less flexibility and room for extending the charge group through the membrane.[51] A longer spacer could not only facilitate the charge group easier to reach a target substrate (here cell membrane), but provide a flexible anchoring on surfaces without requiring a configurational change of the bulky tri-terpene structure.

Next, we explored the effect of molecular weight (M_n) of polymers on the antimicrobial activity (Table 3.1). In case of *P. aeruginosa*, the MICs of higher molecular weight polymers increased. For *E. coli*, the molecular weight at the test range has a minimal effect on the activity. In case of Gram-positive bacteria, *S. aureus*, the lower molecular weight polymer CA_10k_5 exhibited a MIC of ~ 15.3 μg mL^{-1}, whereas the MIC for CA_32k_5 was at 27.4 μg mL^{-1}. These results indicated that CA polymer with ~10, 000 g mol^{-1} molecular weight exhibited better efficacy than the higher molecular weight polymers. This could be explained by the potential trapping of higher molecular weight polymers in the dense, outmost peptidoglycan layer of *S. aureus*. This observation is

consistent with the sieving effect, as also identified by Lienkamp et al.[52] We also evaluated the antimicrobial activity of a cationic cholic acid based monomer (CA_Monomer, Table 3.1), which is lower than that of polymers. This might be due to the increase of the density of local facial amphiphilicity from polycations than monomers, which was similarly observed by many other groups on different systems.[53]

Antimicrobial activity was further investigated using a clinically isolated MDR strain of *E. coli* (ATCC-BAA-197). As shown in Table 3.1, all cholic acid polymers containing a five-methylene spacer inhibited the growth of this strain, and with low MIC values (7- 15 μg mL^{-1}), demonstrating a high efficacy against MDR *E. coli*. These MIC values increased with polymers containing the shorter spacer unit. However, the MIC values are comparatively higher than those for regular strains of *E. coli* (ATCC-11775), which is possibly due to varying phospholipid compositions. It is worth noting that the cholic acid polymers with a molecular weight in the range of 10, 000 – 20, 000 g mol^{-1} is also more efficient at inhibiting bacterial growth than those with higher molecular weight.

To evaluate the possible bacterial resistance of cholic acid-based polymers, we performed an antimicrobial resistance study for one of the most potent polymers, CA_19k_5, against *P. aeruginosa* and *E. coli*. Bacteria were exposed multiple times to the polymer at a sub-MIC level, and the MIC was measured for every consecutive passage. Detailed experimental procedures are provided in the supplementary information. After ten passages, no significant changes in the MIC values were observed, as detailed in Figure 3.6. This important result demonstrated that developing resistance against cholic acid-based cationic polymers is inherently difficult for both *P. aeruginosa* and *E.coli* bacterial strains.

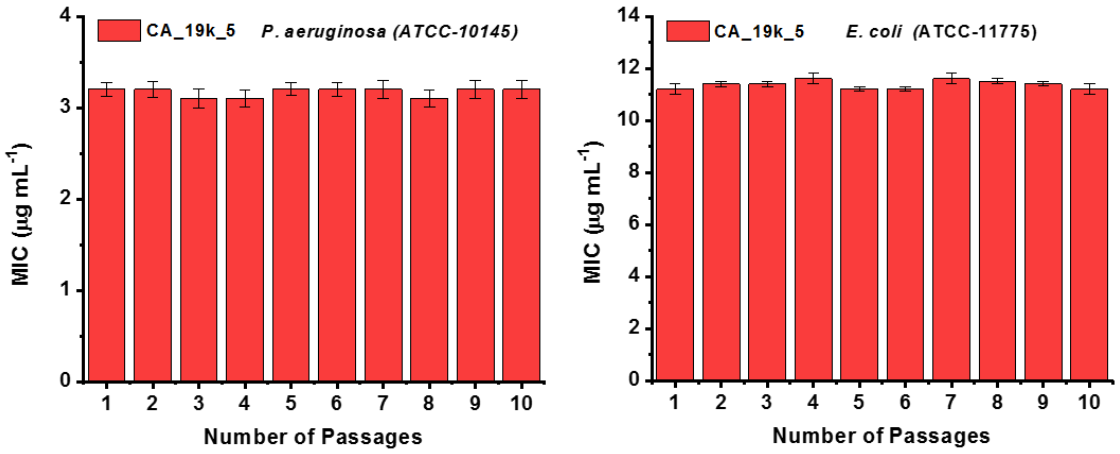

Figure 3.6 Drug resistance study of CA_19k_5 against *P. aeruginosa* and *E. coli* upon multiple sublethal dose treatment. The Data are collected from the three replicates and the error bars represent the s.d. of three replicates.

Hemolytic Activities.

The toxicity of bile acid-derived cationic polymers was evaluated by measuring hemoglobin release from mouse red blood cells (RBCs) at various concentrations. The selectivity for bacterial cells over mammalian cells was determined by the ratio of HC_{50} (the concentration of a polymer that causes 50% hemolysis of RBCs) to MIC values (HC_{50}/MIC). As mentioned previously, the hydrophobic and hydrophilic balance of an antimicrobial polymer plays a critical role for the selective attachment to a bacterial cell membrane. It is well established that a polymer with higher hydrophobicity or lower hydrophilicity produces hemolysis to a greater extent, due to the strong interaction with the lipid portion of a mammalian cell membrane.[25, 47, 54]As shown in Table 3.1, all cholic acid polymers exhibited negligible hemolysis at their respective MIC values, demonstrating excellent selectivity toward a broad range of pathogenic microbes over mammalian cells.

Bile acid derivatives are intrinsically hydrophobic due to the presence of a four fused-ring structure. All cholic acid polymers contain three positive head groups in each repeat unit, which reduces hydrophobicity. In contrast, the deoxycholic acid-based polymer

possesses only two positive charged head groups in each repeat unit, making it more hydrophobic with a substantial level of toxicity. The hemolysis activity of lithocholic acid-based cationic polymers was not determined due to poor solubility in water. Additionally, the molecular weight of polymers was also found to have some effect on hemolysis activity (Table 3.1). We observed that HC_{50} increased with the increase of molecular weight of cholic acid-based polymers. The length of spacers also has an enormous impact on hemolysis, as shown in Table 3.1. We observed that the cholic acid polymers containing shorter spacers (CA_19k_1 and CA_19k_3) are more toxic compared to the longer spacer containing polymer (CA_19k_5). There are many parameters to influence the hemolytic activity, especially the balance of hydrophilicity and hydrophobicity. The low HC_{50} value for CA_19k_1 might be related with insufficient electrostatic interactions due to the short spacer linking cationic charges, which could amplify the hydrophobic effect by cholic acid on the more hydrophobic nature of membranes from mammalian cells.

Mechanisms of Action.

To elucidate the mode of action of bile acid-derived polymers against bacteria, we performed confocal laser scanning microscopy (CLSM) to investigate the membrane permeability changes before and after treatment with CA_19k_5 polymer using a LIVE/DEAD BacLight assay kit. The concentration of polymers is two times that of the MIC value. As shown in Figure 3.7, green colored cells were observed for control bacteria (*E. coli* and *P. aeruginosa*), revealing most cells live with intact bacterial membranes. In contrast, when the bacteria were treated with polymer CA_19k_5, most cells were killed. These findings revealed that the antimicrobial activity of bile acid-based cationic polymers occurred by the disruption of bacterial membrane, consistent with the membrane lytic

mechanism of various synthetic antimicrobial polymers.[28, 39, 46, 55] In case of *S. aureus*, these polymers are less effective (Figure 3.17). The antimicrobial mechanism of action was further investigated through the observation of morphological changes of bacterial cells after CA_19k_5 polymer treatment using scanning electron microscopy (SEM). Bacteria *E. coli* and *P. aeruginosa* under control remained intact with smooth surfaces as shown in Figure 3.7, whereas polymer-treated cells were significantly damaged and highly distorted from the original morphology. Most bacterial cells were shown to be significantly fragmented. The significant physical damage of cell membranes was observed for *S. aureus* only when the concentration of polymers was increased to four times that of the MIC value (Figure 3.18). The loss of original morphology with cell membrane damage was more apparent in the case of Gram-negative bacteria compared to that of Gram-positive bacteria.

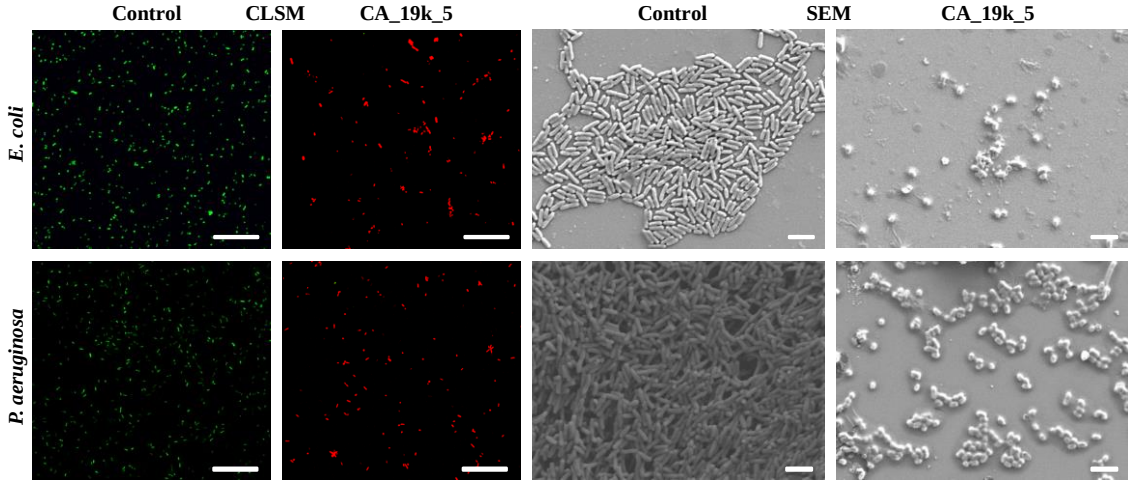

Figure 3.7 CLSM and SEM images of *E. coli* and *P. aeruginosa* under control and CA_19k_5 treatment with two times of MIC concentration. Bacteria concentrations were 1.0×10^6 CFU/mL. Bacterial solutions without CA_19k_5 were used as the control. Scale bar in confocal images is 25 μm and scale bar in SEM images is 2 μm.

Discussion.

Bile acid derivatives (mostly small molecules) have been developed as antimicrobial agents. Moore et al. at reported that cationic bile salts share some structural features with an antibiotic squalamine isolated from sharks.[56] Diamond et al. prepared a family of head-to-tail cationic lipids that combine cholic acid and spermine, which showed enhanced antimicrobial activity related to increased hydrophobicity, although no facial amphiphilicity was explored.[57] Savage and co-workers claimed that membrane-active facial amphiphilic cationic molecules, such as bile acid derivatives, could disrupt bacterial membranes.[58, 59] Cholic acid-derived cationic surfactants can form micellar structures that exhibit antimicrobial activity against Gram-positive and Gram-negative bacteria.[60] However, higher susceptibility to the resistance of these small molecules remains a significant issue.

In the current study, we developed a class of antimicrobial polymers from bile acids, which possess novel macromolecular conformations critical for interactions with bacterial membranes. We observed that cholic acid-based cationic polymers are more effective against Gram-negative bacteria, especially *P. aeruginosa*, than Gram-positive bacteria (e.g. *S. aureus*). Different from Gram-positive bacteria using peptidoglycan as the major periphery enveloping their cell membranes, Gram-negative bacteria possess double membranes with the outer membrane made up of zwitterionic phosphatidylethanolamine (PE) and other anionic phospholipids as their periphery for self-defense. Therefore, in Gram-negative bacteria it is more challenging for antimicrobial agents to balance their hydrophobicity and cationic charges as well as to adopt a conformation that is favorable for interactions with the outer membrane.

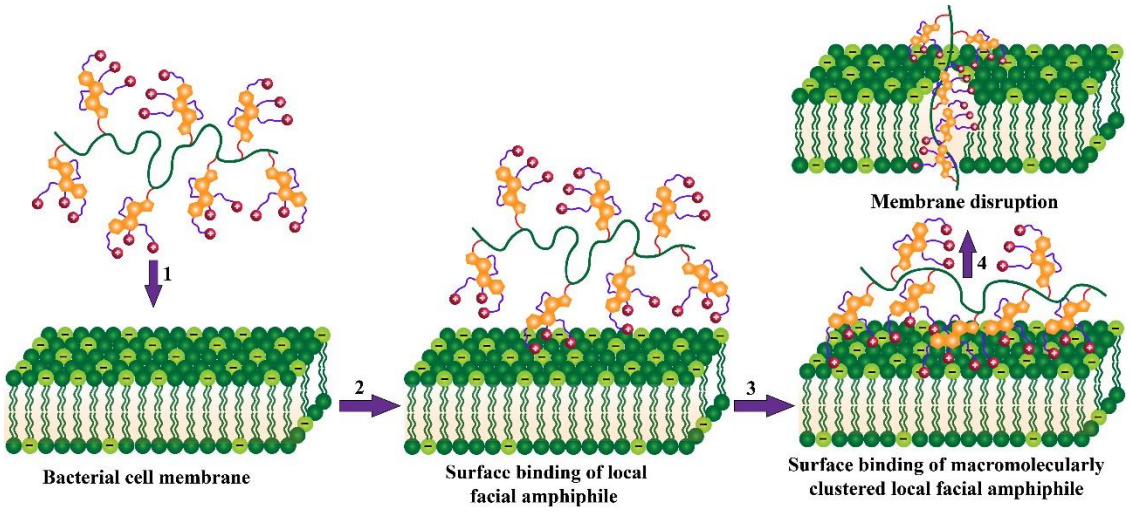

Figure 3.8 A proposed mechanism of action of cholic acid-based polymers on the bacterial cell membrane: **1** diffusion, **2** surface binding, **3** membrane insertion and **4** membrane disruption. The illustrated cholic acid can be replaced by other multicyclic compounds that are modified with facial amphiphilicity.

The hydrophobic multicyclic structure and three oriented cationic charges in the modified cholic acid provide true facial amphiphilicity in contact with bacterial cell membranes. Initially, three cationic charges on each cholic acid unit localize onto the outer membrane as a result of electrostatic interactions (Figure 3.8), then the hydrophobic face of cholic acid inserts into the membrane. Since each of this unique moiety is attached to a flexible macromolecular chain, collectively tens of (or even hundreds of) these local facial amphiphilic structures would facilitate each other and promote the entire macromolecule to penetrate through the membrane (Figure 3.8). Such a concerted penetration of macromolecular chains across the cell membrane would cause its destabilization and fragmentation, ultimately leading to cell death. With this design, there is no need for an entire macromolecule to adopt a globally entropy-unfavorable facial amphiphilic conformation. Conversely, Gram-positive bacteria, like *S. aureus*, have membranes primarily composed of anionic lipids such as phosphatidylglycerol (PG) and cardiolipin

(CL), which is overlain by a dense and thick peptidoglycan layer.[46] Bulky cholic acid-based polymers could be more easily trapped in this layer and thus less effective in disrupting these cell membranes.

3.4 Conclusions

In summary, we reported a design of antimicrobial polymers with repeat units possessing local facial amphiphilicity, which could promote effective interactions of an entire macromolecule with bacterial cell membranes, circumventing the adoption of an energetically-unfavorable global facial amphiphilicity. Specifically, we derivatized three different multicyclic natural products. Among them, cholic acid polymers were shown to be more efficient than their deoxycholic and lithocholic acid counterparts, regarding both antimicrobial activity and selectivity. This is ascribed to the true facial amphiphilic structure from cholic acid derivatives, which have the hydrophobic multicyclic structure as one face and three oriented hydrophilic cationic charges as the other face. It is worth noting that a lot of multicyclic natural and synthetic compounds could be used as the key building block. This macromolecular structure and conformation may open an avenue toward next-generation antimicrobial agents to treat multidrug-resistant Gram-negative bacteria.

3.5 Experimental Section

Materials. All chemicals were purchased from commercial sources and used as received unless otherwise stated. Cholic acid (CA, ≥98%), deoxycholic acid (DCA, ≥98%), lithocholic acid (LCA, ≥98%), 2-hydroxyethyl methacrylate (HEMA, 97%), and 4-dimethylamino pyridine (DMAP, 99%) were purchased from Sigma-Aldrich. 1-(3-dimethylaminopropyl)-3-ethyl carbodiimide hydrochloride (EDC·HCl, 98%) was purchased from TCI. 6-

Bromohexanoyl chloride (97%), 4-bromobutanoyl chloride (97%), bromoacetyl bromide (98%) and trimethylamine (33% w/w in ethanol denatured with 2% cyclohexane) was purchased from Alfa-Aesar. 4-Cyano-4-(thiobenzylthio)pentanoic acid (CTP, 97%) was purchased from Strem Chemicals Inc. Azobisisobutyronitrile (AIBN, Sigma, 98%) and solvents such as hexanes, anhydrous *N, N*-dimethylformamide (DMF, 99.9%), tetrahydrofuran (THF), dichloromethane (DCM), *etc.* were purified by standard procedures. $CDCl_3$ (99.9% D), D_2O (99.9% D) and DMSO-d_6 (99.9% D) were purchased from Cambridge Isotope Laboratories, Inc.

Characterization. The monomer and compound purity and polymer conversion were monitored by proton nuclear magnetic resonance 300 MHz (^{1}H NMR) spectroscopy using Bruker Avance III HD 300 spectrometer. Spectra were recorded in deuterated chloroform, Deuterium oxide or dimethylsulfoxide solvent in ppm (δ) with tetramethylsilane as an internal standard. Molecular weight and molecular weight distribution of polymers were measured by gel permeation chromatography (GPC) in THF equipped with a Waters 1525 Binary Pump, three Styragel columns, and a Waters 2414 Refractive Index (RI) detector. HPLC grade THF solvent was used as eluent at 35 °C with a flow rate of 1.0 mL min^{-1}. A series of narrowly-dispersed polystyrene standards obtained from Polymer Laboratories were used to calibrate the GPC system. GPC samples were prepared by dissolving polymers in HPLC grade THF at a concentration of 5-10 mg mL^{-1} and filtered by PTFE micro-filters with an average pore size of 0.2 μm.

Synthesis of Monomers. (2-methacryloyloxy)ethyl cholate (MAECA) monomer was synthesized via an esterification reaction between CA and 2-hydroxyethyl methacrylate (HEMA) in the presence of EDC·HCL and 4-dimethylamino pyridine (DMAP). Initially, CA (5.0 g, 12.24 mmol) and DMAP (0.16 g, 1.35 mmol) were dissolved in 40 mL of dry

tetrahydrofuran (THF) under nitrogen. 1-(3-dimethylaminopropyl)-3-ethyl carbodiimide hydrochloride (EDC·HCl) (2.58 g, 13.46 mmol) was added to the solution. After placing the reaction mixture in an ice bath, HEMA (1.75 g, 13.56 mmol) was added dropwise to the solution and then progressed for 48 h at room temperature. The reaction mixture was filtered and evaporated. The crude product was redissolved in dichloromethane (DCM) (60 mL) and washed with 5% HCl solution (25 mL × 1), saturated $NaHCO_3$ (25 mL × 3), water (25 mL × 2) and brine solution (25 mL × 2). After drying the organic layer over anhydrous $MgSO_4$, the solvent was removed by rotary evaporation. Silica column chromatography with hexane: ethyl acetate (7 : 3) as eluents was carried out to yield a product with a yield of 60%. ^{1}H NMR (Figure 3.10a) (300 MHz, $CDCl_3$, δ, ppm): 6.13 and 5.59 (2H, s, a), 4.33 (4H, m, b & b'), 3.96 (1H, t, c), 3.84 (1H, q, d), 3.45 (1H, m, e), 1.94 (3H, s, f), 0.97 (3H, d, g), 0.88 (3H, s, h) and 0.67 (3H, s, i). ES-MS (Figure 3.19): observed *m*/*z* for [M + Na^+] 543 and [M + H^+] 521.

(2-methacryloyloxy)ethyl deoxycholate (MAEDA) was synthesized according to a similar procedure to the synthesis of MAECA. ^{1}H NMR (Figure 3.11a) (300 MHz, $CDCl_3$, δ, ppm): 6.13 and 5.59 (2H, s, a), 4.33 (4H, m, b & b'), 3.97 (1H, t, c), 3.61 (1H, m, d), 1.94 (3H, s, e), 0.97 (3H, d, f), 0.88 (3H, s, h) and 0.67 (3H, s, g). ES-MS (Figure 3.20): observed *m*/*z* for [M + Na^+] 527 and [M + H^+] 505.

(2-methacryloyloxy)ethyl lithocholate (MAELA) was also synthesized according to a similar procedure to the synthesis of MAECA, except for the purification process. Silica column chromatography with hexane: ethyl acetate (3 : 2) as eluents was carried out to yield a product with a yield of 50%. ^{1}H NMR (Figure 3.11b) (300 MHz, $CDCl_3$, δ, ppm):

6.12 and 5.59 (2H, s, a), 4.33 (4H, m, b & b'), 3.61 (1H, m, c), 1.94 (3H, s, d), and 0.62 (3H, s, i). Direct-probe mass spectrum (Figure 3.21): observed *m*/*z* 488.

Synthesis of Bile Acid Polymers. Methacrylate monomers were polymerized using a typical RAFT polymerization technique.[45] For example, MAECA (0.70 g, 1.35 mmol), 4-Cyano-4-(thiobenzylthio)pentanoic acid (CTP) (6.27 mg, 0.0224 mmol), and azobisisobutyronitrile (AIBN) (0.74 mg, 4.487 µmol) were placed in a 10 mL Schlenk flask and dissolved in *N*, *N*-dimethylformamide (DMF) (2 mL). The mixture was performed with three freeze-pump-thaw cycles protected under nitrogen and immersed into a preheated oil bath set at 70 °C. After a certain period of time, the polymerization was quenched by exposure to air and cooling under an ice water bath. The reaction mixture was precipitated twice into a mixture of hexane and DCM (50 : 50) and finally dissolved in THF and precipitated into hexane. The polymer was dried under vacuum.

Synthesis of Bromoalkyl-Containing Bile Acid Polymers. CA polymer (300 mg) was placed in a 25 mL round bottom flask and dissolved in anhydrous DMF (3 mL). Excess 6-bromohexanoyl chloride (3 mL) or 4-bromobutanoyl chloride (3 mL) or bromoacetyl bromide (3 mL) was added to the polymer solution dropwise at room temperature. The reaction mixture was allowed to stir at 55 ºC for 48 hrs and precipitated into methanol. The product was redissolved in DCM (2 mL), precipitated in methanol twice, and dried under vacuum. The reaction was confirmed by ^{1}H NMR and FTIR. Similarly, DCA and LCA polymers were modified. ^{1}H NMR spectra of post-modified CA, DCA, LCA polymer with 6-bromohexanoyl chloride is shown in Figure 3.10a, Figure 3.11a and b respectively**.** FTIR spectra of modified CA, DCA, LCA polymers with 6-bromohexanoyl chloride are shown in Figure 3.10b, 3.12a and b respectively. ^{1}H NMR spectra of modified CA polymer

with 4-bromobutanoyl chloride and bromoacetyl bromide are shown in the Figure 3.13a and b, respectively**.**

Synthesis of QAC-Containing Polymers. As an example: 6-bromohexyl-modified CA polymer (300 mg) was dissolved in DMF (4 mL). Then, trimethylamine solution (33wt%, 9 mL) in ethanol was added to the reaction mixture and stirred for 24 hrs at 55 ^{o}C. After cooling and concentrating the reaction mixture, the resulting solution was precipitated in THF and centrifuged to collect the product. The product was washed with THF and dried under vacuum. Finally, the product was further purified by dialysis against DI water (1 L × 3) for 24 hrs. The solution in dialysis bag was collected and freeze-dried to obtain a white product. DCA and LCA polymers were similarly quaternized.

Synthesis of QAC-Containing CA Monomer. MAECA (0.50 g, 0.96 mmol), triethyl amine (2.91 g, 28.84 mmol), hydroquinone (0.19 mmol, 0.021 g) and catalytic DMAP (0.035 g, 0.29 mmol) were dissolved in dry THF (10 mL) under nitrogen. Then, 6-bromohexanoyl chloride (2.59 g, 14.42 mmol) was added dropwise to the mixture at 0 ^{o}C was then stirred at room temperature for 36 hrs. The reaction mixture was filtered and evaporated. The residue was diluted with DCM and washed with water (3 times), Saturated $NaHCO_3$ (3 times) and Brine solution (one times). The organic phase was dried over magnesium sulfate and concentrated, then precipitated in hexane twice to remove unreacted 6-bromohexanoyl chloride. The product was further purified by the silica column chromatography with hexane: ethyl acetate (1 : 4) as eluents to obtain a product with a yield of 55%. The yellow product was dried under vacuum. The reaction was confirmed by ^{1}H NMR (Figure 3.14) and FTIR (Figure 3.15). ^{1}H NMR (300 MHz, $CDCl_3$, δ, ppm):

6.13 and 5.59 (2H, s, e), 5.18 (1H, t, a), 5.01 (1H, q, b), 4.53 (1H, m, c), 4.29 (4H, m, d & d'), 3.5 (6H, t, g, g'& g"), 2.48 (6H, t, h, h' & h") and 1.91 (3H, s, f).

Compound **1** (200 mg, 0.19 mmol) (Figure 3.9b) was dissolved in DMF (3 mL). Then, trimethylamine solution (33wt%, 10 mL) in ethanol was added to the reaction mixture and stirred for 24 hrs in a closed reaction vessel at 55 ^{o}C. After cooling and concentrating the reaction mixture, the resulting solution was precipitated in THF and centrifuged to collect the product. The product was further washed with THF and dried under vacuum. The reaction product was confirmed by ^{1}H NMR (Figure 3.14).

Measurements of Antimicrobial Activity. The introduction of cationic charges to each polymer showed increased solubility in water. However, only cholic acid-based polymers are well soluble in water (~200 mg mL^{-1}). Deoxycholic acid polymers show limited solubility, while lithocholic acid polymers are not well soluble in water, due to the low charge density and high hydrophobicity. All polymers are well soluble in dimthyl sulfoxide (DMSO).

Bacteria Cell Culture. *Escherichia coli* (*E. coli*, ATCC-11775), *Pseudomonas aeruginosa* (*P. aeruginosa*, ATCC-10145), *Escherichia coli* (*E. coli*, ATCC- BAA-197), and *Staphylococcus aureus* (*S. aureus*, ATCC-33591) were purchased from ATCC. For these bacteria, a single colony was inoculated in 30 mL Tryptic Soy broth (TSB) at 37 °C for 24 h, shaking at 190 rpm min^{-1}. All bacteria were grown to an optical density of about l.00 (OD_{600} = 1.00) for further use.

Disk-diffusion Assays. The agar disk-diffusion assays were conducted by following literature.[28] At first, actively growing cultures of each bacterial strain on Mannitol salt agar

(MSA) were inoculated on TSB agar plates. The bacterial growth culture (cell concentrations were 1.0×10^6 CFU/mL; 10 μL) was diluted to 1 mL in TSB solution. Subsequently, 100 μL of that bacterial solution was spread on TSB agar plates to form a bacterial lawn covering the plate surface. Then, 6 mm (diameter) filter discs were added to the plate surface. Each bile acid-containing polymer at different concentrations in DMSO was added to disks, and the plates were incubated at 28 °C for 18 h. The development of a clear zone around the disk is known as the inhibition zone, where bacteria are unable to grow. This inhibition zone indicates the ability of agents to kill bacteria.

Minimum Inhibitory Concentration (MIC) Measurements. The MIC of cationic bile acid-containing homopolymers and bile acid compounds were determined using a broth microdilution method.[4] DMSO solution of homopolymer or compound with different concentrations was placed into each well of a 96-well plate. Different amount of TSB solution was added to antibiotic containing each well to get the volume of 150 μL. Then, 50 μL of bacterial TSB solution (OD_{600} = 0.07) was added into each well containing polymer solutions. The bacterial TSB solution without polymers or compounds was used as the control. The 96-well plate was incubated at 37 °C under constant shaking of 100 rpm for ~18 h until satisfactory growth. Bacterial growth was detected at OD_{600}, and was compared to controls of bacterial TSB solution without polymers. All assays were carried out in triplicates in the same assay plate. Optical density was plotted against polymer concentration, and linear regression analysis was used to determine the lowest concentration at which the optical density reading becomes zero. The MIC was taken as the concentration of bile acid-based polymers and compounds at which no microbial growth was observed.

Drug Resistance Study. A drug resistance study was performed against *P. aeruginosa* and *E. coli* for one of the active antimicrobial polymers named as CA_19k_5. Initially, the MIC of the polymer was measured as described above. The 10 μL bacterial solution was taken from the well that contains polymer solution of 2×MIC and incubated for over night at 37 ^{o}C. Then, using this newly grown bacterial solution previously exposed to the polymer sample, the new MIC was determined. This assay was repeated for ten passes and MIC values were determined each time. Development of drug resistance was analyzed by observing the change in MIC after every pass. A polymer showing the same MIC in each successive passage indicates the bacteria did not develop resistance to the polymer.

Hemolysis Evaluation. Blood was collected from mice in heparinized tubes and diluted by mixing 800 μL of blood with 1000 μL of PBS. Polymer samples were prepared in PBS at concentrations of 0.5, 1, 2 4, 16, 31, 62, 125, 250, and 500 μg mL^{-1}, and 60 μL of the diluted blood samples was added to 3 mL of polymers, PBS, or 0.1% Triton-X100 in PBS. The samples were incubated for 1 h at 37 °C followed by centrifugation for 10 min at 1500 rpm. Supernatants were collected, and OD was measured at 545 nm to calculate hemolysis rate by using the equation, HR = (AS – AN)/(AP – AN), where AS, AN, and AP are OD values of the supernatants from test samples, negative control (PBS), and positive control (0.1% Triton-X100), respectively.

LIVE/DEAD Bacterial Viability Assays. Confocal laser scanning microscopy (CLSM) analysis was used to study the bacterial membrane permeability after polymer treatment. The bacterial strains were inoculated at 37 °C together with polymer CA_19k_5 at two times the MIC value following the same procedure for MIC determination. An untreated bacterial solution was used as controls. After 18 h incubation at 37 °C, 1 μL of

LIVE/DEAD BacLight (Bacterial Viability Kit; Invitrogen Inc.) was added to 5 μL incubated solution and incubated for 15 min. The LIVE/DEAD BacLight bacterial viability kit consists of propidium iodide (PI), and FITC-labeled SYTO 9 dye used to stain nucleic acid (DNA). Green-fluorescing SYTO 9 can enter all cells, live or dead, whereas red fluorescing PI can only stain the DNA of damaged cytoplasmic membranes of dead or dying cells. Cells were imaged under a Leica TCS SP5 CLSM with a 63× oil immersion lens. When excited at 488 nm with argon and helium/neon lasers, bacteria with intact membranes display green fluorescence (emission = 500 nm), and bacteria with disrupted membranes fluoresce red (emission = 635 nm).

Bacterial Morphology Assays. The scanning electron microscopy (SEM) was used to examine morphologies of different bacteria with a similar procedure. In general, 10 μL of bacterial cell solution was grown on one glass slide in a 12-well plate containing 1 mL of TSB medium at 37 °C overnight. Cell suspensions were diluted to OD_{600} = 1.0. The polymer at twice the MIC was added to the 1 mL bacteria stock solution and incubated at 37 °C overnight. A bacterial solution without any polymers was used as the control. The samples were then fixed in cacodylate buffer with 2.5% glutaraldehyde solution (pH = 7.2) for 2–3 h at 4 °C and post-fixed with 1% osmium tetraoxide at 4 °C for 1 h. The samples were dried at a critical point, then coated with gold using a Denton Dest II Sputter Coater for 120 s, and observed by FE-SEM. An untreated cell suspension was used as the control.

Additional Figures

a

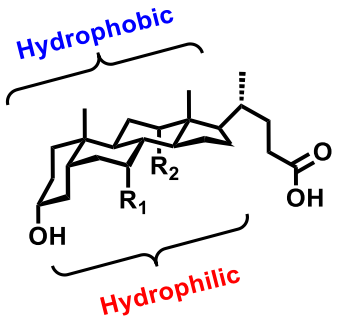

Bile Acid	R_1	R_2
Cholic Acid	OH	OH
Deoxycholic Acid	H	OH
Chenodeoxycholic Acid	OH	H
Lithocholic Acid	H	H

b

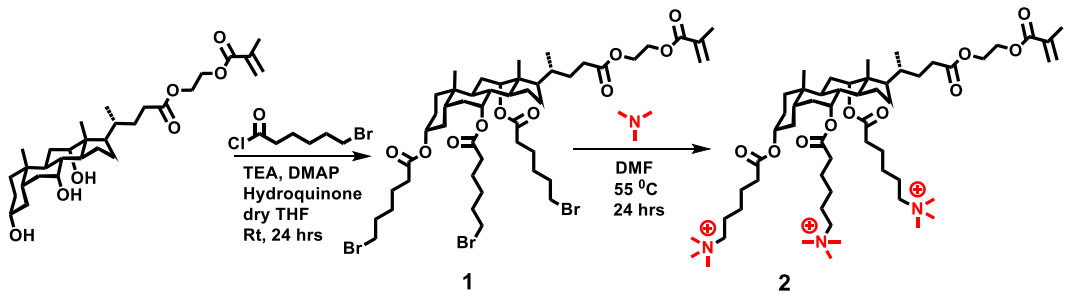

Figure 3.9 Bile acid derivatives and cationic monomer synthesis. **a** Structures of bile acid derivatives; **b** Reaction scheme for the synthesis of cholic acid-containing QAC monomer (labeled as CA_Monomer).

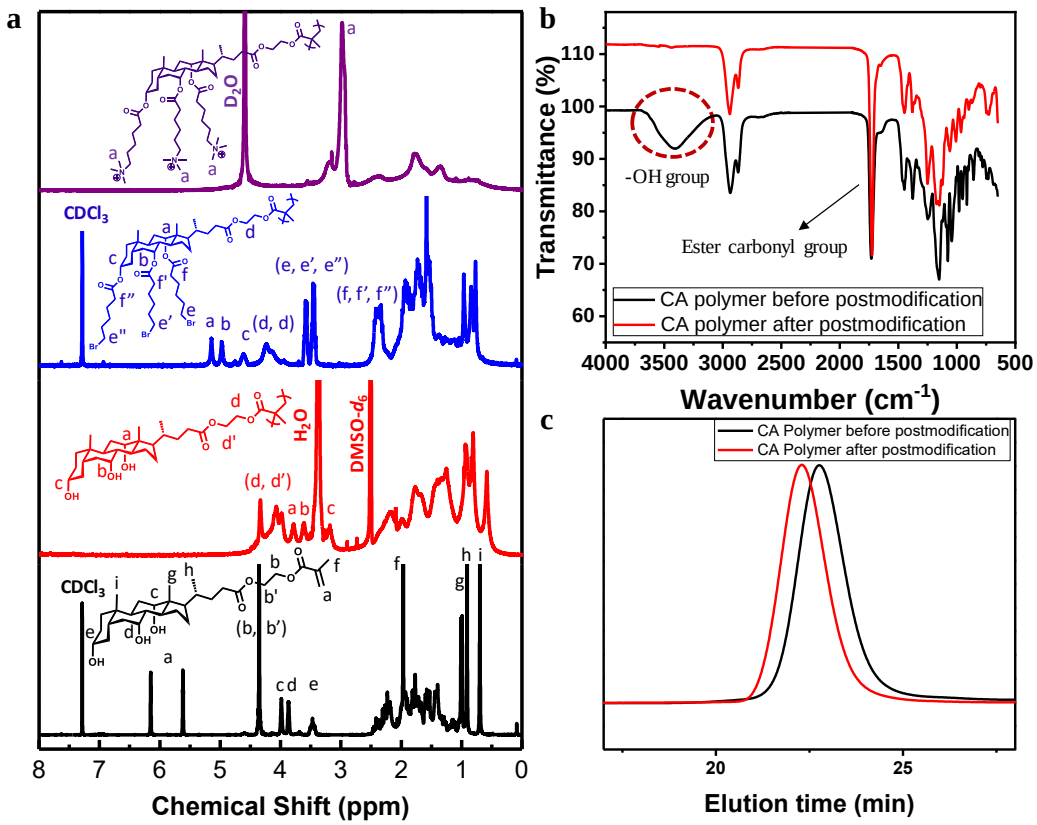

Figure 3.10 Characterization of cholic acid polymer. **a** ^{1}H NMR spectra for cholic acid polymers; **b** FTIR spectra of cholic acid polymers (black) and polymers after post-polymerization modification (red); **c** GPC traces of the CA_19k_5 polymers before and after post-polymerization modification.

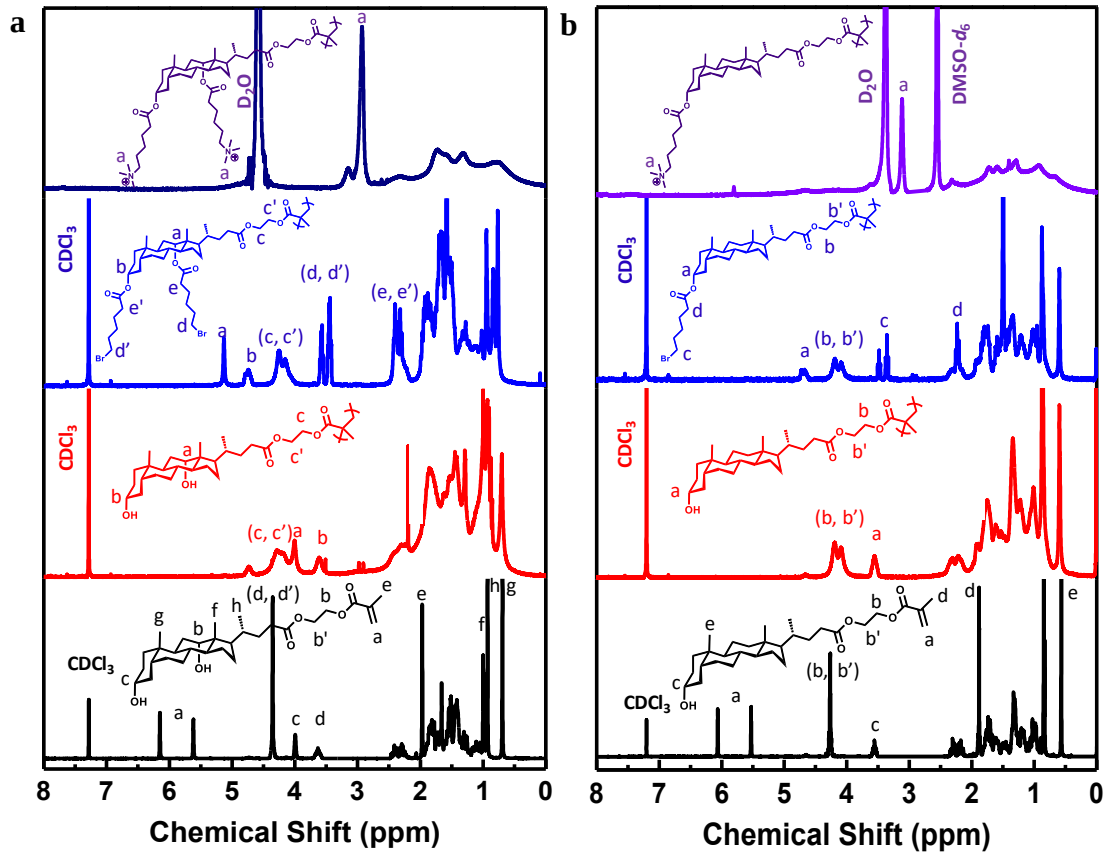

Figure 3.11 ^{1}H NMR spectra of **a** Deoxycholic acid polymers; **b** Lithocholic acid polymers.

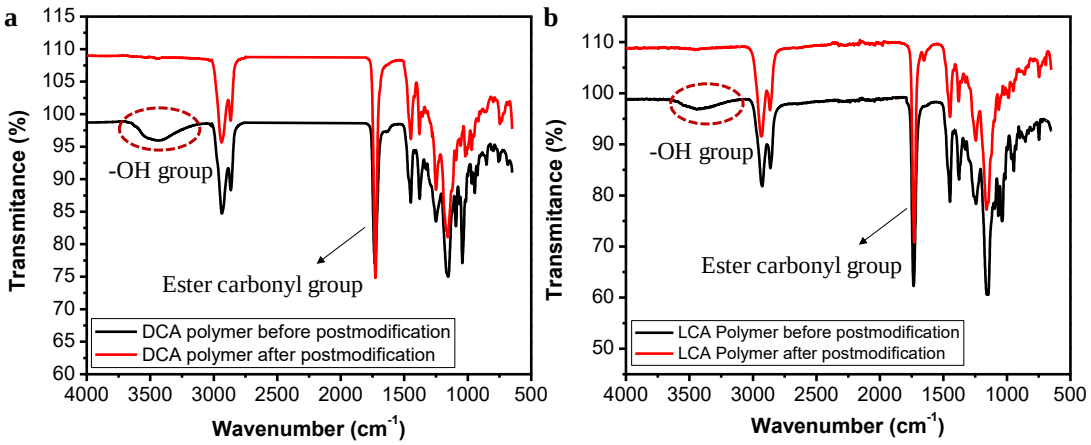

Figure 3.12 FTIR spectra of **a** Deoxycholic polymers (black) and polymers after post-polymerization modification (red); **b** Lithocholic polymers (black) and polymers after post-polymerization modification (red).

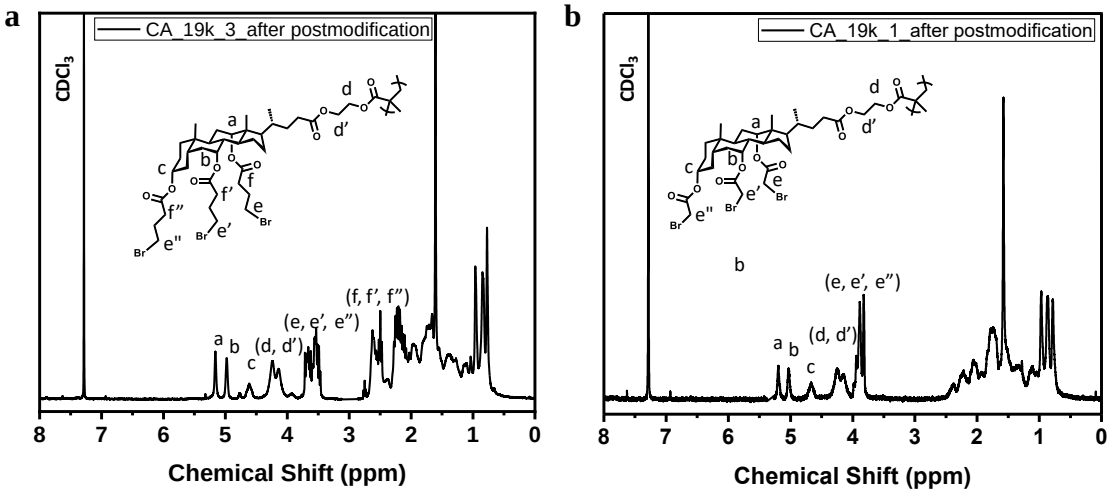

Figure 3.13 ^{1}H NMR spectra for **a** the CA_19k_3 polymer after post-polymerization modification; **b** the CA_19k_1 polymer after post-polymerization modification.

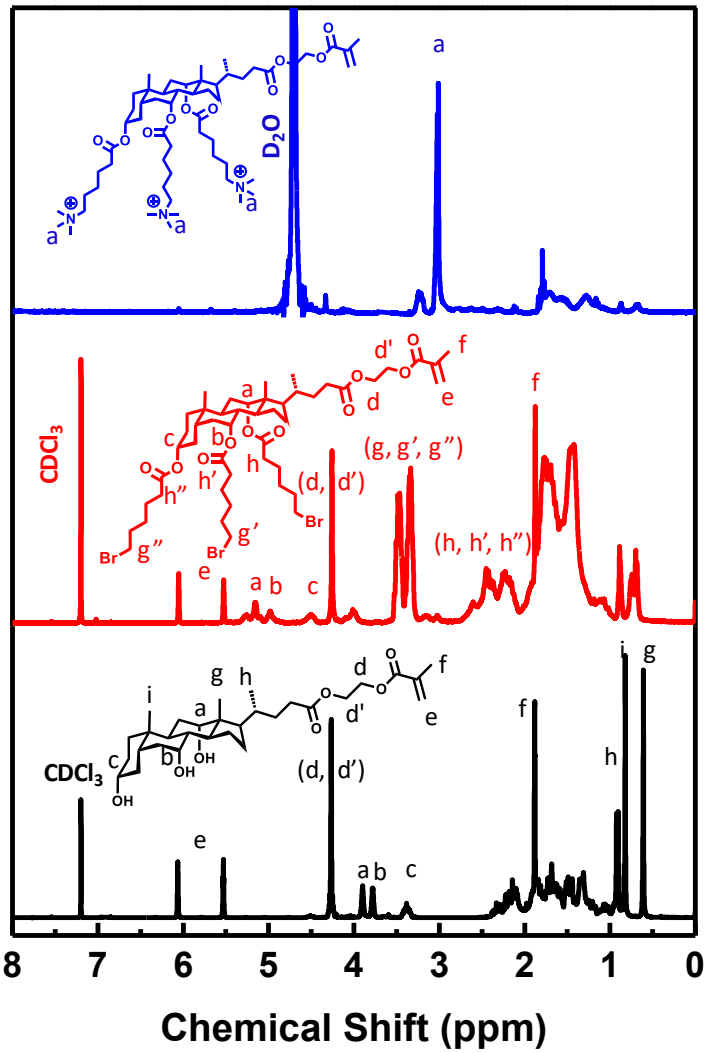

Figure 3.14 ^{1}H NMR spectra of QAC-containing cholic acid monomer.

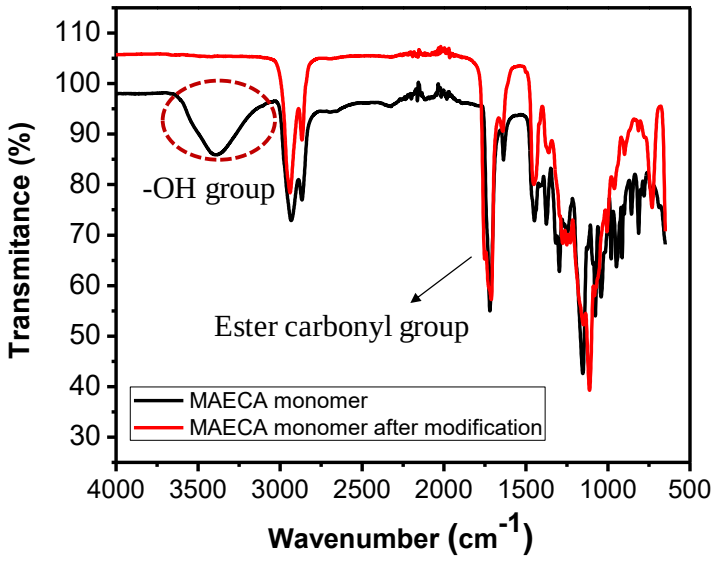

Figure 3.15 FTIR spectra of MAECA monomer (black) and MAECA monomer after modification (red).

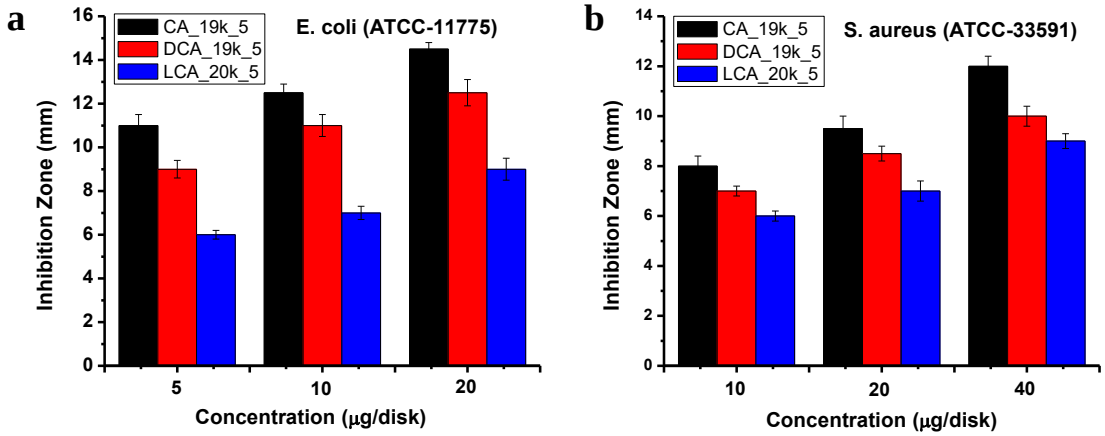

Figure 3.16 Antimicrobial activities of polymers CA_19k_5, DCA_19k_5 and LCA_19k_5 as demonstrated by disk diffusion assay against **a** *E. coli* and **b** *S. aureus*. The error bars represent the s.d. of three replicates.

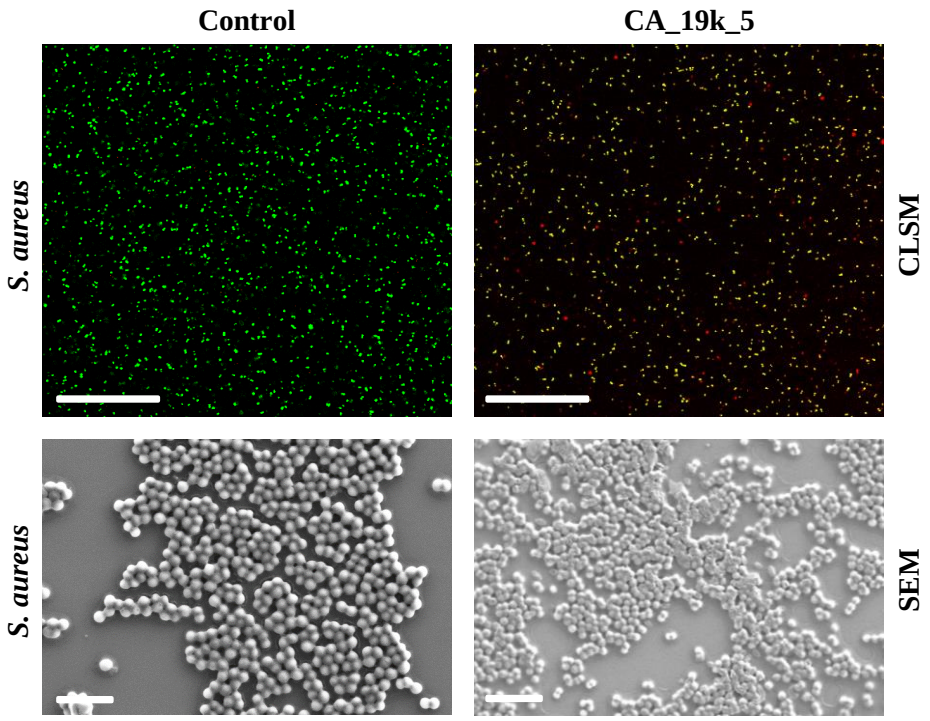

Figure 3.17 CLSM and SEM images of control and CA_19k_5 polymer. CA_19k_5 treatment with two times of MIC concentration. Bacterial solutions without CA_19k_5 were used as the control. Scale bar in confocal images is 50 µm and scale bar in SEM images is 2 µm.

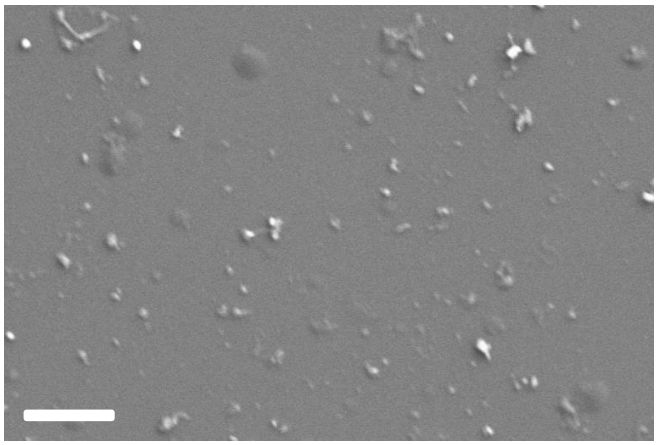

Figure 3.18 SEM image of *S. aureus* with CA_19k_5 polymer treatment of four times MIC concentration. Scale bar in SEM images is 2 µm.

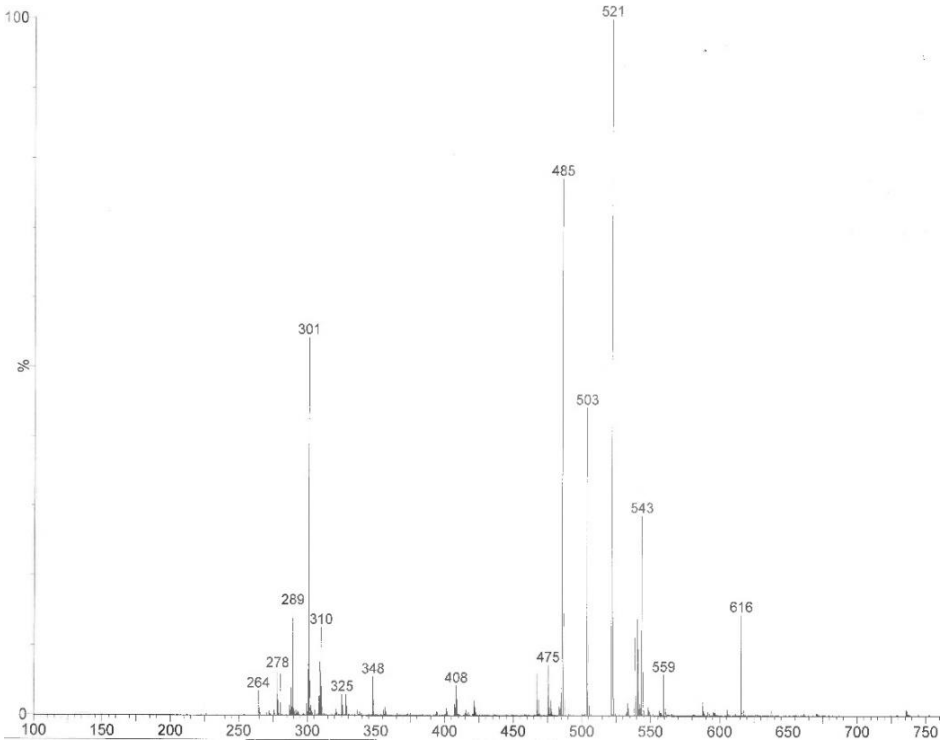

Figure 3.19 Mass spectrum of MAECA monomer.

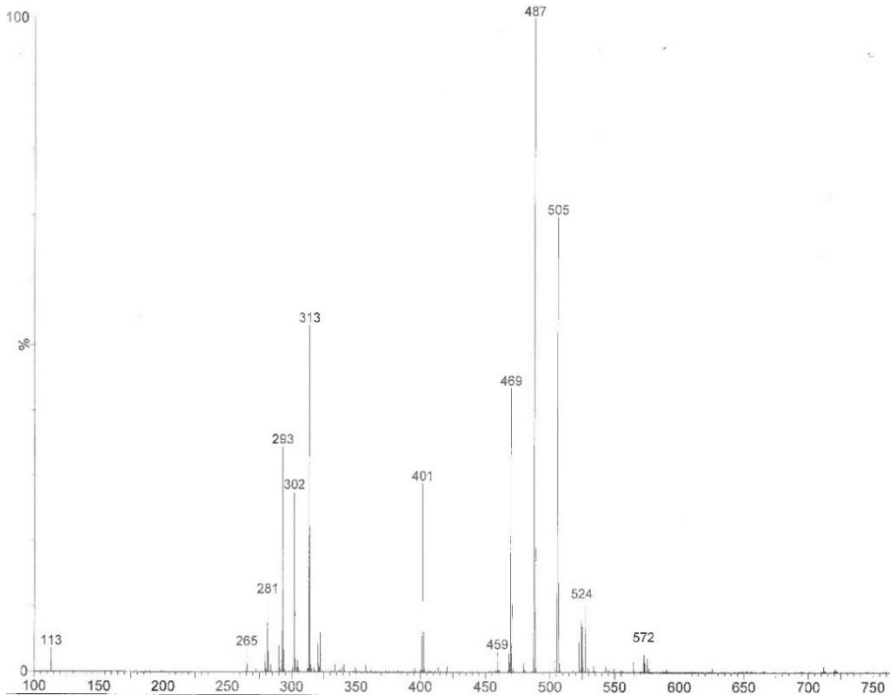

Figure 3.20 Mass spectrum of MAEDA monomer.

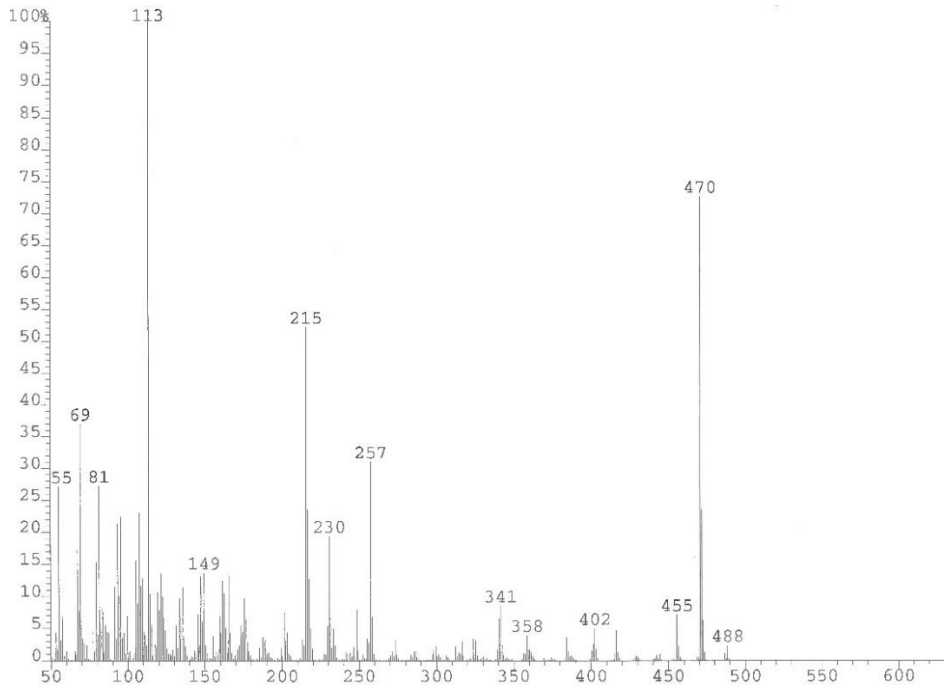

Figure 3.21 Mass spectrum of MAELA monomer.

Table 3.2 Molecular weight and dispersity of bile acid-derived polymers.

Polymer Symbol	M_n (g mol^{-1}) (GPC) Before post-polymerization modification	$Đ$	M_n (g mol^{-1}) (GPC) After post-polymerization modification	$Đ$
CA_19k_5	19,000	1.10	23,000	1.10
DCA_19k_5	19,000	1.11	22,000	1.14
LCA_19k_5	20,000	1.12	21,000	1.12
CA_10k_5	10,000	1.07	13,000	1.15
CA_19k_3	19,000	1.10	21,000	1.13
CA_19k_1	19,000	1.10	19,000	1.10
CA_25k_5	25,000	1.16	38,000	1.23
CA_32k_5	32,000	1.26	45,000	1.28

3.6 References

1. Bush, K.; Courvalin, P.; Dantas, G.; Davies, J.; Eisenstein, B.; Huovinen, P.; Jacoby, G. A.; Kishony, R.; Kreiswirth, B. N.; Kutter, E.; Lerner, S. A.; Levy, S.; Lewis, K.; Lomovskaya, O.; Miller, J. H.; Mobashery, S.; Piddock, L. J. V.; Projan, S.; Thomas, C. M.; Tomasz, A.; Tulkens, P. M.; Walsh, T. R.; Watson, J. D.; Witkowski, J.; Witte, W.; Wright, G.; Yeh, P.; Zgurskaya, H. I., Tackling antibiotic resistance. *Nat. Rev. Microbiol.* **2011,** *9* (12), 894-896.
2. Centers for Disease Control and Prevention (CDC). (2013) Antibiotic resistance threats in the United States, Atlanta, GA, https://www.cdc.gov/drugresistance/threat-report-2013.
3. Taubes, G., The Bacteria Fight Back. *Science* **2008,** *321* (5887), 356-361.
4. Lam, S. J.; O'Brien-Simpson, N. M.; Pantarat, N.; Sulistio, A.; Wong, E. H. H.; Chen, Y.-Y.; Lenzo, J. C.; Holden, J. A.; Blencowe, A.; Reynolds, E. C.; Qiao, G. G., Combating multidrug-resistant Gram-negative bacteria with structurally nanoengineered antimicrobial peptide polymers. *Nat. Microbiol.* **2016,** *1*.
5. Chin, W.; Zhong, G.; Pu, Q.; Yang, C.; Lou, W.; De Sessions, P. F.; Periaswamy, B.; Lee, A.; Liang, Z. C.; Ding, X.; Gao, S.; Chu, C. W.; Bianco, S.; Bao, C.; Tong, Y. W.; Fan, W.; Wu, M.; Hedrick, J. L.; Yang, Y. Y., A macromolecular approach to eradicate multidrug resistant bacterial infections while mitigating drug resistance onset. *Nat. Commun.* **2018,** *9* (1).
6. Lam, S. J.; Wong, E. H. H.; Boyer, C.; Qiao, G. G., Antimicrobial polymeric nanoparticles. *Prog. Polym. Sci.* **2018,** *76*, 40-64.
7. Nederberg, F.; Zhang, Y.; Tan, J. P. K.; Xu, K.; Wang, H.; Yang, C.; Gao, S.; Guo, X.

D.; Fukushima, K.; Li, L.; Hedrick, J. L.; Yang, Y.-Y., Biodegradable nanostructures with selective lysis of microbial membranes. *Nat. Chem.* **2011,** *3*, 409-414.

8. Brogden, K. A., Antimicrobial peptides: pore formers or metabolic inhibitors in bacteria? *Nat. Rev. Microbiol.* **2005,** *3*, 238-250.
9. Kohanski, M. A.; Dwyer, D. J.; Collins, J. J., How antibiotics kill bacteria: from targets to networks. *Nat. Rev. Microbiol.* **2010,** *8*, 423-435.
10. Ling, L. L.; Schneider, T.; Peoples, A. J.; Spoering, A. L.; Engels, I.; Conlon, B. P.; Mueller, A.; Schäberle, T. F.; Hughes, D. E.; Epstein, S.; Jones, M.; Lazarides, L.; Steadman, V. A.; Cohen, D. R.; Felix, C. R.; Fetterman, K. A.; Millett, W. P.; Nitti, A. G.; Zullo, A. M.; Chen, C.; Lewis, K., A new antibiotic kills pathogens without detectable resistance. *Nature* **2015,** *517*, 455-459.
11. Shi, Y.; Teng, P.; Sang, P.; She, F.; Wei, L.; Cai, J., γ-AApeptides: Design, Structure, and Applications. *Acc. Chem. Res.* **2016,** *49* (3), 428-441.
12. Radzishevsky, I. S.; Rotem, S.; Bourdetsky, D.; Navon-Venezia, S.; Carmeli, Y.; Mor, A., Improved antimicrobial peptides based on acyl-lysine oligomers. *Nat. Biotechnol.* **2007,** *25*, 657-659.
13. Takahashi, H.; Caputo, G. A.; Vemparala, S.; Kuroda, K., Synthetic Random Copolymers as a Molecular Platform To Mimic Host-Defense Antimicrobial Peptides. *Bioconj. Chem.* **2017,** *28* (5), 1340-1350.
14. Xiong, M.; Han, Z.; Song, Z.; Yu, J.; Ying, H.; Yin, L.; Cheng, J., Bacteria-Assisted Activation of Antimicrobial Polypeptides by a Random-Coil to Helix Transition. *Angew. Chem. Int. Ed.* **2017,** *56* (36), 10826-10829.
15. Zasloff, M., Antimicrobial peptides of multicellular organisms. *Nature* **2002,** *415*, 389-

395.

16. Mowery, B. P.; Lindner, A. H.; Weisblum, B.; Stahl, S. S.; Gellman, S. H., Structure−activity Relationships among Random Nylon-3 Copolymers That Mimic Antibacterial Host-Defense Peptides. *J. Am. Chem. Soc.* **2009,** *131* (28), 9735-9745.
17. Lienkamp, K.; Madkour, A. E.; Musante, A.; Nelson, C. F.; Nüsslein, K.; Tew, G. N., Antimicrobial Polymers Prepared by ROMP with Unprecedented Selectivity: A Molecular Construction Kit Approach. *J. Am. Chem. Soc.* **2008,** *130* (30), 9836-9843.
18. Ganewatta, M. S.; Tang, C., Controlling macromolecular structures towards effective antimicrobial polymers. *Polymer* **2015,** *63*, A1-A29.
19. Ong, Z. Y.; Wiradharma, N.; Yang, Y. Y., Strategies employed in the design and optimization of synthetic antimicrobial peptide amphiphiles with enhanced therapeutic potentials. *Adv. Drug Del. Rev.* **2014,** *78*, 28-45.
20. Porter, E. A.; Wang, X.; Lee, H.-S.; Weisblum, B.; Gellman, S. H., Non-haemolytic β-amino-acid oligomers. *Nature* **2000,** *404*, 565.
21. Porter, E. A.; Weisblum, B.; Gellman, S. H., Mimicry of Host-Defense Peptides by Unnatural Oligomers: Antimicrobial β-Peptides. *J. Am. Chem. Soc.* **2002,** *124* (25), 7324-7330.
22. Chongsiriwatana, N. P.; Patch, J. A.; Czyzewski, A. M.; Dohm, M. T.; Ivankin, A.; Gidalevitz, D.; Zuckermann, R. N.; Barron, A. E., Peptoids that mimic the structure, function, and mechanism of helical antimicrobial peptides. *Proc. Natl. Acad. Sci. U.S.A.* **2008,** *105* (8), 2794-2799.
23. Reuther, J. F.; Goodrich, A. C.; Escamilla, P. R.; Lu, T. A.; Del Rio, V.; Davies, B. W.; Anslyn, E. V., A Versatile Approach to Noncanonical, Dynamic Covalent Single- and

Multi-Loop Peptide Macrocycles for Enhancing Antimicrobial Activity. *J. Am. Chem. Soc.* **2018,** *140* (10), 3768-3774.

24. Ilker, M. F.; Nüsslein, K.; Tew, G. N.; Coughlin, E. B., Tuning the Hemolytic and Antibacterial Activities of Amphiphilic Polynorbornene Derivatives. *J. Am. Chem. Soc.* **2004,** *126* (48), 15870-15875.
25. Geng, Z.; Finn, M. G., Thiabicyclononane-Based Antimicrobial Polycations. *J. Am. Chem. Soc.* **2017,** *139* (43), 15401-15406.
26. Ergene, C.; Yasuhara, K.; Palermo, E. F., Biomimetic antimicrobial polymers: recent advances in molecular design. *Polym. Chem.* **2018,** *9* (18), 2407-2427.
27. Chen, Y.; Wilbon, P. A.; Chen, Y. P.; Zhou, J.; Nagarkatti, M.; Wang, C.; Chu, F.; Decho, A. W.; Tang, C., Amphipathic antibacterial agents using cationic methacrylic polymers with natural rosin as pendant group. *RSC Adv.* **2012,** *2* (27), 10275-10282.
28. Ganewatta, M. S.; Chen, Y. P.; Wang, J.; Zhou, J.; Ebalunode, J.; Nagarkatti, M.; Decho, A. W.; Tang, C., Bio-inspired resin acid-derived materials as anti-bacterial resistance agents with unexpected activities. *Chem. Sci.* **2014,** *5* (5), 2011-2016.
29. Ganewatta, M. S.; Miller, K. P.; Singleton, S. P.; Mehrpouya-Bahrami, P.; Chen, Y. P.; Yan, Y.; Nagarkatti, M.; Nagarkatti, P.; Decho, A. W.; Tang, C., Antibacterial and Biofilm-Disrupting Coatings from Resin Acid-Derived Materials. *Biomacromolecules* **2015,** *16* (10), 3336-3344.
30. Zhang, J.; Chen, Y. P.; Miller, K. P.; Ganewatta, M. S.; Bam, M.; Yan, Y.; Nagarkatti, M.; Decho, A. W.; Tang, C., Antimicrobial Metallopolymers and Their Bioconjugates with Conventional Antibiotics against Multidrug-Resistant Bacteria. *J. Am. Chem. Soc.* **2014,** *136* (13), 4873-4876.

31. Yang, P.; Bam, M.; Pageni, P.; Zhu, T.; Chen, Y. P.; Nagarkatti, M.; Decho, A. W.; Tang, C., Trio Act of Boronolectin with Antibiotic-Metal Complexed Macromolecules toward Broad-Spectrum Antimicrobial Efficacy. *ACS Infect. Dis.* **2017,** *3* (11), 845-853.

32. Yan, Y.; Zhang, J.; Ren, L.; Tang, C., Metal-containing and related polymers for biomedical applications. *Chem. Soc. Rev.* **2016,** *45* (19), 5232-5263.

33. Pageni, P.; Yang, P.; Bam, M.; Zhu, T.; Chen, Y. P.; Decho, A. W.; Nagarkatti, M.; Tang, C., Recyclable magnetic nanoparticles grafted with antimicrobial metallopolymer-antibiotic bioconjugates. *Biomaterials* **2018,** *178*, 363-372.

34. Zhu, T.; Sha, Y.; Yan, J.; Pageni, P.; Rahman, M. A.; Yan, Y.; Tang, C., Metallo-polyelectrolytes as a class of ionic macromolecules for functional materials. *Nat. Commun.* **2018,** *9* (1).

35. Ganewatta, M. S.; Rahman, M. A.; Mercado, L.; Shokfai, T.; Decho, A. W.; Reineke, T. M.; Tang, C., Facially amphiphilic polyionene biocidal polymers derived from lithocholic acid. *Bioact Mater* **2018,** *3* (2), 186-193.

36. Mowery, B. P.; Lee, S. E.; Kissounko, D. A.; Epand, R. F.; Epand, R. M.; Weisblum, B.; Stahl, S. S.; Gellman, S. H., Mimicry of Antimicrobial Host-Defense Peptides by Random Copolymers. *J. Am. Chem. Soc.* **2007,** *129* (50), 15474-15476.

37. Liu, R.; Chen, X.; Chakraborty, S.; Lemke, J. J.; Hayouka, Z.; Chow, C.; Welch, R. A.; Weisblum, B.; Masters, K. S.; Gellman, S. H., Tuning the Biological Activity Profile of Antibacterial Polymers via Subunit Substitution Pattern. *J. Am. Chem. Soc.* **2014,** *136* (11), 4410-4418.

38. Tew, G. N.; Liu, D.; Chen, B.; Doerksen, R. J.; Kaplan, J.; Carroll, P. J.; Klein, M. L.;

DeGrado, W. F., De novo design of biomimetic antimicrobial polymers. *Proc. Natl. Acad. Sci. U.S.A.* **2002,** *99* (8), 5110-5114.

39. Kuroda, K.; DeGrado, W. F., Amphiphilic Polymethacrylate Derivatives as Antimicrobial Agents. *J. Am. Chem. Soc.* **2005,** *127* (12), 4128-4129.
40. Thaker, H. D.; Cankaya, A.; Scott, R. W.; Tew, G. N., Role of Amphiphilicity in the Design of Synthetic Mimics of Antimicrobial Peptides with Gram-Negative Activity. *ACS Med. Chem. Lett.* **2013,** *4* (5), 481-485.
41. Gabriel, G. J.; Maegerlein, J. A.; Nelson, C. F.; Dabkowski, J. M.; Eren, T.; Nüsslein, K.; Tew, G. N., Comparison of Facially Amphiphilic versus Segregated Monomers in the Design of Antibacterial Copolymers. *Chem. Eur. J.* **2009,** *15* (2), 433-439.
42. Zhu, X.-X.; Nichifor, M., Polymeric Materials Containing Bile Acids. *Acc. Chem. Res.* **2002,** *35* (7), 539-546.
43. Zhang, M.; Strandman, S.; Waldron, K. C.; Zhu, X. X., Supramolecular hydrogelation with bile acid derivatives: structures, properties and applications. *J. Mater. Chem. B* **2016,** *4* (47), 7506-7520.
44. di Gregorio, M. C.; Travaglini, L.; Del Giudice, A.; Cautela, J.; Pavel, N. V.; Galantini, L., Bile Salts: Natural Surfactants and Precursors of a Broad Family of Complex Amphiphiles. *Langmuir* **2018**.
45. Pal, S.; Ghosh Roy, S.; De, P., Synthesis via RAFT polymerization of thermo- and pH-responsive random copolymers containing cholic acid moieties and their self-assembly in water. *Polym. Chem.* **2014,** *5* (4), 1275-1284.
46. Qiao, Y.; Yang, C.; Coady, D. J.; Ong, Z. Y.; Hedrick, J. L.; Yang, Y.-Y., Highly dynamic biodegradable micelles capable of lysing Gram-positive and Gram-negative

bacterial membrane. *Biomaterials* **2012,** *33* (4), 1146-1153.

47. Liu, S.; Ono, R. J.; Wu, H.; Teo, J. Y.; Liang, Z. C.; Xu, K.; Zhang, M.; Zhong, G.; Tan, J. P. K.; Ng, M.; Yang, C.; Chan, J.; Ji, Z.; Bao, C.; Kumar, K.; Gao, S.; Lee, A.; Fevre, M.; Dong, H.; Ying, J. Y.; Li, L.; Fan, W.; Hedrick, J. L.; Yang, Y. Y., Highly potent antimicrobial polyionenes with rapid killing kinetics, skin biocompatibility and in vivo bactericidal activity. *Biomaterials* **2017,** *127*, 36-48.
48. Palermo, E. F.; Vemparala, S.; Kuroda, K., Cationic Spacer Arm Design Strategy for Control of Antimicrobial Activity and Conformation of Amphiphilic Methacrylate Random Copolymers. *Biomacromolecules* **2012,** *13* (5), 1632-1641.
49. Jaud, S.; Fernández-Vidal, M.; Nilsson, I.; Meindl-Beinker, N. M.; Hübner, N. C.; Tobias, D. J.; von Heijne, G.; White, S. H., Insertion of short transmembrane helices by the Sec61 translocon. *Proc. Natl. Acad. Sci. U.S.A.* **2009,** *106* (28), 11588-11593.
50. Schow, E. V.; Freites, J. A.; Cheng, P.; Bernsel, A.; von Heijne, G.; White, S. H.; Tobias, D. J., Arginine in Membranes: The Connection Between Molecular Dynamics Simulations and Translocon-Mediated Insertion Experiments. *J. Membr. Biol.* **2011,** *239* (1), 35-48.
51. Mondal, J.; Zhu, X.; Cui, Q.; Yethiraj, A., Sequence-Dependent Interaction of β-Peptides with Membranes. *J. Phys. Chem. B* **2010,** *114* (42), 13585-13592.
52. Lienkamp, K.; Kumar, K.-N.; Som, A.; Nüsslein, K.; Tew, G. N., "Doubly Selective" Antimicrobial Polymers: How Do They Differentiate between Bacteria? *Chem. Eur. J.* **2009,** *15* (43), 11710-11714.
53. Kenawy, E.-R.; Worley, S. D.; Broughton, R., The Chemistry and Applications of Antimicrobial Polymers: A State-of-the-Art Review. *Biomacromolecules* **2007,** *8* (5),

1359-1384.

54. Singh, M.; Singh, A.; Kundu, S.; Bansal, S.; Bajaj, A., Deciphering the role of charge, hydration, and hydrophobicity for cytotoxic activities and membrane interactions of bile acid based facial amphiphiles. *Biochim. Biophys. Acta* **2013,** *1828* (8), 1926-1937.
55. Pageni, P.; Yang, P.; Chen, Y. P.; Huang, Y.; Bam, M.; Zhu, T.; Nagarkatti, M.; Benicewicz, B. C.; Decho, A. W.; Tang, C., Charged Metallopolymer-Grafted Silica Nanoparticles for Antimicrobial Applications. *Biomacromolecules* **2018,** *19*, 417-425.
56. Moore, K. S.; Wehrli, S.; Roder, H.; Rogers, M.; Forrest, J. N.; McCrimmon, D.; Zasloff, M., Squalamine: an aminosterol antibiotic from the shark. *Proc. Natl. Acad. Sci. U.S.A.* **1993,** *90* (4), 1354-1358.
57. Randazzo, R. A. S.; Bucki, R.; Janmey, P. A.; Diamond, S. L., A series of cationic sterol lipids with gene transfer and bactericidal activity. *Biorg. Med. Chem.* **2009,** *17* (9), 3257-3265.
58. Li, C.; Budge, L. P.; Driscoll, C. D.; Willardson, B. M.; Allman, G. W.; Savage, P. B., Incremental Conversion of Outer-Membrane Permeabilizers into Potent Antibiotics for Gram-Negative Bacteria. *J. Am. Chem. Soc.* **1999,** *121* (5), 931-940.
59. Li, C.; Peters, A. S.; Meredith, E. L.; Allman, G. W.; Savage, P. B., Design and Synthesis of Potent Sensitizers of Gram-Negative Bacteria Based on a Cholic Acid Scaffolding. *J. Am. Chem. Soc.* **1998,** *120* (12), 2961-2962.
60. Willemen, H. M.; Smet, L. C. P. M. d.; Koudijs, A.; Stuart, M. C. A.; Jong, I. G. A. M. H. d.; Marcelis, A. T. M.; Sudhölter, E. J. R., Micelle Formation and Antimicrobial Activity of Cholic Acid Derivatives with Three Permanent Ionic Head Groups. *Angew. Chem. Int. Ed.* **2002,** *41* (22), 4275-4277.

CHAPTER 4

FACIAL AMPHIPHILICITY-INDUCED SELF-ASSEMBLY (FAISA) OF GRADIENT COPOLYMERS

4.1 Abstract

Amphiphilic species, such as block copolymers or surfactants, inherently self-assembled into a wide variety of nanostructures in a selective solvent. We report the self-assembly of facially amphiphilic multicyclic natural product-based gradient copolymers. Depending on the ratio of hydrophilic and hydrophobic segments, these copolymers can self-assemble in water to produce spherical, lenticular and rod-like nanostructures via supramolecular interactions. The hydrophobic interaction from multicyclic natural product initiates the self-assembly process that can be tuned by changing the amount of neutral hydrophilic PEG moiety. Incorporation of PEG into the copolymers not only increased the biocompatibility but also improved the colloidal stability of the aggregates. The formation of nanostructures such as spheres, vesicles, and tubular shape can be expedited applying temperature.

4.2 Introduction

Natural biomolecules, including peptides, proteins, lipids, nucleic acids, etc., are able to self-assemble into highly sophisticated structures in order to perform their unique functions.[1-3] Inspired by nature, a variety of synthetic macromolecules with complex self-assembled structures have been developed for a wide range of applications primarily in the areas of nanotechnology and biomedical sciences.[4-5] Amphiphilic homopolymers and copolymers comprising solvophilic and solvophobic segments can self-assemble to form a rich spectrum of morphologies or aggregates, where the solvophobic portions form the core to reduce contacts with solvents and the solvophilic segments constitute corona to stabilize aggregates.[6] The self-assembly behaviors of amphiphilic polymers largely depend on the polymer chain compositions, architectures, and balance of solvophobicity and

solvophilicity.[7-8] Most compositions adopt an architecture of block copolymers,[9-11] though other topologies, including random,[12-14] gradient[15-17] and alternating[18] copolymers, have been much less developed. Self-assembly of amphiphilic block copolymers can provide precisely controlled and well-defined morphologies in 0D, 1D, 2D, and 3D spaces.[9-11, 19-21] Recently, some sophisticated self-assembly techniques have been developed to prepare wide variety of morphologies. Manners, Winnik and coworkers explored crystallization-driven self-assembly (CDSA), a living supramolecular strategy that yields nanostructures with a narrow dispersity.[22-25] Steven Armes and coworkers developed polymerization-induced self-assembly (PISA) that involve very simple operation, and form rich morphologies with high solid content.[26-28] However, most of these involve the block copolymers, and the synthesis of many block copolymers is tedious and time-consuming because their preparation involves sequential controlled polymerization or post-polymerization treatments,[29] with the precaution for possible contamination by homopolymers during the synthesis.

Therefore, the self-assembly of homopolymers, random and gradient copolymers (or aperiodic copolymers) is appealing due to their easy preparation, scalability, and the potential to control sequences of monomeric units. Recently some reports revealed that the amphiphilic homopolymers are capable of self-assembly but only into vesicles or spherical aggregates with 10 to 1000 nm size.[30-31] Sawamoto, Terashima, and coworkers reported self-assembly of amphiphilic random copolymers bearing hydrophilic poly(ethylene glycol) (PEG) and hydrophobic linear alkyl groups in water.[32-34] A few other groups reported various supramolecular assemblies based on amphiphilic copolymers in water.[33-35] The self-assembly behaviors of gradient copolymers is very rare.[15-17] The self-assembly

behaviors of gradient copolymers mostly depend on the hydrophilic-hydrophobic balance of their compositions. The scope of these copolymer compositions requires in-depth understanding of structure-property relationships on the origin of various mechanisms of assembly, which is critical for a rational design.

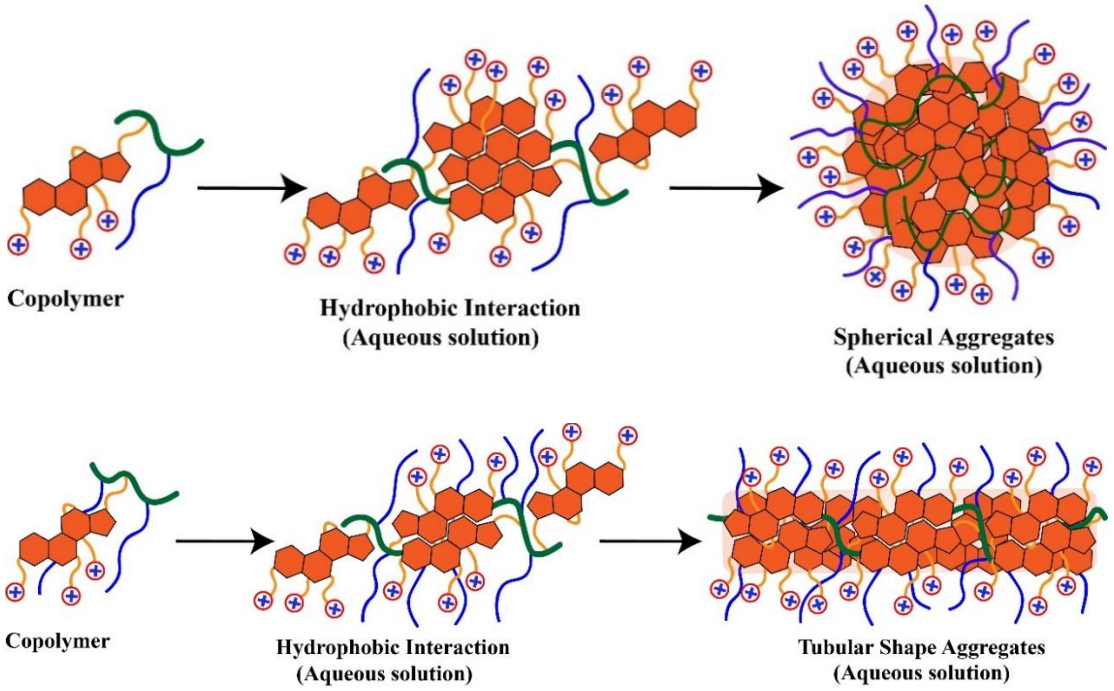

Figure 4.1 Formation of spherical and tubular aggregates in water.

Herein we report a new methodology on the compositions of gradient copolymers toward controlled self-assembled nanostructures. The key design is to construct facial amphiphilic moieties as monomeric units together with water-soluble co-monomer compositions, which can tune the balance of enthalpy and entropy for controlled self-assembly. The facial amphiphilic moieties consist of large cross-sectional multicyclic hydrocarbons on one side and multiple charged polar head groups on the other side. The charge repulsion reduces the aggregation of hydrocarbons due to van der Waals attraction (i.e., London force). The presence of hydrophilic co-monomer compositions enhances

excluded volume repulsions. The interplay of these three different forces dictates self-assembled morphologies, an analog to grafted hairy polymer nanoparticles. We hypothesized that a gradient/blocky copolymer composition is desirable to allow the precise interplay of the above-mentioned three different interactions.

To address this hypothesis, we chose multicyclic natural products, e.g., bile acids, as key building blocks to construct facial amphiphilicity in monomeric units, which were copolymerized with PEGylated methacrylate, leading to novel copolymers with tunable charged density, hydrophobicity, and hydrophilicity. Bile acids are biologically active surfactants with inherent facial structures including large cross-sectional tetracyclic hydrocarbons (constituted as the convex β-face) and polar functionalities such as hydroxyl and carboxylic groups a (positioned in the concave α-face).[36] Their facial amphiphilicity allows them to form very ordered aggregates with different morphologies in aqueous solutions, which also can be tuned with different stimuli such as temperature and added electrolyte, etc.[37] However, the bile acid derivatives mostly form large aggregates, and some of them are not well controlled. Due to their unique structural feature, these acids have been widely used in many fields including drug delivery,[38-39] sensors,[40] polymeric gels,[41-42] antimicrobials[43-44], and other biological applications.[45] In the biomedical field, these nanomaterials are mainly developed for regenerative medicines and drug delivery cargoes. However, there are recent efforts to foster nanostructures or self-assembled materials for antimicrobial applications, though still at the infancy stage. Recently, we developed bile-acid based facially amphiphilic cationic homopolymers that act as a strong antibacterial agent.[46] We hypothesized that the facial amphiphilicity of bile acid containing polymers could facilitate the phase segregation to self-assemble into nanoobjects.

Herein we design the cationic bile acid-based facial amphiphilic copolymers and investigate their self-assembly behavior. We have synthesized the cationic bile acid-based facial amphiphilic copolymers with different amount of neutral poly (ethylene glycol) (PEG) units. PEG can improve biocompatibility as well as colloidal stability of the copolymers self-assembly.[47] Due to the presence of facial amphiphilic cationic moieties, these types of amphiphilic copolymers can form a wide range of aggregates via supramolecular interaction such as hydrophobic interaction (Figure 4.1). Three different bile acid derivatives, lithocholic, deoxycholic, and cholic acid were used to construct one, two, and three quaternary ammonium charge (QAC) containing copolymers respectively. We performed a more comprehensive investigation of the self-assembly behavior of three bile acid derived copolymers with different PEG content and examine how the resulting change in hydrophilicity and hydrophobicity affect the morphology. The temperature-induced morphology of copolymers is also investigated to expedite the self-assembly process.

4.3 Results and Discussion

Synthesis of amphiphilic copolymers. A series of amphiphilic random/gradient (or, aperiodic) copolymers bearing hydrophilic PEG and hydrophobic bile acid derivatives were synthesized via living reversible addition fragmentation transfer (RAFT) using polymerization utilizing 4-cyano-4-(thiobenzylthio)pentanoic acid (CTP) as a chain transfer agent. Bile acid-based methacrylate monomers were prepared following our recently reported method.[46] QAC containing homopolymer was synthesized from bile acids derivatives (such as, cholic acid and deoxycholic acid) following our previously reported method.[46] The neutral PEG was chosen to increase hydrophilicity as well as

biocompatibility of the polymer, which is widely used as a polymeric material for the biomedical application.[48] Moreover, PEG increases the colloidal stability that allows for the formation of spheres, polymersomes, and fibers in aqueous solution.[48] In order to study the influence of the hydrophilic PEG block on the copolymer self-assembly, five copolymers (Figure 4.2) with varying the numbers of PEG blocks were prepared. The PEG content was changed from 10% to 50% in mole ratio. The polymerization was well controlled with the molecular weight Mn = 10000-20000 Da and a low polydispersity index ($Đ$ = 1.12), as determined by Gel Permeation Chromatography (GPC) calibrated against polystyrene standards. The molecular weight of all copolymers obtained by GPC was higher than the molecular weight calculated by ^{1}H NMR. This is because of bulky multicyclic ring structures occupy larger hydrodynamic volume. ^{1}H NMR was used to determine the degree of polymerization (DP) and the monomer feed ratio (MAECA/PEGMA). Hydroxyl groups of the cholic acid moiety of the random copolymers were functionalized to bear QAC groups by following our previous report. In the post-polymerization modification, hydroxyl groups of copolymers were modified through an esterification reaction with bromohexanoyl chloride and the bromine groups were substituted by trimethylamine to offer QAC containing polymers. The post-polymerization modification was confirmed by FTIR (Figure 4.12b) (disappearance of a broad peak at 3500-3600 cm^{-1} corresponding to hydroxyl groups) and ^{1}H NMR (Figure 4.12a) (the peaks next to the alcohol group in ^{1}H NMR at ~ 3.2 to 3.8 ppm shifted to 4.7 to 5.2 ppm). The monomer reactivity ratios were obtained from the Fineman-Ross plot that confirm the formation of gradient copolymers (Figure 4.17).[49] To evaluate the effect of charge density on self-assembly, ~ 20 and 40 mole % PEG containing gradient copolymers with double

(C_DCA) QAC head groups and 40 mole % PEG with single (C_LCA) head groups containing gradient copolymers were prepared similarly from deoxycholic acid and lithocholic acid respectively. Polymers were denoted according to their architecture and respective derivative resource (i.e. C_CA1 is a copolymer of cholic acid).

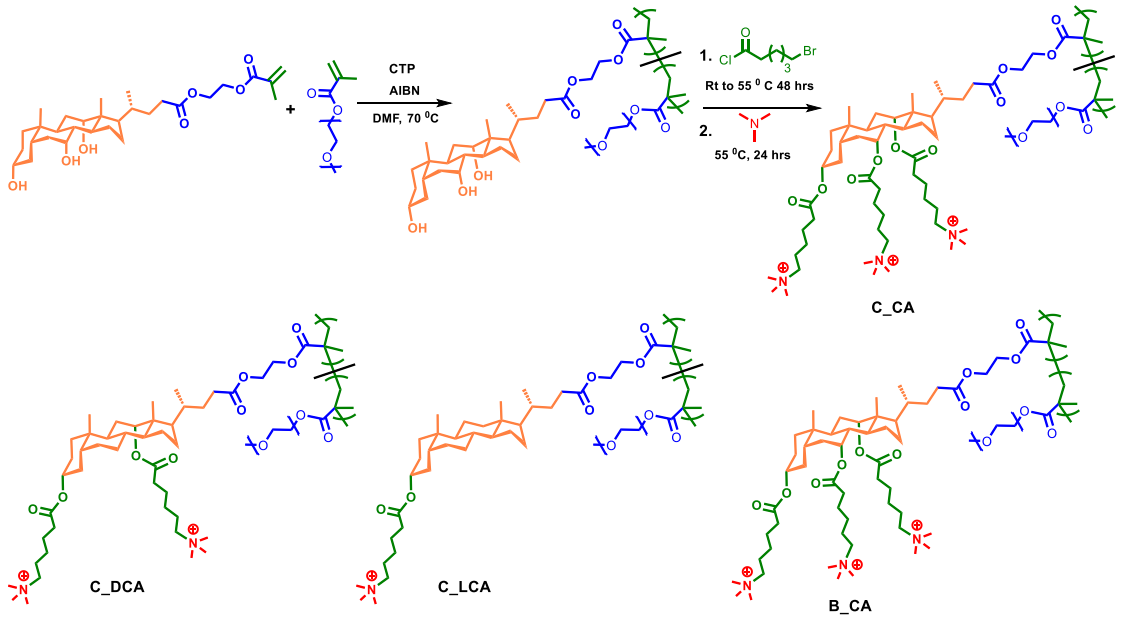

Figure 4.2 Synthesis of QAC charge containing a random copolymer.

One block copolymer with 40% mole ratio of PEG was synthesized by one-pot sequential RAFT polymerization in order to investigate the influence of the block copolymer on self-assembly. In a first step, MAECA was polymerized by RAFT using CTP as chain transfer agent. Once all the monomers were consumed, PEGMA was introduced and polymerized on the same reaction pot at 70 °C (Figure 4.11). The clear shift in GPC traces in each step to high molecular weight indicating the successful chain extension shown in Figure 4.16c. Polymerization was well controlled with a narrow molecular weight distribution ($Đ < 1.1$). A similar procedure was followed to do the post-polymerization modification to make quaternary ammonium groups containing block copolymers. All characterization data and

experimental details are given in the supplementary information. All characterization data and experimental details are provided in the supplementary information.

Table 4.1 Copolymer Characterization by NMR, GPC, DLS, and Zeta Potential Analysis

Co-polymers	Bile Acid Feed (mole %)	PEGMA Feed (mole % by ^{1}H NMR)	Molecular Weight M_n[a] (g/mol) (^{1}H NMR)	Molecular Weight M_n[b] (g/mol) (GPC)	Dispersity ($Đ$)	D_h[c] of Aggregates by DLS (nm)	Zeta potential, ζ (mV)[d]
C_CA1	90	10	12000	18000	1. 16	312.3 ±8.6	+69.4±3.3
C_CA2	80	20	13000	21000	1.11	302.4±7.4	+68.4±2.1
C_CA3	70	30	8000	10000	1.08	205.2 ± 12.4	+64.6±0.9
C_CA4	58	42	8000	14000	1.09	248.7 ±27	+50.4±4.1
C_CA5	47	53	9000	11000	1.08	375.3 ± 30.9	+46.5±3.1
C_DCA1	80	20	13000	21000	1.20	223.9 ± 23.1	+58.8±7.2
C_DCA2	55	45	8000	10000	1.07	332.2 ± 23.1	+55.7±1.1
C_LCA	60	40	10000	15000	1.12	119.4 ± 31	+50.1±1.2
B_CA	57	43	14000	20000	1.20	322.2 ± 6.5	+59.8±2
H_CA	100		13000	19000	1.10	329.3± 15.4	+70.2±2.1
H_DCA	100		13000	19000	1.11	250.9± 20.6	+58.1±3.4

a. Number-average molecular weight calculated from ^{1}H NMR spectrum.
b. Number-average molecular weight determined by GPC calibrated by polystyrene standard.
c. The mean hydrodynamic diameter, D_h (Z-average) of particles determined by DLS (at 25 ^{o}C) after one-month annealing at room temperature (Concentration 1 mg/mL).
d. Zeta potential (mV) was measured by DLS (Concentration 1 mg/mL).

Self-Assembly Behaviors

At first, the self-assembly behavior of bile acid-based copolymers was investigated by ^{1}H NMR spectroscopy. Initially, the formation of aggregates of C_CA1, C_CA4, and C_CA5 were studied by ^{1}H NMR spectroscopy in two different solvents, D_2O and DMSO-d_6, shown in Figure 4.13. The ^{1}H NMR peaks for methyl groups in the cholic acid moieties disappeared (0.6–1.0 ppm) in the D_2O solvent but were observed in the DMSO-d_6. In D_2O solvent, only PEG and QAC groups are soluble, but the hydrophobic ring of cholic acid moieties are not soluble and covered by the hydrophilic (PEG and QAC) groups. On the other hand, the DMSO-d_6 is a suitable solvent for all the components in the copolymer and showed clear peaks at 0.6–1.0 ppm for methyl groups. This result indicates that facial amphiphilicity leads all the copolymers to form higher order aggregates in aqueous solutions through the arrangement of hydrophilic and hydrophobic components in the copolymers where the hydrocarbon-rich ring structures of bile acids constitute the core and the hydrophilic groups line the periphery.

Dynamic light scattering (DLS) experiments were employed to measure the size of the aggregates of all copolymers, summarized in Table 4.2. The hydrodynamic diameter (D_h) of all the copolymers is between 180 to 400 nm demonstrating that all the copolymers formed nanoaggregates in aqueous solution. The aggregate size decreases along with an increase in PEG blocks of the copolymers until 30 mol %, after that size increases along with an increase in PEG blocks of the copolymers (Figure 4.3a). Size decreases with increasing certain amount of PEG because of the decrease of electrostatic repulsion among the positive charge of cholic acid moiety leading to shrinkage aggregate size. In addition, the higher the number of multicyclic cholic acid moiety increases the higher the charge

density that increases the charge repulsion and extends the volume to minimize the repulsion and leading to occupy the larger hydrodynamic volume. The stability of all the copolymers was also studied by measuring the zeta potential (Table 4.2). All copolymers showed positive zeta potential values obtained around 45-70 mV also suggests the colloidal stability of the aggregates and QAC groups were located on the outer surface of the aggregates. The zeta potential of C_CA1 has determined to be 69 mV due to the presence of higher cholic acid block with higher charge density that creates larger electrostatic repulsion between particles. The C_CA5 copolymer showed the lowest zeta potential as 46 mV indicating that a higher PEG ratio in the copolymer reduces the zeta potential. The zeta potential decreases with increasing neutral PEG content because the cationic charge was shielded by the more extended PEG corona (Figure 4.3b).[48]

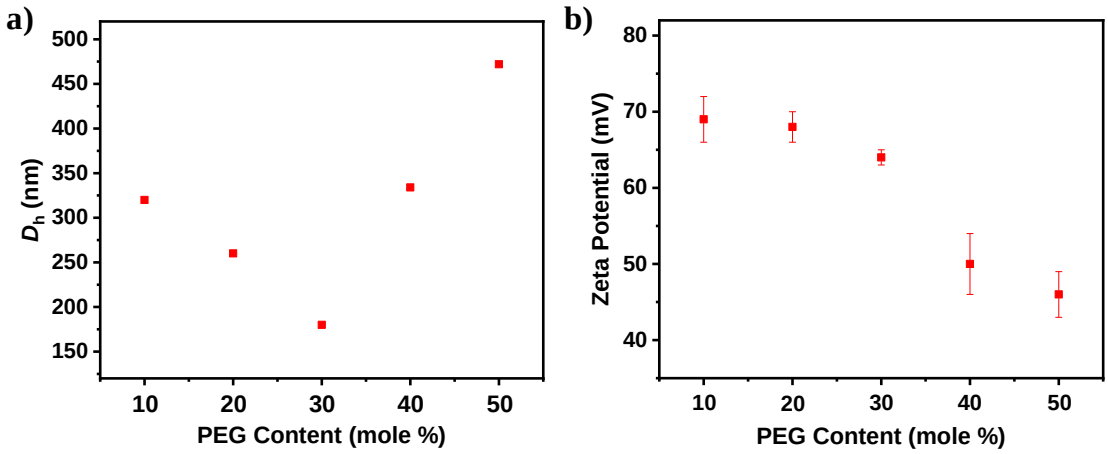

Figure 4.3 DLS study of nanoaggregates; **a)** DLS hydrodynamic diameter (D_h) of aggregates in water as a function of PEG feed ratio. Hydrodynamic diameter was measured after 7 days annealing at room temperature; **b**) Zeta potential of copolymer aggregates as a function of PEG content.

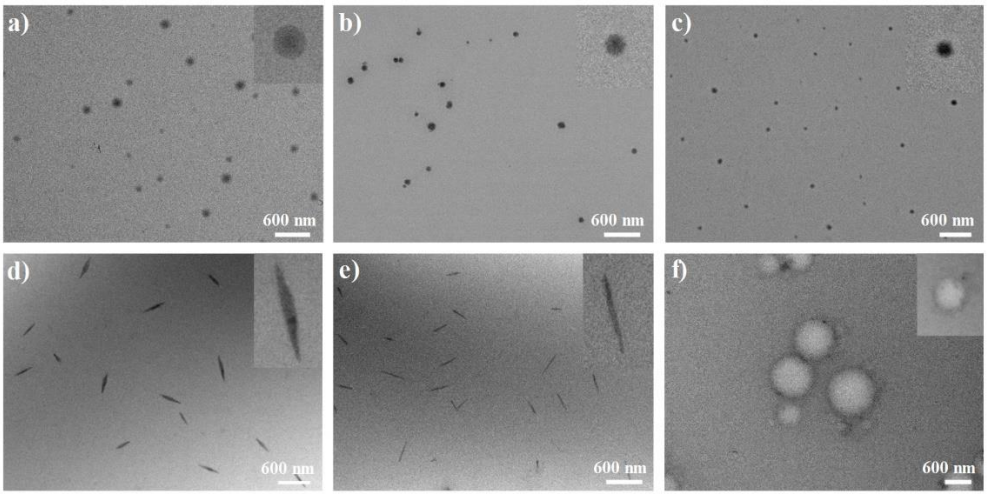

Figure 4.4 TEM images of the copolymers of **a)** C_CA1, **b)** C_CA2, **c)** C_CA3, **d)** C_CA4, **e)** C_CA5 and **d)** B_CA. TEM images were taken from an aqueous solution at a concentration of 5 mg/mL after one-month annealing at room temperature. Inset images show the local zoom in morphologies.

The morphology of the aggregates formed by different copolymers in pure DI water was visualized by TEM and AFM. All the copolymers self-assembled into different morphologies in water. The aqueous solution of copolymers was stabilized at room temperature for one month; then the solution was drop cast on the carbon coated TEM grid for imaging (Figure 4.4). The morphology of C_CA1, C_CA2 and C_CA3 copolymers was observed to be a spherical aggregate. TEM images also showed the size decreases with increasing the certain mole % of PEG (until 30%). The C_CA4 and C_CA5 copolymers were exhibited lenticular and rod-like aggregates respectively. The average diameter of C_CA1 is around 350-350 nm, and the average length of C_CA4 and C_CA5 is 350-500 and 350-600 nm with center diameters of 85-90 and 30-35 nm respectively, as measured by TEM. The result indicates that block copolymers with a lower PEG (<30 mole %) or higher cholic acid preferably form sphere type aggregates, while copolymers with higher PEG blocks tend to form a fiber or rod-like shaped aggregates. This is due to the higher percentage of the neutral PEG unit increasing the overall solubility of the copolymer,

allowing the more hydrophilic units of the copolymer to come in contact with water. Moreover, the addition of the neutral PEG unit significantly decreases the repulsive interactions among the positively charged cholic acid moiety, thus the lower interfacial area is favored and leading to an extended conformational rearrangement in the polymer chain. This allows the higher PEG-containing copolymers to form lenticular or rod-like shaped aggregates. The central region of the spheres and rods in TEM images show darker contrast represent the rigid skeleton from the bile acid derivatives where the electron beam can traverse through more materials than in the edge. The AFM images (Figure 4.18) also confirms the same type of morphology.

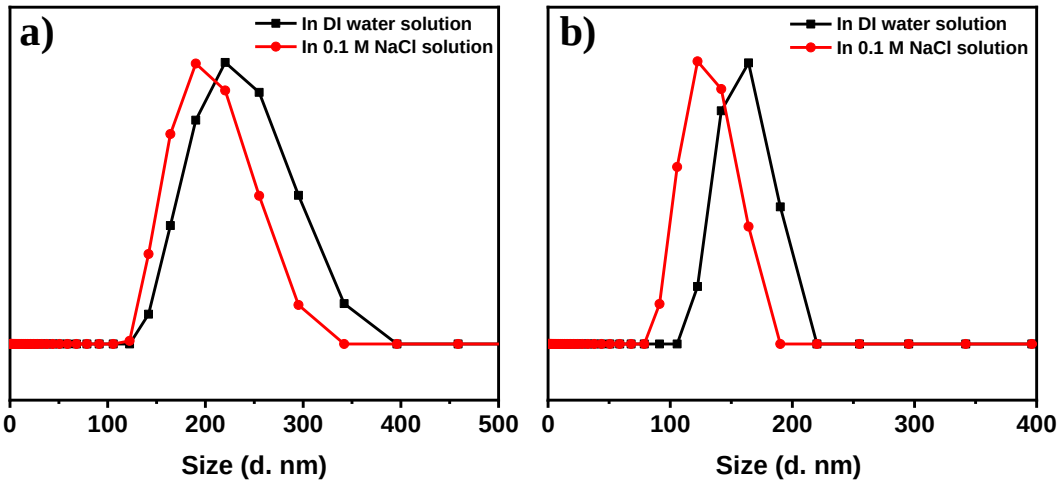

Figure 4.5 Average size distribution graph from DLS measurement of the aqueous solution of the copolymers with concentration 1mg/mL after one week annealing at 25 ^{o}C: a) C_CA1 in DI water (black) and 0.1 M NaCl solution (red); b) C_CA4 in DI water (black) and 0.1 M NaCl solution (red).

Aggregation behavior of the positively charged copolymers in aqueous solution can also be regulated by the refinement of ionic interaction. Herein, external electrolyte (0.1 M NaCl) was added to the copolymer solutions. All the copolymers were formed spherical aggregates after the addition of 0.1M NaCl salt in the solution, which was confirmed by

the TEM images (Figure 4.19). The DLS measurement showed that the hydrodynamic diameter (D_h) of all the copolymers was significantly decreased (Figure 4.4) which is potentially due to the salt ion minimizing the repulsion between the positively charged blocks leading to chain contraction. Moreover, the solution will lead to a Debye-Huckel shielding effect, where the polymer chains undergo a conformational transition adopting a collapsed, more entropically favored conformation. The size of the aggregates decreases with a decrease of hydrophilic blocks within the copolymers. We observed that a higher cholic acid block-containing copolymer formed larger size aggregates due to the repulsive force among the positive charges allow the polymer coils to occupy a larger volume in solution.

The aggregation behavior can be further influenced by varying the charge density of the polyelectrolyte chain. To investigate the effect of charge density on the morphology, we synthesized different mole % PEG-containing one and two QAC group containing lithocholic acid (C_LCA) and deoxycholic acid (C_DCA) copolymers respectively. The dialyzed solution of both copolymers also formed aggregates confirmed by the TEM imaging (Figure 4.6). C_DCA1 and C_DCA2 both formed rod-like aggregates. The average diameter of C_DCA1 is around 45-50 nm with varying lengths of 220-260 nm, whereas the average diameter of C_DCA2 is around 20-25 nm with a varying length of 300-400 nm. These results also demonstrate that the higher the mole % of PEG decreases the diameter of the rod-like aggregates. On the other hand, the C_LCA copolymer formed fiber-like aggregates with diameter around 8-10 nm and an elongated length to several micrometers. Therefore, the lower charge density leads to form rod-like structures.

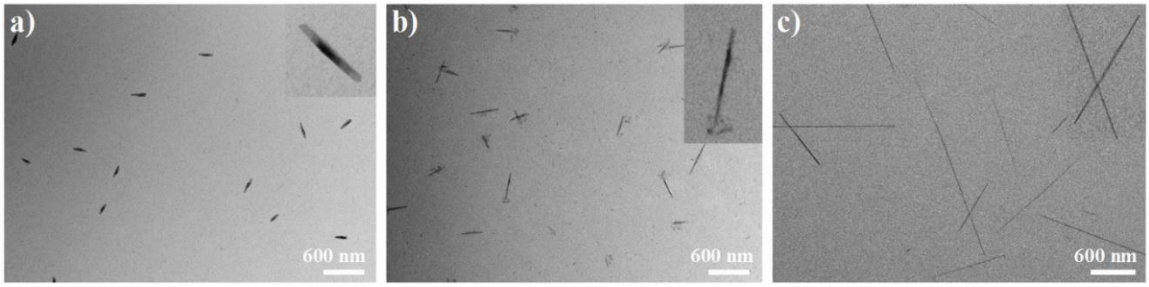

Figure 4.6 TEM images of the copolymers of (a) C_DCA1, (b) C_DCA2, (c) C_LCA. TEM images were taken from the water solution at a concentration of 5 mg/mL after one-month annealing at room temperature.

We also investigated the self-assembly behavior of 40 mole % PEG-containing cholic acid-based cationic block copolymers (B_CA). B_CA block copolymer only formed large vesicle type aggregates with an average diameter of 0.6-1 μm in aqueous solution after one-month incubation at room temperature. The central region in the TEM images of B_CA (Figure 4.4f) appears brighter because the electron beams need to pass through the fewer materials, which also confirms the formation of the vesicles with hollow centers.[50] The block copolymer (B_CA) from vesicles because the curvature in the vesicles is stabilized by preferential segregation of the short cationic hydrophilic segments to the inside of the vesicles, and the long chains to the outside. The repulsion among the longer corona chains is clearly greater than that among, the shorter chains. Therefore, segregation of the hydrophilic blocks, which allows the formation of an asymmetric lamella, stabilizes the curvature of the vesicles.[51]

To expedite the self-assembly process, we further investigated the morphological behavior of the aqueous solution of copolymers at elevated temperature; we choose 37 ^{o}C as an example because it is body temperature and our copolymer potentially can be applied in the body. Usually, amphiphilic copolymers are organized via various supramolecular interactions or reversible associations such as hydrophobic interactions, hydrogen bonding,

van der Waals forces, and electrostatic interactions. Because of the weak interactions, the self-assembly process can be affected by environmental conditions.[52] Normally, cationic and poly (ethylene glycol) (PEG) containing copolymers changed their morphology in aqueous solution with response to temperature.[53] Moreover, the hydrophobic interactions are favored by increasing the temperatures.[36, 50] An aqueous solution of C_CA1, C_CA4, C_DCA1, and C_DCA2 was incubated at 37 ºC for the different time intervals (2, 4, 6, 12, and 24 hrs) and monitored by TEM. From the TEM images, we observed that temperature is able to expedite the formation of the spherical, lenticular and rod-like or fiber-like aggregates. C_CA1 and C_CA4 are able to form the sphere and lenticular shape within 24 hrs, whereas the C_DCA1 and C_DCA2 can from a rod-like shape within two hours (Figure 4.20). The rate of the formation of aggregation quantities decrease with an increasing number of QAC groups in the bile acid derivatives (such as from deoxycholic acid to cholic acid), the similar results have been observed by others.[37] These results demonstrate that the higher the hydrophobicity faster the formation of aggregates. This is because a higher content of hydrophobic segments will result in stronger interactions between the hydrophobic face (convex β-face, shown in Figure 4.10) of bile acid derivatives, leading to a more stable structure (Figure 4.1). Aggregation numbers are decreasing with increasing the number hydroxyl group in the bile acid derivatives, which also can be tuned with different stimuli such as temperature and added electrolyte, etc.[37]

The time-dependent temperature effect study also demonstrates the aggregation behavior (such as the formation of the sphere and rod-like type aggregates) of the copolymers in DI water. TEM images (Figure 4.7a) of C_CA1 reveals that after 2 hrs of incubation at 37 ºC, the copolymers initially associate as unimers or small aggregates in aqueous solution. After

successive time under incubation, the unimers starts forming vesicle type aggregates. After 12 hrs, clear vesicles with size around 600-700 nm appeared. These vesicles subsequently collapse into spherical shape aggregates with diameters averaging around 440 ± 100 nm (measured from TEM images at 24 hrs). Similarly, the aggregation behavior of C_CA4 in DI water was observed in the TEM images (Figure 4.21) that also displayed the association of unimers into fibrous supramolecular aggregates (4 hrs TEM images). As the aggregates approach each other, they begin to fuse linearly after 4 hrs of incubation. After 6 hrs, aggregates continually expand to a fused rod-like structure. The diameter of the spherical aggregates is similar to the width of the fused rod-like structure, which confirms the linear fusion of the spherical aggregates fused to form a long rod. The rod then begins to split into individual molecular rods that may be because of the static charge repulsion of QAC groups arrayed at the tubular surface. The molecular rod subsequently starts to show the signs of fragmentation after 12 hrs, and ultimately detach into multiple lenticular shapes. The possible mechanism for the whole process is graphically represented in Figure 4.8. The copolymers solutions in DI water go through different intermediate/ metastable states to form the sphere and lenticular or rod-like aggregates, which we speculate the equilibrium states. These spheres and rod-like structures are stable at same environmental conditions. These structures are preserved even for six months in room temperature. The self-assembly behavior of all the bile acid-based amphiphilic copolymers in water suggests that the formation of sphere and lenticular or rod-like shape aggregates are dictated by the supramolecular interaction of the facial amphiphilic structure of bile acid derivatives and the hydrophilic PEG contents. Notably, the main driving force is the hydrophobic interaction between the convex β-face of bile acid derivatives that form the core of the

aggregates. Then depending on the charge density and neutral PEG content reveals different morphology (Figure 4.1). Lower the amount of PEG drives the formation the of spherically shaped aggregates, where higher PEG content leads to the formation of lenticular or rod-like aggregates. Higher PEG ratio reduces the repulsion of the cationic charge and leading to form the stable lenticular or rod-like shaped structures (Figure 4.1).

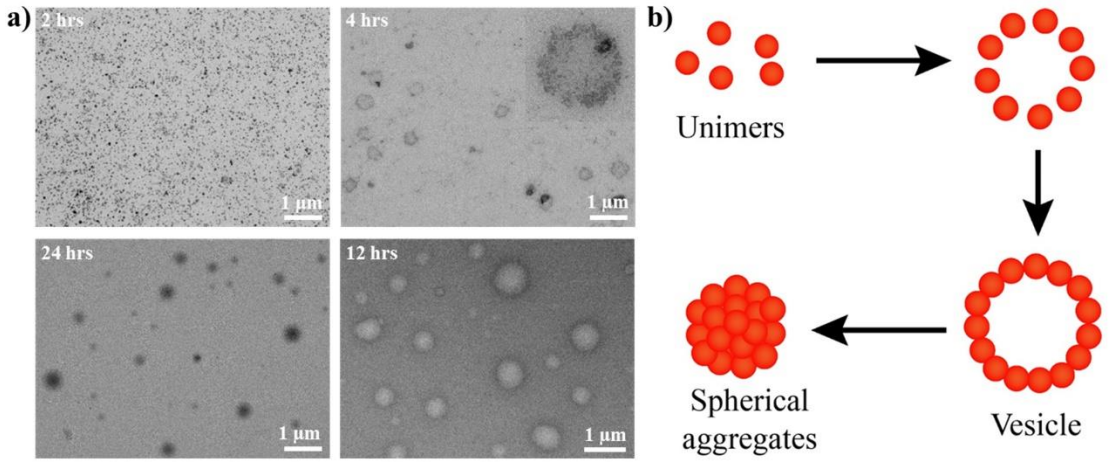

Figure 4.7 TEM images evidencing the formation of spherical aggregates; **a)** TEM images of the copolymers of C_CA1 after 2, 4, 12, and 24 hrs annealing at 37 ºC temperature. TEM images were taken from the water solution of C_CA1 at a concentration of 5 mg/mL; **b)** Proposed mechanism for the formation of spherical aggregates.

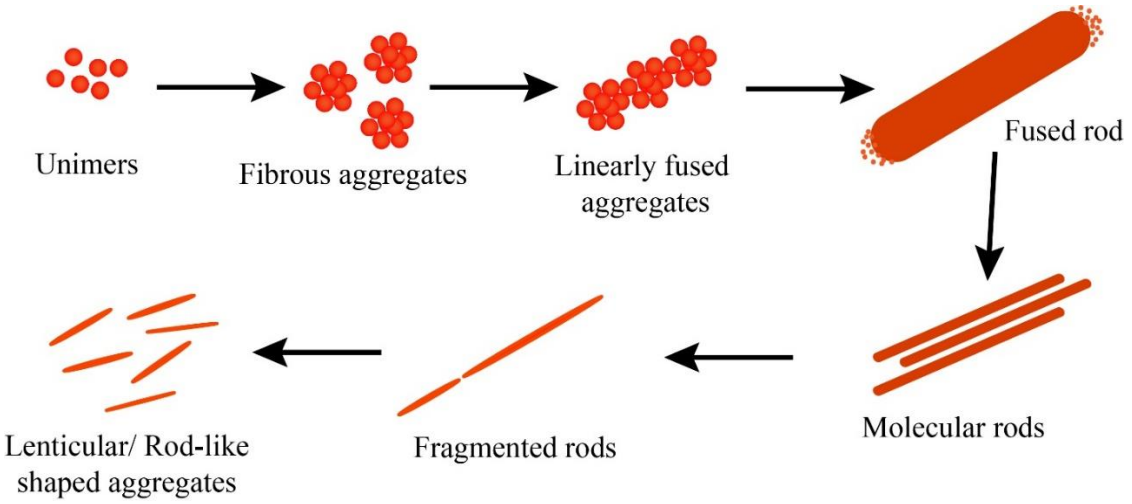

Figure 4.8 Proposed mechanism for the formation of lenticular or rod-like shaped aggregates.

Finally, we investigated the homopolymer morphology to confirm the effect of facial amphiphilicity. The DLS results indicated that the homopolymer also forms some aggregates. The DLS size of the cholic acid-based homopolymer (H_CA) is around 300 nm. Similar to the copolymer solutions, H_CA polymer was also incubated for one-month in aqueous solution at room temperature to investigate the self-assembly behavior. TEM images revealed that H_CA formed large size vesicles (Figure 4.22) while H_DCA formed some irregular shape aggregates, which is may be due to the lake of facial amphiphilicity and lower charge density. This result demonstrated that facial amphiphilicity leads all the polymers to form higher order aggregates in aqueous solutions through the arrangement of hydrophilic and hydrophobic components in the polymers (Figure 4.9).

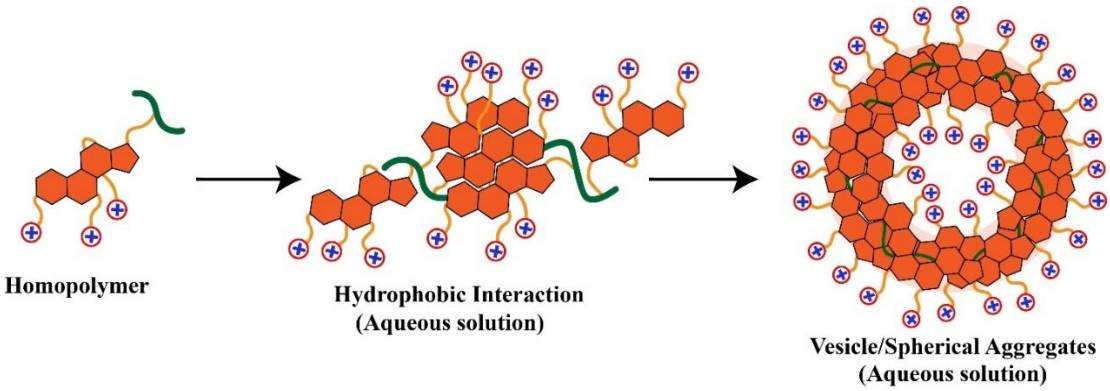

Figure 4.9 Formation of vesicles in water by homopolymers.

4.4 Conclusions

In summary, we have reported the synthesis of cationic amphiphilic gradient/blocky copolymers bearing a hydrophilic PEG chain and a hydrophobic steroid moiety (such as bile acid derivatives) possessing local facial amphiphilicity via living

reversible addition fragmentation transfer (RAFT) polymerization. All the copolymers are self-assembled in water to form spherical, lenticular or rod-like aggregates depending on the mole % of hydrophilic segments. These aggregates are driven towards formation by the hydrophobic interaction of the *β*-phase of the bile acid derivatives. Incorporation of PEG into the polymer improves the biocompatibility of the bile acid-based cationic copolymers. The supramolecular interaction from multicyclic natural product induced self-assembly can open a unique avenue for making different morphology such as spheres, vesicles and tubular shape structure via gradient/blocky copolymerization by tuning the level of amphiphilicity.

4.5 Experimental Section

Materials. All chemicals were purchased from commercial sources and used as received unless otherwise stated. Cholic acid (CA, ≥98%), deoxycholic acid (DCA, ≥98%), lithocholic acid (LCA, ≥98%), 2-hydroxyethyl methacrylate (HEMA, 97%), and 4-dimethylamino pyridine (DMAP, 99%), Poly(ethylene glycol) methyl ether methacrylate (PEGMA, average M_n = 500) were purchased from Sigma-Aldrich and used without further purification. 1-(3-dimethylaminopropyl)-3-ethyl carbodiimide hydrochloride (EDC.HCl, 98%) was purchased from TCI and used without further purification. 6-Bromohexanoyl chloride (97%), 4-bromobutanoyl chloride (97%), bromoacetyl bromide (98%) and trimethylamine (33% w/w in ethanol denatured with 2% cyclohexane) was purchased from Alfa-Aesar. 4-Cyano-4-(thiobenzylthio)pentanoic acid (CTP, 97%) was purchased from Strem Chemicals Inc. Azobisisobutyronitrile (AIBN, Sigma, 98%) and solvents such as hexanes, anhydrous N, N-dimethylformamide (DMF, 99.9%), tetrahydrofuran (THF), dichloromethane (DCM), etc. were purified by standard procedures. The (2-methacryloyloxy)ethyl cholate (MAECA), (2-

methacryloyloxy)ethyl deoxycholate (MAEDA), and (2-methacryloyloxy)ethyl lithocholate (MAELA) monomers were synthesized following our previous report. $CDCl_3$ (99.9% D), D_2O (99.9% D) and DMSO-d_6 (99.9% D) were purchased from Cambridge Isotope Laboratories, Inc.

Characterization. The monomer and compound purity and polymer conversion were monitored by proton nuclear magnetic resonance 300 MHz (^{1}H NMR) spectroscopy using Bruker Avance III HD 300 spectrometer. Spectra were recorded in deuterated chloroform, deuterium oxide or dimethylsulfoxide solvent in ppm (δ) with tetramethylsilane as an internal standard. Molecular weight and molecular weight distribution of polymers were measured by gel permeation chromatography (GPC) in THF equipped with a Waters 1525 Binary Pump, three Styragel columns, and a Waters 2414 Refractive Index (RI) detector. HPLC grade THF solvent was used as eluent at 35 °C with a flow rate of 1.0 mL/min. A series of narrowly-dispersed polystyrene standards obtained from Polymer Laboratories were used to calibrate the GPC system. GPC samples were prepared by dissolving polymers in HPLC grade THF at a concentration of 5-10 mg/mL and filtered by PTFE micro-filters with an average pore size of 0.2 μm.

Dynamic light scattering (DLS) and Zeta potential. A Zetasizer Nano series ZEN3690 (Malvern Instruments, Malvern, UK) instrument was used to measure the hydrodynamic diameter (Z-average) and Zeta potential of the aggregates. The samples were prepared by dissolving dry copolymer in filtered (0.2 μm GHP membrane filter) deionized water with a concentration of 1 mg/mL. The solutions were at pH 7.0, and the measurements were carried out at 25 °C. The data processing was done using the general-purpose algorithms

provided in the Zetasizer Software. Sample measurements were acquired in triplicate and reported as an average and standard error.

Atomic Force Microscopy (AFM). AFM was accomplished using a Multimode Nanoscope V system (Bruker, Santa Barbara, CA). Tapping mode AFM was used to map the topography by tapping the surface using an oscillating tip. The measurements were achieved using commercial Si cantilevers with a nominal spring constant and resonance frequency at 20–80 Nm^{-1} and 230–410 kHz, respectively (TESP, Bruker AFM Probes, Santa Barbara, CA).

Preparation of Thin Films. Thin films were prepared by drop casting from a water solution of copolymers onto an oxidized silicon wafer (100 nm thick thermal oxide). The silicon wafers were cleaned using acetone–water mixture and then isopropyl alcohol or ethanol and dried under nitrogen flow. After drop casting, the films were dried over-night under the open air.

Transmission Electron Microscopy (TEM). A JOEL 1400 plus transmission electron microscope (TEM) was applied to take images at an operating voltage of 120 kV. TEM samples were prepared by dropping solution on carbon-supported copper grids and then dried before observation.

Synthesis of Gradient Copolymers. Methacrylate monomers (MAECA and PEGMA) were copolymerized using a typical RAFT polymerization technique.[1] For example, C_CA4 copolymer was synthesized using the predetermined ratios (e. g. [Monomer] : [AIBN] : [CTP] = 60: 0.2: 1). MAECA (0.40 g, 0.769 mmol), PEGMA (0.384g, 0.769 mmol), 4-Cyano-4-(thiobenzylthio)pentanoic acid (CTP) (7.16 mg, 0.0256 mmol), and

azobisisobutyronitrile (AIBN) (0.84 mg, 5.12 µmol) were placed in a 10 mL Schlenk flask and dissolved in N, N-dimethylformamide (DMF) (1 mL). The mixture was performed with three freeze-pump-thaw cycles protected under nitrogen and immersed into a preheated oil bath set at 70 °C. After a certain period (17 hrs), the polymerization was quenched by exposure to air and cooling under an ice water bath. The reaction mixture was precipitated twice into a mixture of hexane and DCM (80 : 20) and finally dissolved in THF and precipitated into hexane. The polymer was dried under vacuum.

Synthesis of Block Copolymers. Block copolymer was synthesized using living one-pot sequential RAFT polymerization technique. At first, MAECA was polymerized with predetermined ratios (e. g. [MAECA] : [AIBN] : [CTP] = 30: 0.2: 1). MAECA (0.40 g, 0.769 mmol), CTP (7.16 mg, 0.256 mmol), and AIBN (0.84 mg, 5.13 µmol) were dissolve in dry DMF (1 mL) in a schlenk flask. The mixture was performed with three freeze-pump-thaw cycles protected under nitrogen and immersed into a preheated oil bath set at 70 °C. Once all the monomers were consumed (after 6hrs) confirmed by ^{1}H NMR, second batch of monomer such as PEGMA (0.384 g, 0.769 mmol), AIBN (0.42 mg, 2.56 µmol) and dry DMF (0.5 mL) were mixed together and performed three freeze-pump-thaw cycles protected under nitrogen. Then, this mixture was added to the previous reaction mixture and continued stirring for another 36 hrs. The reaction mixture was quenched by cooling in ice. The final product was isolated by precipitating in cold hexanes for three times. The reaction was confirmed by ^{1}H NMR (Figure 4.16), and the molecular weight was measured by GPC (Figure 4.16).

Post-polymerization Modification. Post-polymerization modification was carried out by following our previous method. Briefly, the C_CA4 copolymer (400 mg) was placed in a

25 mL round bottom flask and dissolved in anhydrous DMF (2 mL). An excess amount of 6-bromohexanoyl chloride (3 mL) was added to the polymer solution dropwise at room temperature. The reaction mixture was allowed to stir at 55 ^{0}C for 48 hrs. After the completion of the reaction, the reaction mixture was precipitated into methanol. The product was redissolved in DCM (2 mL), precipitated in methanol twice, and dried under high vacuum. The reaction was confirmed by ^{1}H NMR and FTIR spectroscopy (Figure 4.12**)**. Similarly, C_CA1, CCA2, C_CA3, C_CA5, C_DCA1, C_DCA2, C_LCA, and B_CA copolymers were modified. ^{1}H NMR spectra of post-modified C_DCA2, C_LCA and B_CA copolymer with 6-bromohexanoyl chloride is shown in Figure 4.15a, b, and 4.16a respectively**.**

Synthesis of QAC Containing Polymers. Quaternization of all copolymers was carried out by following our previous method. As an example: the product of post-modified C_CA2 polymer (300 mg) was placed in a 25 mL round bottom flask and sealed with a rubber septa and dissolved in DMF (4 mL). Then, trimethylamine solution (33wt%, 9 mL) in ethanol was added to the reaction mixture at room temperature. The reaction mixture was stirred for 24 hrs in a closed reaction vessel at 55 ^{o}C. After cooling and concentrating the reaction mixture, the resulting solution was precipitated in THF and centrifuged to collect the product. The product was washed with THF and dried under high vacuum. Finally, the product was further purified by dialysis against DI water (1 L × 3) for 24 hrs. The solution in a dialysis bag was collected and freeze-dried to obtain a white product. All the copolymers and block copolymer were similarly quaternized.

Additional Figures and Tables

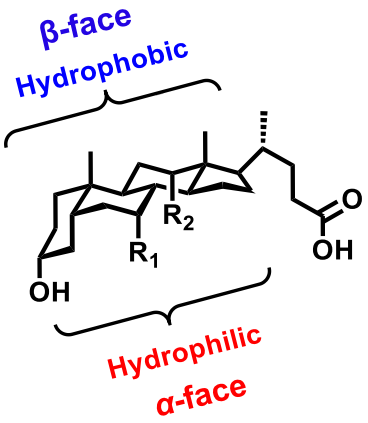

Cholic acid (R_1 and R_2 = OH)

Deoxycholic acid (R_1 = H and R_2 = OH)

Lithocholic acid (R_1 and R_2 = H)

Figure 4.10 Structures of bile acid derivatives.

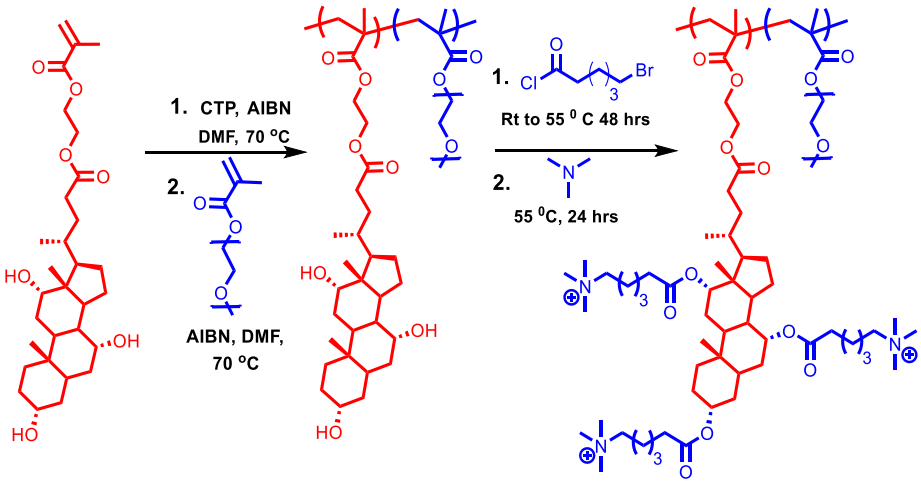

Figure 4.11 Synthesis of QAC charge containing block copolymer (B_CA)**.**

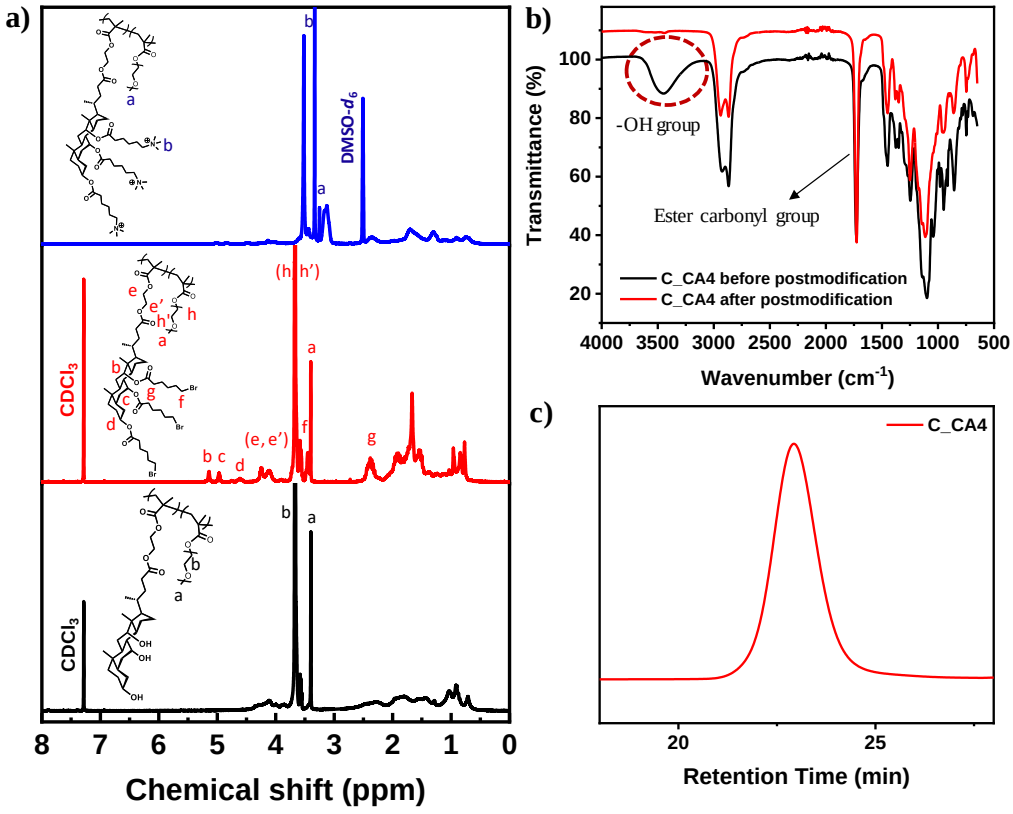

Figure 4.12 a) ^{1}H NMR Spectra of C_CA4 copolymer; b) FTIR spectra of C_CA4 copolymer before modification (black) and copolymer after post-polymerization modification (red); c) GPC traces of the C_CA4.

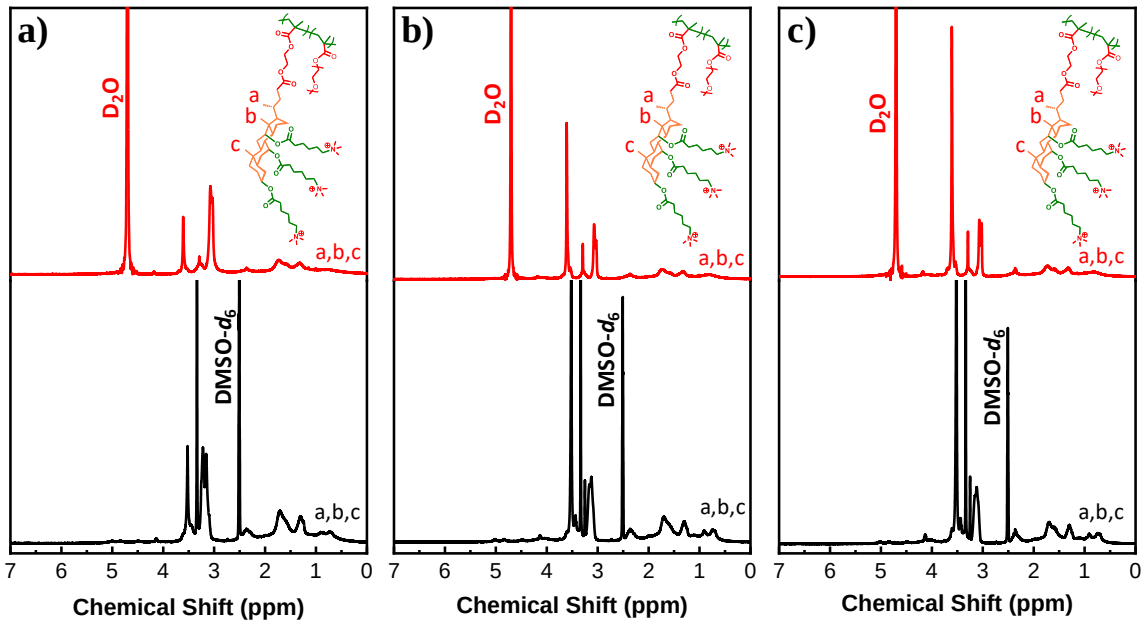

Figure 4.13 ^{1}H NMR Spectra of a) C_CA1; b) C_CA4 and c) C_CA5 in DMSO and D_2O solvent at 25 ^{o}C.

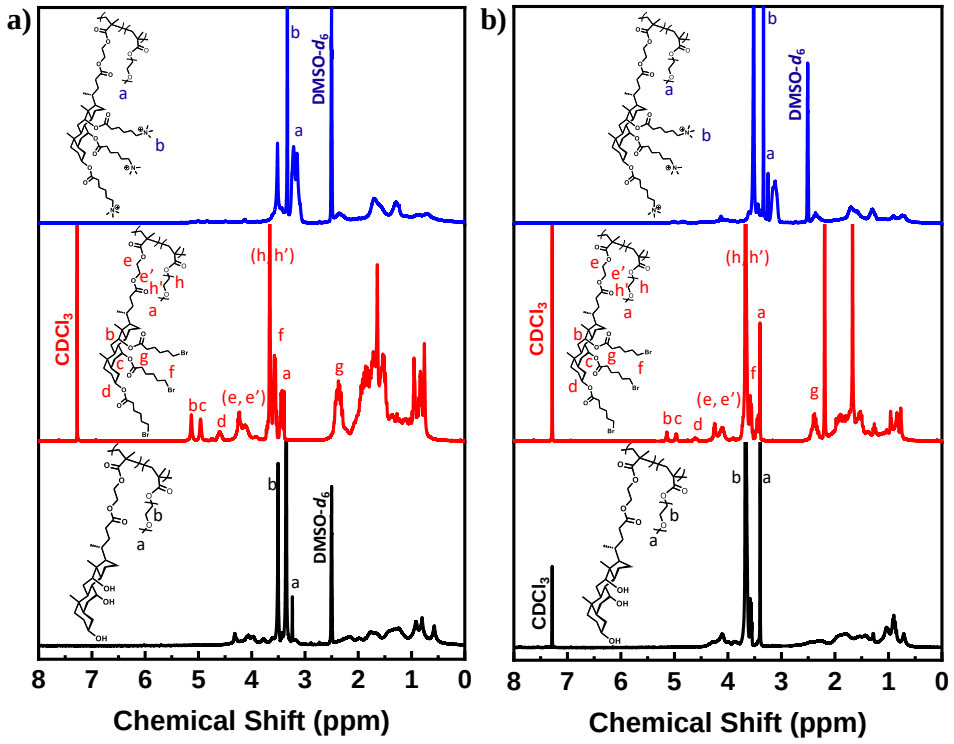

Figure 4.14 ^{1}H NMR spectra of **a)** C_CA1; **b)** C_CA5 copolymer;

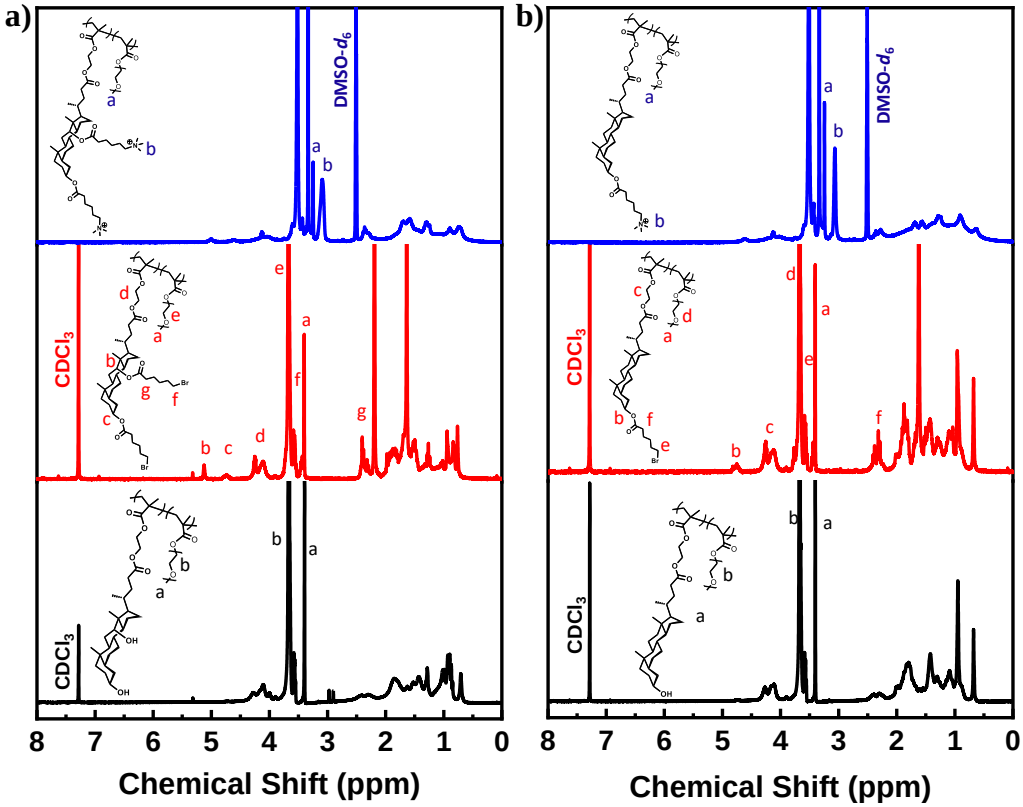

Figure 4.15 ^{1}H NMR spectra of **a)** C_DCA2; **b)** C_LCA copolymer.

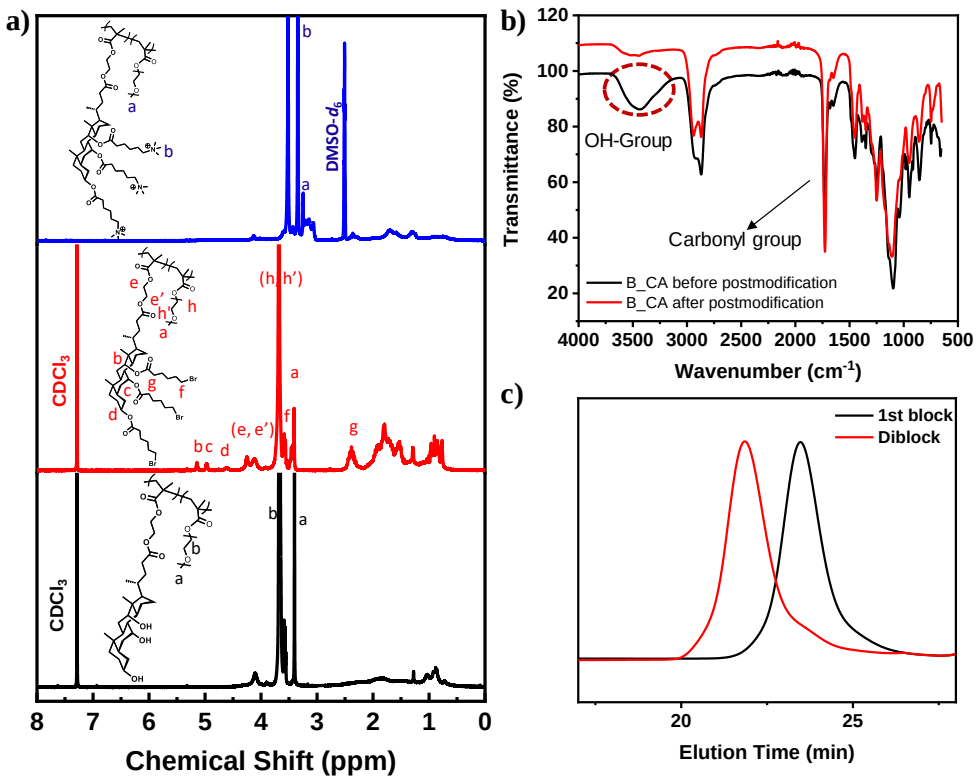

Figure 4.16 Characterization of B_CA block copolymer. **a)** ^{1}H NMR spectra; **b)** FTIR spectra; **c)** GPC traces for the B_CA block copolymer.

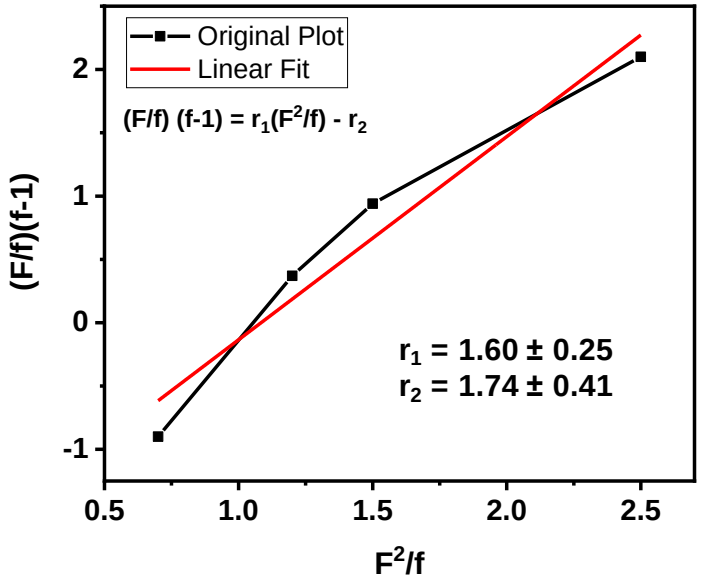

Figure 4.17 Fineman-Ross plot for the RAFT copolymerization of MAECA and PEGMA monomer.

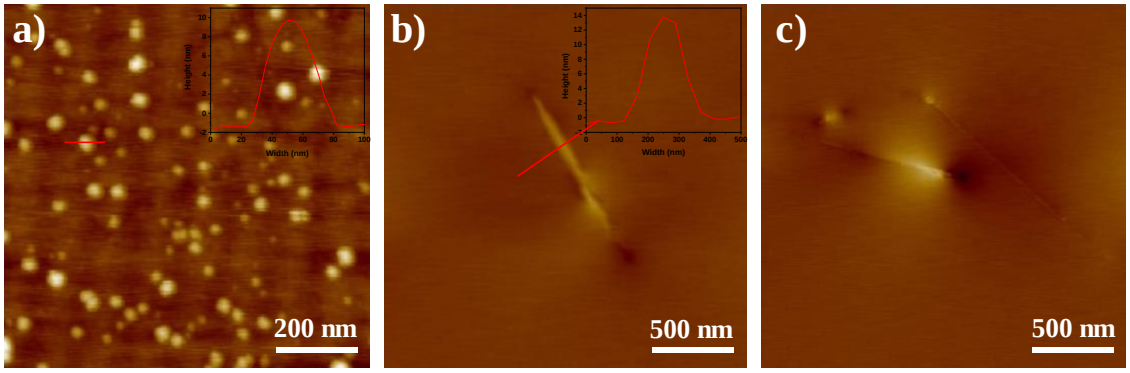

Figure 4.18 AFM images of the copolymers of (a) C_CA1, (b) C_CA4, (c) C_CA5. AFM images were taken from the water solution at a concentration of 5 mg/mL after one-week annealing at room temperature.

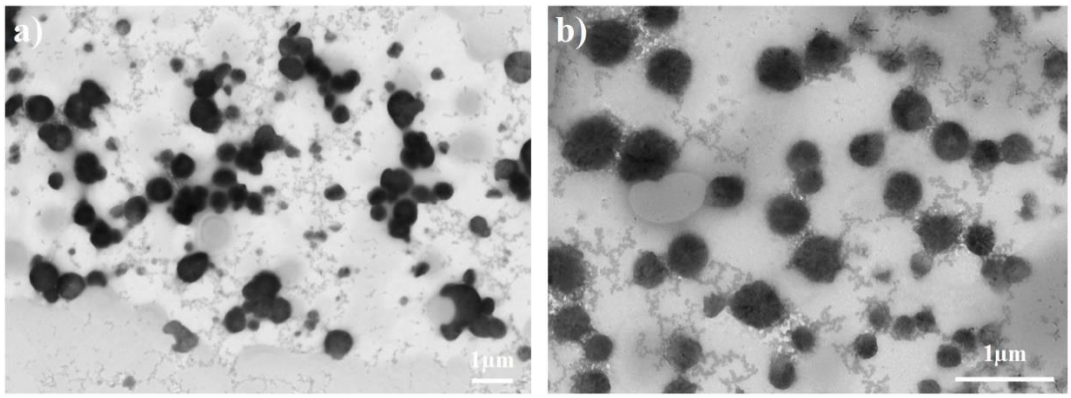

Figure 4.19 TEM images of the copolymers of (a) C_CA1, (b) C_CA4. TEM images were taken from the salt (0.1 M NaCl) solution at a concentration of 5 mg/mL after one-week annealing at room temperature.

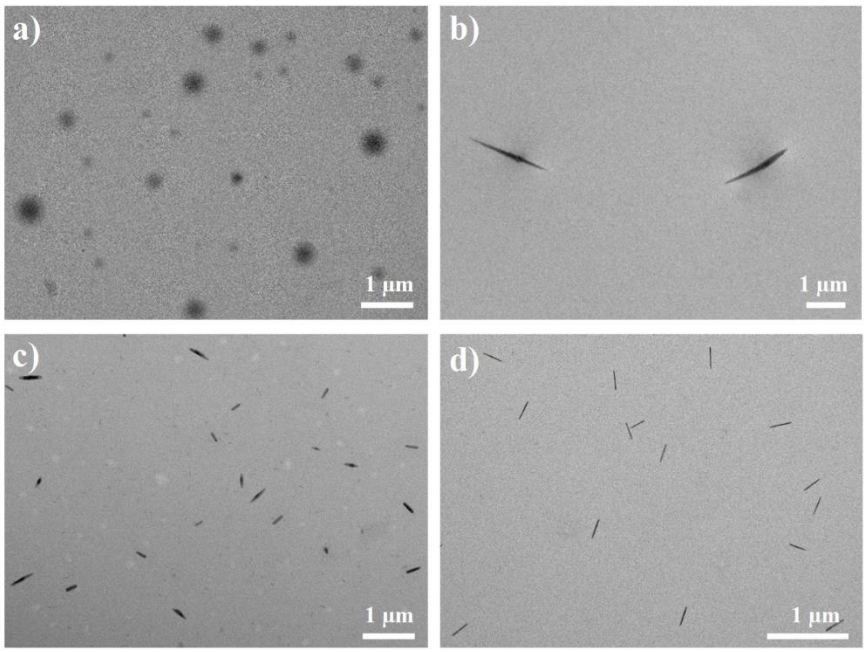

Figure 4.20 TEM images of the copolymers of (a) C_CA1 (18 hrs), (b) C_CA4 (24 hrs), (c) C_DCA1 (2 hrs), (d) C_DCA2 (2 hrs). TEM images were taken from the water solution of C_CA1, C_CA4, C_DCA1, and C_DCA2 at a concentration of 5 mg/mL after annealing at 37 ^{o}C temperature.

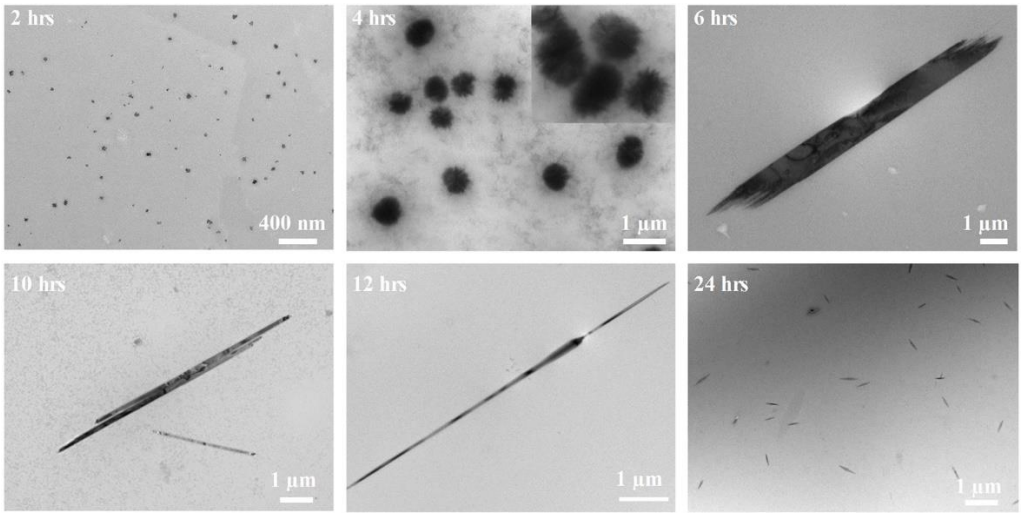

Figure 4.21 TEM images of the copolymers of C_CA4 after 2, 4, 6, 10, 12, and 24 hrs. TEM images were taken from the water solution at a concentration of 5 mg/mL after annealing at 37 ^{o}C temperature.

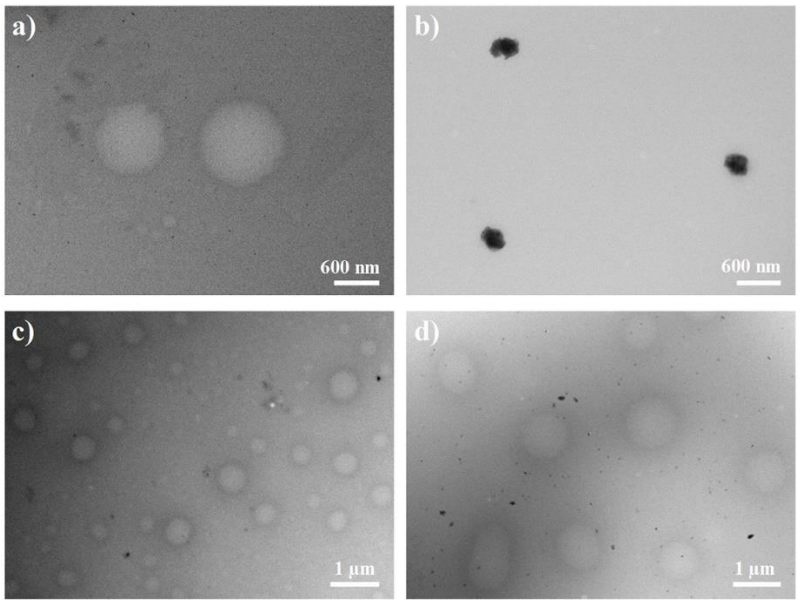

Figure 4.22 TEM images of homopolymers; a) H_CA after one-month incubation at RT; b) H_CDA after one-month incubation at RT; c) H_CA after 24 hrs incubation at 37 ^{o}C temperature; d) H_CA after 24 hrs incubation at 37 ^{o}C temperature.

Table 4.2 Size distribution graph from DLS measurement of the aqueous solution of the copolymers (concentration 2mg/mL) at 25 ^{o}C.

Co-polymers	D_h of Aggregates (nm)				Zeta potential (ζ) (mV)	
	In DI water after 4 hrs	In DI water after one week	0.1M NaCl Solution after 4 hrs	0.1M NaCl Solution after one week	In DI water	0.1M NaCl Solution
C_CA1	310.3 ±	320.0±6.1	220±2	203.7 ± 8.9	+69.4±3.3	25.7±1.2
C_CA2	304.1±32.7	259.7±19.4	190.6±12.9	152.2±21.3	+68.4±2.1	+24.7±1.2
C_CA3	237.3±32.1	180.7±3.1	175.1±12.2	145.8±15.1	+64.6±0.9	+20.5±2.2
C_CA4	260.3 ±	334.9± 41.2	174±1	135.1±16.7	+50.4±4.1	+20±1
C_CA5	431.6 ±	472.3±180	110±3	145.4±15.3	+46.5±3.1	+19±1
C_DCA1	404.1±13.7	318.4± 17			+58.8±7.2	
C_DCA2	405.2±52.3	342.2± 16	166.2 ± 6.8	93.7 ± 17.8	+55.7±1.1	+15.1±2
C_LCA	314.5±13.7	120.3±14		40.9 ± 1.9	+50.1±1.2	
B_CA	322.2 ±	277.8±13.4	156 ±21.7	150.0 ±2.6	+59.8±2	+12.5±0.7

4.6 References

1. Karsenti, E., Self-organization in cell biology: a brief history. *Nature Reviews Molecular Cell Biology* **2008,** *9*, 255.
2. Whitesides, G. M.; Grzybowski, B., Self-Assembly at All Scales. *Science* **2002,** *295* (5564), 2418.
3. Dill, K. A.; MacCallum, J. L., The Protein-Folding Problem, 50 Years On. *Science* **2012,** *338* (6110), 1042-1046.
4. Stupp, S. I., Self-Assembly and Biomaterials. *Nano Lett.* **2010,** *10* (12), 4783-4786.
5. Bates, F. S.; Hillmyer, M. A.; Lodge, T. P.; Bates, C. M.; Delaney, K. T.; Fredrickson, G. H., Multiblock Polymers: Panacea or Pandora's Box? *Science* **2012,** *336* (6080), 434-440.
6. Mai, Y.; Eisenberg, A., Self-assembly of block copolymers. *Chem. Soc. Rev.* **2012,** *41* (18), 5969-5985.
7. Moughton, A. O.; O'Reilly, R. K., Thermally induced micelle to vesicle morphology transition for a charged chain end diblock copolymer. *Chem. Commun.* **2010,** *46* (7), 1091-1093.
8. Blanazs, A.; Madsen, J.; Battaglia, G.; Ryan, A. J.; Armes, S. P., Mechanistic Insights for Block Copolymer Morphologies: How Do Worms Form Vesicles? *J. Am. Chem. Soc.* **2011,** *133* (41), 16581-16587.
9. Bhargava, P.; Zheng, J. X.; Li, P.; Quirk, R. P.; Harris, F. W.; Cheng, S. Z. D., Self-Assembled Polystyrene-block-Poly(ethylene Oxide) Micelle Morphologies in Solution. *Macromolecules* **2006,** *39*, 4880.
10. Jain, S.; Bates, F. S., On the Origins of Morphological Complexity in Block

Copolymer Surfactants. *Science* **2003,** *300*, 460.

11. Discher, D. E.; Eisenberg, A., Polymer Vesicles. *Science* **2002,** *297*, 967.
12. Li, L.; Raghupathi, K.; Song, C.; Prasad, P.; Thayumanavan, S., Self-Assembly of Random Copolymers. *Chem. Commun.* **2014,** *50*, 13417.
13. Mavila, S.; Eivgi, O.; Berkovich, I.; Lemcoff, N. G., Intramolecular Cross-Linking Methodologies for the Synthesis of Polymer Nanoparticles. *Chem. Rev.* **2016,** *116*, 878.
14. Terashima, T.; Sugita, T.; Fukae, K.; Sawamoto, M., Synthesis and Single-Chain Folding of Amphiphilic Random Copolymers in Water. *Macromolecules* **2014,** *47*, 589.
15. Ogura, Y.; Artar, M.; Palmans, A. R. A.; Sawamoto, M.; Meijer, E. W.; Terashima, T., Self-Assembly of Hydrogen-Bonding Gradient Copolymers: Sequence Control via Tandem Living Radical Polymerization with Transesterification. *Macromolecules* **2017,** *50*, 3215.
16. Ogura, Y.; Terashima, T.; Sawamoto, M., Amphiphilic PEG-Functionalized Gradient Copolymers via Tandem Catalysis of Living Radical Polymerization and Transesterification. *Macromolecules* **2017,** *50*, 822.
17. Hattori, G.; Hirai, Y.; Sawamoto, M.; Terashima, T., Self-Assembly of PEG/dodecyl-Graft Amphiphilic Copolymers in Water: Consequences of the Monomer Sequence and Chain Flexibility on Uniform Micelles. *Polym. Chem.* **2017,** *8*, 7248.
18. Ueda, M.; Hashidzume, A.; Sato, T., Unicore–Multicore Transition of the Micelle Formed by an Amphiphilic Alternating Copolymer in Aqueous Media by Changing Molecular Weight. *Macromolecules* **2011,** *44*, 2970.
19. Jain, S.; Bates, F. S., On the Origins of Morphological Complexity in Block Copolymer Surfactants. *Science* **2003,** *300* (5618), 460-464.

20. Discher, D. E.; Eisenberg, A., Polymer Vesicles. *Science* **2002,** *297* (5583), 967-973.

21. Cui, H.; Chen, Z.; Zhong, S.; Wooley, K. L.; Pochan, D. J., Block Copolymer Assembly via Kinetic Control. *Science* **2007,** *317* (5838), 647-650.

22. Wang, X.; Guerin, G.; Wang, H.; Wang, Y.; Manners, I.; Winnik, M. A., Cylindrical Block Copolymer Micelles and Co-Micelles of Controlled Length and Architecture. *Science* **2007,** *317* (5838), 644.

23. Gilroy, J. B.; Gädt, T.; Whittell, G. R.; Chabanne, L.; Mitchels, J. M.; Richardson, R. M.; Winnik, M. A.; Manners, I., Monodisperse cylindrical micelles by crystallization-driven living self-assembly. *Nat. Chem.* **2010,** *2*, 566.

24. Rupar, P. A.; Chabanne, L.; Winnik, M. A.; Manners, I., Non-Centrosymmetric Cylindrical Micelles by Unidirectional Growth. *Science* **2012,** *337* (6094), 559.

25. Qiu, H.; Hudson, Z. M.; Winnik, M. A.; Manners, I., Multidimensional hierarchical self-assembly of amphiphilic cylindrical block comicelles. *Science* **2015,** *347* (6228), 1329.

26. Derry, M. J.; Fielding, L. A.; Armes, S. P., Polymerization-induced self-assembly of block copolymer nanoparticles via RAFT non-aqueous dispersion polymerization. *Prog. Polym. Sci.* **2016,** *52*, 1-18.

27. Warren, N. J.; Armes, S. P., Polymerization-Induced Self-Assembly of Block Copolymer Nano-objects via RAFT Aqueous Dispersion Polymerization. *J. Am. Chem. Soc.* **2014,** *136* (29), 10174-10185.

28. Canning, S. L.; Smith, G. N.; Armes, S. P., A Critical Appraisal of RAFT-Mediated Polymerization-Induced Self-Assembly. *Macromolecules* **2016,** *49* (6), 1985-2001.

29. Li, L.; Raghupathi, K.; Song, C.; Prasad, P.; Thayumanavan, S., Self-assembly of

random copolymers. *Chem. Commun.* **2014,** *50* (88), 13417-13432.

30. Kale, T. S.; Klaikherd, A.; Popere, B.; Thayumanavan, S., Supramolecular Assemblies of Amphiphilic Homopolymers. *Langmuir* **2009,** *25* (17), 9660-9670.
31. Zhu, Y.; Yang, B.; Chen, S.; Du, J., Polymer vesicles: Mechanism, preparation, application, and responsive behavior. *Prog. Polym. Sci.* **2017,** *64*, 1-22.
32. Hattori, G.; Hirai, Y.; Sawamoto, M.; Terashima, T., Self-assembly of PEG/dodecyl-graft amphiphilic copolymers in water: consequences of the monomer sequence and chain flexibility on uniform micelles. *Polym. Chem.* **2017,** *8* (46), 7248-7259.
33. Shibata, M.; Matsumoto, M.; Hirai, Y.; Takenaka, M.; Sawamoto, M.; Terashima, T., Intramolecular Folding or Intermolecular Self-Assembly of Amphiphilic Random Copolymers: On-Demand Control by Pendant Design. *Macromolecules* **2018,** *51* (10), 3738-3745.
34. Hattori, G.; Takenaka, M.; Sawamoto, M.; Terashima, T., Nanostructured Materials via the Pendant Self-Assembly of Amphiphilic Crystalline Random Copolymers. *J. Am. Chem. Soc.* **2018,** *140* (27), 8376-8379.
35. Shao, M.; Chang, Q.; Dodelet, J.-P.; Chenitz, R., Recent Advances in Electrocatalysts for Oxygen Reduction Reaction. *Chem. Rev.* **2016,** *116* (6), 3594-3657.
36. di Gregorio, M. C.; Travaglini, L.; Del Giudice, A.; Cautela, J.; Pavel, N. V.; Galantini, L., Bile Salts: Natural Surfactants and Precursors of a Broad Family of Complex Amphiphiles. *Langmuir* **2018**.
37. di Gregorio, M. C.; Varenik, M.; Gubitosi, M.; Travaglini, L.; Pavel, N. V.; Jover, A.; Meijide, F.; Regev, O.; Galantini, L., Multi stimuli response of a single surfactant presenting a rich self-assembly behavior. *RSC Adv.* **2015,** *5* (47), 37800-37806.

38. Patil, S.; Patil, S.; Gawali, S.; Shende, S.; Jadhav, S.; Basu, S., Novel self-assembled lithocholic acid nanoparticles for drug delivery in cancer. *RSC Adv.* **2013,** *3* (43), 19760-19764.

39. Zhang, K.; Jia, Y.-G.; Tsai, I. H.; Strandman, S.; Ren, L.; Hong, L.; Zhang, G.; Guan, Y.; Zhang, Y.; Zhu, X. X., "Bitter-Sweet" Polymeric Micelles Formed by Block Copolymers from Glucosamine and Cholic Acid. *Biomacromolecules* **2017,** *18* (3), 778-786.

40. Khatri, V. K.; Chahar, M.; Pavani, K.; Pandey, P. S., Bile Acid-Based Cyclic Bisbenzimidazolium Receptors for Anion Recognition: Highly Improved Receptors for Fluoride and Chloride Ions. *J. Org. Chem.* **2007,** *72* (26), 10224-10226.

41. Pal, A.; Basit, H.; Sen, S.; Aswal, V. K.; Bhattacharya, S., Structure and properties of two component hydrogels comprising lithocholic acid and organic amines. *J. Mater. Chem.* **2009,** *19* (25), 4325-4334.

42. Zhang, M.; Strandman, S.; Waldron, K. C.; Zhu, X. X., Supramolecular hydrogelation with bile acid derivatives: structures, properties and applications. *J. Mater. Chem. B* **2016,** *4* (47), 7506-7520.

43. Ye, W.; Li, Y.; Zhou, Z.; Wang, X.; Yao, J.; Liu, J.; Wang, C., Synthesis and antibacterial activity of new long-chain-alkyl bile acid-based amphiphiles. *Bioorg. Chem.* **2013,** *51*, 1-7.

44. Nascimento, P. G. G.; Lemos, T. L. G.; Almeida, M. C. S.; de Souza, J. M. O.; Bizerra, A. M. C.; Santiago, G. M. P.; da Costa, J. G. M.; Coutinho, H. D. M., Lithocholic acid and derivatives: Antibacterial activity. *Steroids* **2015,** *104*, 8-15.

45. Hofmann, A. F., Bile acids: Trying to understand their chemistry and biology with the

hope of helping patients. *Hepatology* **2009,** *49* (5), 1403-1418.

46. Rahman, M. A.; Bam, M.; Luat, E.; Jui, M. S.; Ganewatta, M. S.; Shokfai, T.; Nagarkatti, M.; Decho, A. W.; Tang, C., Macromolecular-clustered facial amphiphilic antimicrobials. *Nat. Commun.* **2018,** *9* (1), 5231.
47. Grossen, P.; Witzigmann, D.; Sieber, S.; Huwyler, J., PEG-PCL-based nanomedicines: A biodegradable drug delivery system and its application. *J. Control. Release* **2017,** *260*, 46-60.
48. Jiang, Y.; Lodge, T. P.; Reineke, T. M., Packaging pDNA by Polymeric ABC Micelles Simultaneously Achieves Colloidal Stability and Structural Control. *J. Am. Chem. Soc.* **2018,** *140* (35), 11101-11111.
49. Moraes, J.; Simionca, I.-M.; Ketari, H.; Klok, H.-A., Avoiding compositional drift during the RAFT copolymerization of N-(2-hydroxypropyl)methacrylamide and N-acryloxysuccinimide: towards uniform platforms for post-polymerization modification. *Polym. Chem.* **2015,** *6* (17), 3245-3251.
50. Soto Tellini, V. H.; Jover, A.; Meijide, F.; Vázquez Tato, J.; Galantini, L.; Pavel, N. V., Supramolecular Structures Generated by a p-tert-Butylphenyl-amide Derivative of Cholic Acid: From Vesicles to Molecular Tubes. *Adv. Mater.* **2007,** *19* (13), 1752-1756.
51. Luo, L.; Eisenberg, A., Thermodynamic Size Control of Block Copolymer Vesicles in Solution. *Langmuir* **2001,** *17* (22), 6804-6811.
52. Jeong, W.-j.; Kwon, S. h.; Lim, Y.-b., Modular Self-Assembling Peptide Platform with a Tunable Thermoresponsiveness via a Single Amino Acid Substitution. *Adv. Funct. Mater.* **2018,** *28* (35), 1803114.
53. Rakhmatullina, E.; Braun, T.; Chami, M.; Malinova, V.; Meier, W., Self-Organization

Behavior of Methacrylate-Based Amphiphilic Di- and Triblock Copolymers. *Langmuir* **2007,** *23* (24), 12371-12379.

CHAPTER 5

ADVANCED MACROMOLECULAR NANOSTRUCTURES FOR ANTIMICROBIAL APPLICATION

5.1 Abstract

New antimicrobial agents are badly needed to address the current ever-increasing antimicrobial resistance bacterial and the growing epidemic of infections caused by multidrug resistant pathogens. We design the strong antimicrobial nano-objects from the multicyclic natural product based facial amphiphilic cationic copolymers. Steroid based macromolecular architectures of these nanostructures can interact preferentially with bacterial membranes using facially amphiphilicity. Advanced nanostructures such as spheres, vesicles, and lenticular or rod-shaped aggregates are formed in water from the facial amphiphilic cationic copolymers via supramolecular interactions. Incorporation of PEG into the copolymer improves not only the colloidal stability of the aggregates but also biocompatibility. These nanoaggregates were particularly sensitive towards bacterial cell membranes, especially against Gram-negative bacteria, and showed almost no toxicity against mammalian cells.

5.2 Introduction

Bacterial infections, especially those caused by multidrug-resistant (MDR) bacteria, present a globally significant threat to human health.[1-2] The ever-increasing emergency of bacterial resistance to traditional antibiotics is a puzzling issue in battling infectious diseases.[1] Most life-saving antibiotics are resistant by several bacterial pathogens, e.g. multidrug-resistant Gram-negative bacteria is one of the most dangerous bacteria.[3] The presence of a second outer membrane in Gram-negative bacteria acts as an impermeable barrier to antibiotics.[4] Therefore, there persists an urgent need for new-generation antimicrobials with potent therapeutic activity and novel modes of action. It is also

important that in combating the growing epidemic of infections caused by MDR pathogens, agents do not drive the current increase of antimicrobial resistance.

Natural host defense peptides (HDPs) are amphiphilic in nature, combining cationic charges with hydrophobic components, and can bind electrostatically to anionic bacterial membranes. The membrane induces the structural rearrangement of the peptide, forming of an α-helix with globally segregated cationic and lipophilic side chains (also referred to as facial amphiphilicity). [2, 5-11] Due to their membrane-disruptive mechanism of action, bacteria are less likely to develop resistance against HDPs. In contrast, bacteria more easily develop resistance against most antibiotics because they kill bacteria by attacking specific targets, which can be quickly overcome through recombination or particular mutation. Clinical applications of HDPs are severely limited due to their high manufacturing cost and in many cases nonspecific toxicity to mammalian cells. Extensive research has been done to develop HDP-mimicking antimicrobial polymers as pioneered by DeGrado,[12] Gellman,[13] Tew,[14-15] Kuroda[16-17] and Hedrick, and Yang and their coworkers,[18-20] widely considered as robust broad-spectrum antimicrobial agents. Our group has also developed several antimicrobial macromolecules using bulky hydrophobic structures containing natural resin acids and antibiotic-metal bioconjugates. They exhibit low hemolysis against red blood cells (RBCs) and excellent activities against bacteria, particularly against Gram-positive bacteria such as methicillin-resistant *Staphylococcus aureus* (MRSA). Recently, we have developed a new class of true facially amphiphilic cationic polymers with strong antibacterial activity against Gram-negative bacteria, where each repeating unit possesses local facial amphiphilicity and promotes effective interactions of an entire macromolecule with bacterial cell membranes.[21] Few studies have been carried out on the development of

polymer nanoparticles or self-assembling materials with antibacterial activity and improved mammalian cell biocompatibility.[4, 22-25]

Preparation of amphiphilic copolymers that are manipulated to form various morphologies, from spherical micelles to rods, tubes, vesicles, and more complex structures is still challenging. We hypothesized that nanostructured architectures (such as spherical micelles, rods, tubes, vesicles) could be a promising approach for combating MDR bacteria because the formation of nanostructures significantly increases the local mass and cationic charge density of macromolecules. These factors could possibly result in the enhanced ability for continuous disruption of bacterial membranes particularly Gram-negative bacteria (has two cell membranes), while simultaneously exhibiting low hemolysis against RBCs.

To address this hypothesis, we chose multicyclic natural products, e.g., bile acid, as a functionalized building block possessing local facial amphiphilicity. Bile acids are produced by the mammalians and acts as biologically active surfactants. These acids are produced in the liver that exhibits inherent facial amphiphilicity with a rigid four-membered hydrocarbon ring structure (constituted as the convex β-face) and polar functionalities such as hydroxyl groups and a carboxylic acid (positioned in the concave α-face).[26] Due to their unique structural features, these acids are used in many areas including drug delivery,[27-28] sensors,[29] polymeric gels,[30-31] antimicrobials[32-33], and other biological applications.[34] Moreover, the facial amphiphilicity, biocompatibility, and aggregation-capability of bile acid derivatives make them attractive to prepare highly favorable for antimicrobial nanoobjects.

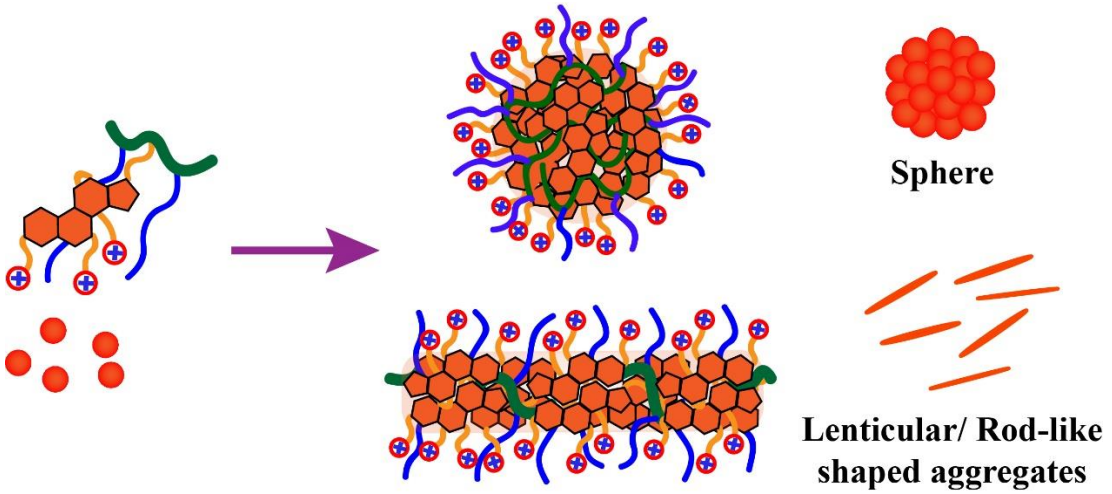

Figure 5.1 Multicyclic natural product-based cationic copolymers form spherical and rod-like aggregates in water.

In this study, we report the effect of the antimicrobial activity of different morphologies from cationic bile acid-based facially amphiphilic copolymers. We have synthesized the cationic copolymers from bile acid derivatives and different amounts of neutral PEG units (Figure 5.1). These quaternary ammonium charges (QAC) containing copolymers self-assembled into spheres, rods, and vesicles. The antimicrobial assay of different morphologies has been investigated.

5.3 Results and Discussion

Synthesis of amphiphilic copolymers. A series of amphiphilic random/gradient (or, aperiodic) copolymers bearing hydrophilic PEG and hydrophobic multicyclic ring containing cholic acid were synthesized via living reversible addition-fragmentation chain transfer (RAFT) using polymerization utilizing 4-cyano-4-(thiobenzylthio)pentanoic acid (CTP) as a chain transfer agent (Figure 5.2). Copolymers with 10, 20, 42, 53 % cholic acid denoted as C_CA1, C-CA2, C_CA3, and C_CA4 respectively were synthesized from long PEG chain containing monomer and cholic acid monomer. All copolymers were post-

modified to convert cationic charge containing polymers following our previously reported method. Single (C_LCA) and double (C_DCA) cationic charge containing copolymers were synthesized similarly. Three cationic charge-based block copolymer (B_CA) was also synthesized to investigate the architecture effect on antimicrobial activity.

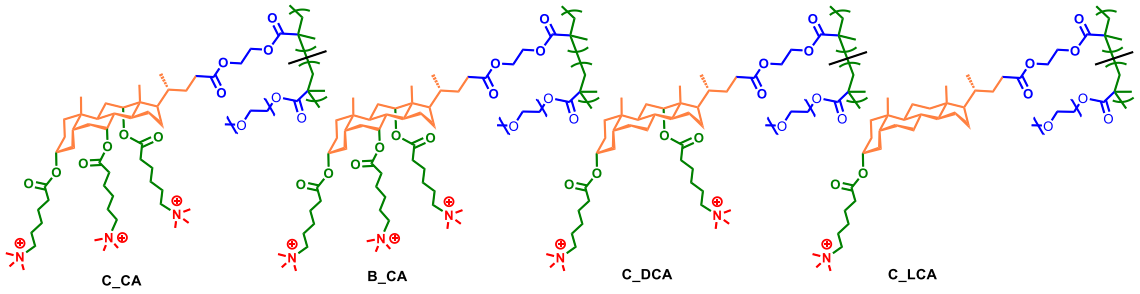

Figure 5.2 Chemical structure of cationic facial amphiphilic copolymers.

Self-Assembly Behaviors. All the copolymers self-assembled into different morphologies in water at 37^{o}C, which was explained in the previous chapter. Formation of spheres, vesicles, and rod-like nanoaggregates are confirmed by TEM images (Figure 5.3). Depending on the PEG feed ratio, three QAC charge containing copolymers are formed spheres and rod-like structures after 24 hrs incubation at 37 ^{o}C. Vesicle type morphology obtained from cholic acid containing block copolymers (B_CA) after 6 hrs incubation at 37 ^{o}C. Deoxycholic (C_DCA) and lithocholic acid (C_LCA) based copolymers formed rod/fiber-like nanostructures in water at 37 ^{o}C after 2 hrs incubation.

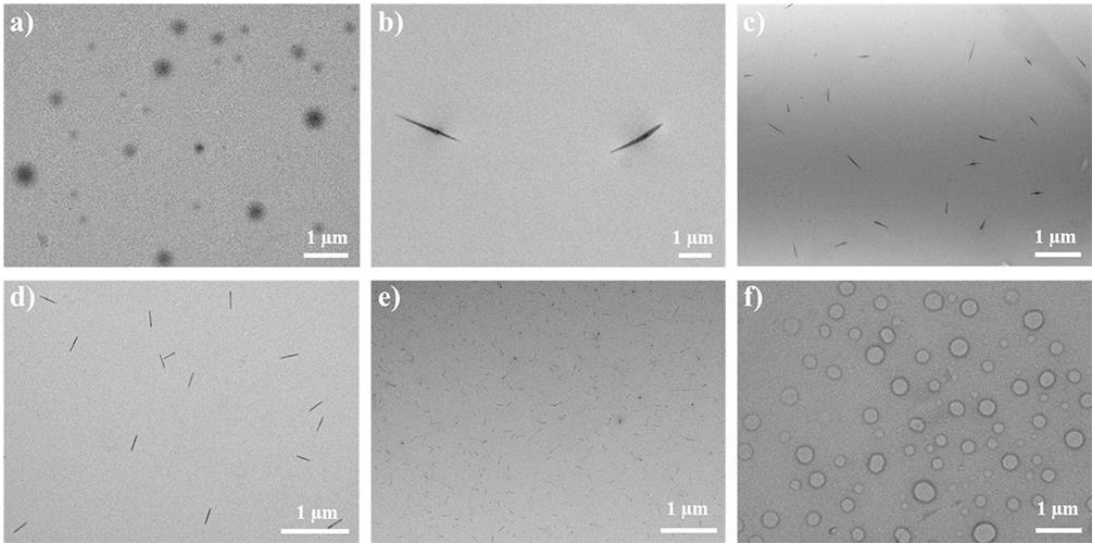

Figure 5.3 TEM images of copolymers; a) C_CA1, b) C_CA3, c) C_CA4, d) C_DCA, e) C_LCA f) B_CA after different time incubation at 37 ºC temperature.

Table 5.1 Antimicrobial activity of different multicyclic natural product-based cationic copolymers.

Polymers	Bile Acid Feed (mole %)	Molecular Weight M_n[a] (g/mol) (GPC)	Minimum Inhibitory Concentration (MIC) (µg/ml)				HC_{50} (µg/mL)	Selectivity of *E. coli* (ATCC-11775) (HC_{50}/MIC)	Selectivity of *S. aureus* (ATCC-33591) (HC_{50}/MIC)
			E. coli (ATCC-11775)	*P. aerugin osa* (ATCC-10145)	*E. coli* (ATCC-BAA-197)	*S. aureus* (ATCC-33591)			
C_CA1	90	18000	12.8	12.8	12.8	25.6	>715	>56	>28
C_CA2	80	21000	18.0	25.6	18.8	51.2	>865	>48	>17
C_CA3	58	14000	25.6	38.4	25.6	51.2	>1366	>53	>26
C_CA4	47	10000	38.4	51.2	38.4	102.4	>1745	>45	>17
B_CA	55	20000	51.2	102.4	51.2	>102.4	>662	>13	<6
C_DCA	60	10000	51.2	38.4	51.2	>102.4	>411	>8	<4
C_LCA	60	15000	>102.4	25.6	>102.4	>102.4	NT	NT	NT

a. Number-average molecular weight determined by GPC calibrated by polystyrene standard.

Antimicrobial Activities. The antimicrobial activities of bile acid-based cationic copolymers polymers were evaluated against clinically-relevant Gram-positive bacteria *S. aureus* and Gram-negative bacteria *E. coli* and *P. aeruginosa*. Recently, we demonstrated that bile acid-based facially amphiphilic homopolymers are potent antimicrobial agents, especially towards Gram-negative bacteria.[21] Here, we evaluated the antimicrobial activity of different aggregates formed in aqueous solution by bile acid-based copolymers. All copolymers were incubated at 37 ºC for specified time to form small aggregates. Then, this incubated solution was used to determine the minimum inhibitory concentration (MIC). The MIC of all copolymers was determined by a broth microdilution method following our previous report. [21] The C_CA1 copolymer exhibited the most potent antimicrobial potency in comparison to other copolymers. The MIC results (Table 5.1) demonstrated that increasing the neutral PEG block ratio in the copolymers results in a loss of antibacterial activity, which was also observed by the others. Consequently, a delicate balance of hydrophobicity and hydrophilicity is one of the essential factors for selective interactions with bacterial membranes. We also observed that single (C_LCA) and double (C_DCA) headed QAC charge containing copolymers with the same PEG feed ratio are less sensitive towards Gram-positive and Gram-negative bacteria in comparison to C_CA3. The lack of sufficient charge density may be the main reason for the decreased activity against bacteria. Higher charge densities of a polymer could lead to more significant interactions with bacterial membranes, and thus enhanced antimicrobial behavior. All of the copolymers showed stronger sensitivity for Gram-negative bacteria (*E. coli)* over Gram-positive bacteria (*S. aureus).* The BCA block copolymer exhibited the weakest activity against bacteria, likely due to their larger sized aggregates in water. Overall, the MIC values for

all copolymers are higher because of the larger size of aggregates impeding penetration through the bacterial cell membrane. Another reason is that the PEG can shield the QAC groups, reducing the targeting ability of copolymers. In addition, many copolymer chains are required to form larger-sized aggregates and are spatially inhibited from multiple binding bacteria at a time.

Bacteria can develop resistance against repeated use of drugs through a variety of methods. To address this ever-growing drug resistance issue, we also studied the antimicrobial resistance for two cholic acid-based cationic copolymers, such as C_CA1 and C_CA3, against *E. coli*. Bacteria were exposed multiple times to the polymer at a sub-MIC level, and the MIC was measured for every following passage. After ten passages, no significant changes in the MIC values were observed, as detailed in Figure 5.4. This important result demonstrated that developing resistance against cholic acid-based cationic copolymers is inherently difficult for *E. coli* bacterial strains. Yang and colleagues observed that the MIC value of ciprofloxacin against *E. coli* increased after four passages, meaning *E. coli* developed resistance against ciprofloxacin after only a few passages.[46]

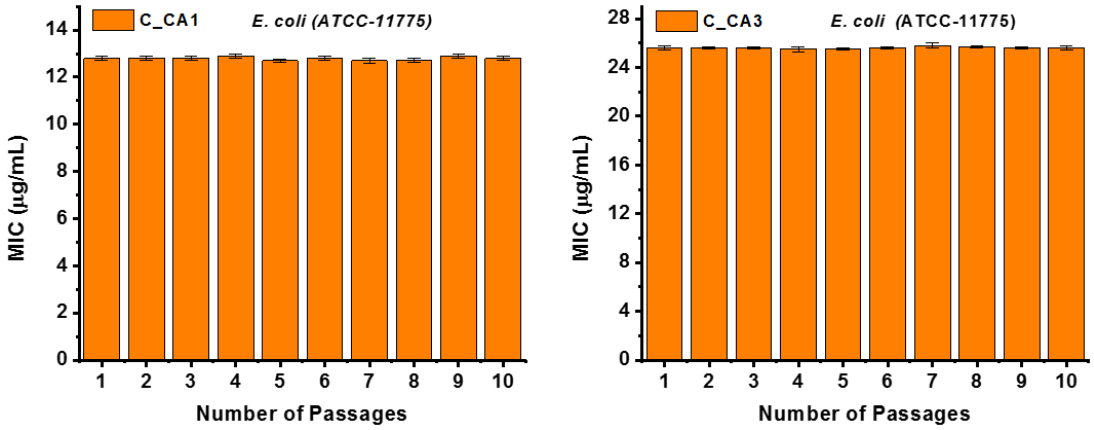

Figure 5.4 Drug resistance study of C_CA1 and C_CA3 against *E. coli* upon multiple sublethal dose treatment.

Hemolytic Activities. The hemolysis activity of bile acid-derived cationic copolymers was evaluated by measuring hemoglobin release from mouse red blood cells (RBCs) at various concentrations. Bile acid derivatives are intrinsically hydrophobic due to the presence of a four fused-ring structure. To increase the hydrophilicity, we incorporated PEG into the copolymers. The results showed that the increasing the composition of neutral PEG improved hemolysis activity. It is well established the PEG can increase the biocompatibility by increasing the hydrophilicity of the polymers. The HC_{50} value, the concentration that causes 50 % hemolysis of RBCs, is measured for all copolymers (Figure 5.5). The selectivity for bacterial cells over mammalian cells was determined by the ratio of HC_{50} values to MIC values (HC_{50}/MIC) (Table 5.1). All of the cholic acid-based cationic copolymers exhibited negligible hemolysis at their respective MIC values, demonstrating excellent selectivity toward a broad range of pathogenic microbes over mammalian cells. The hemolysis and antimicrobial activity result of the copolymers suggest that the selectivity decreases with increasing PEG ratio in the copolymers.

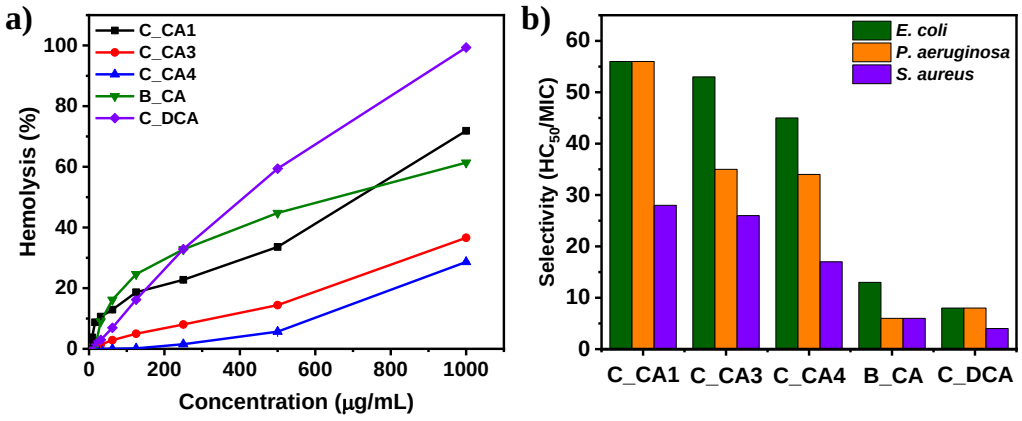

Figure 5.5 **a)** Hemolysis activity of copolymers measured by hemoglobin release from mouse RBCs at various concentrations; **b)** Selectivity of copolymers towards the bacterial membrane.

To elucidate the mode of action of the aggregates derived from bile acid-based copolymers against Gram-negative bacteria, we performed confocal laser scanning microscopy (CLSM) to investigate the membrane permeability changes before and after treatment with C_CA1 and C_CA3 copolymer using a LIVE/DEAD BacLight assay kit. The concentration of polymers used was two times that of the MIC value. As shown in Figure 4.8, green stained cells were observed for control bacteria (*E. coli*), revealing most cells as alive with intact bacterial membranes. In contrast, when the bacteria were treated with copolymers, most cells were killed as indicated by a red coloration. These findings revealed that the antimicrobial activity of bile acid-based cationic polymers occurred by the disruption of the bacterial membrane, consistent with the membrane lytic mechanism of various synthetic antimicrobial polymers.

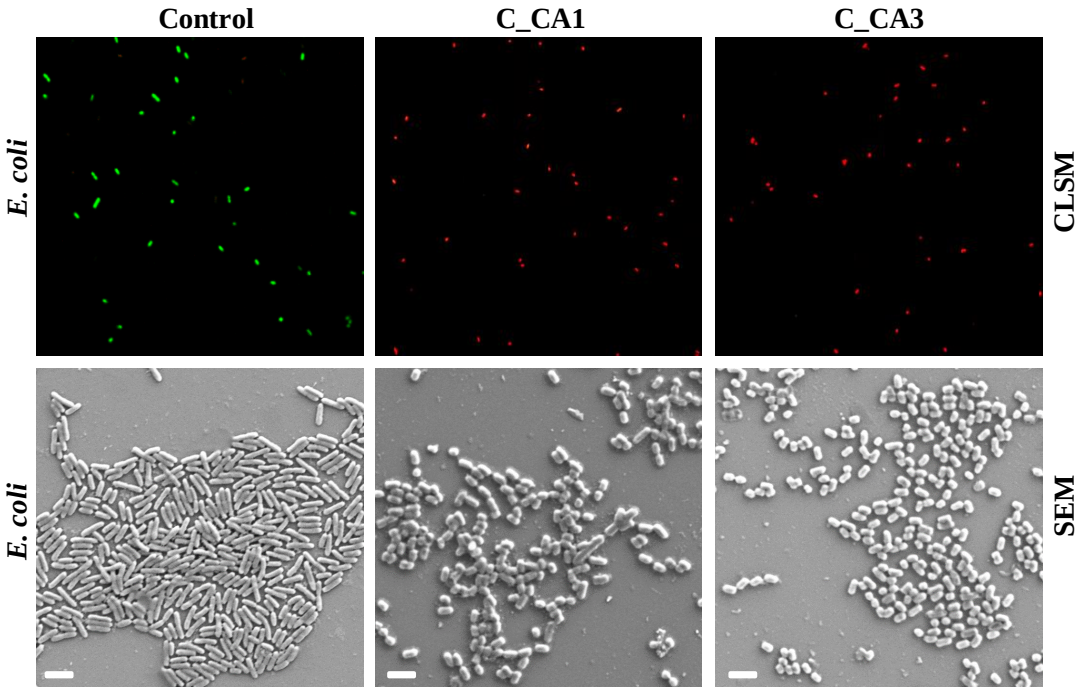

Figure 5.6 CLSM and SEM images of *E. coli* under control, C_CA1 and C_CA3 treatment with two times of MIC concentration. Bacteria concentrations were 1.0×10^6 CFU/mL. Bacterial solutions without polymer were used as the control.

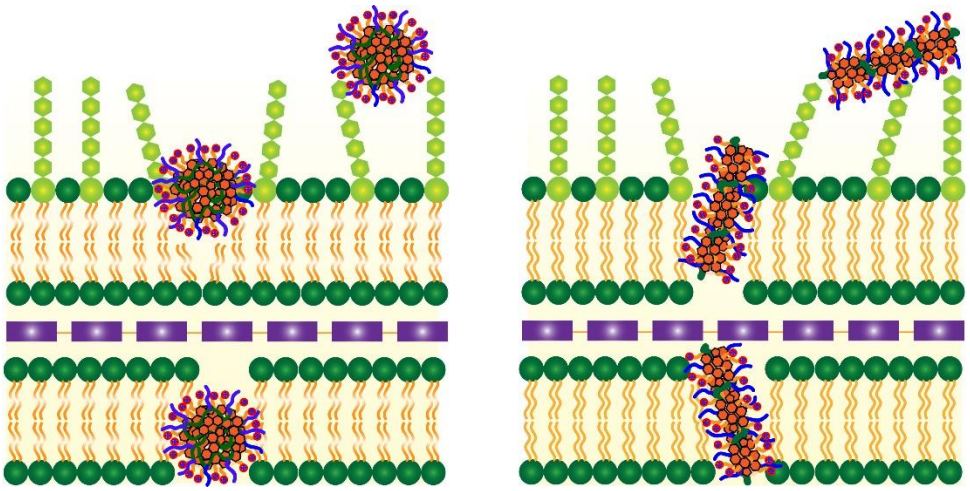

Figure 5.7 A proposed mechanism of action of cholic acid-based amphiphilic copolymers derived spherical and rod-like aggregates on the Gram-negative bacterial cell membrane.

The antimicrobial mechanism of action was further investigated through the observation of morphological changes of bacterial cells after copolymers treatment using scanning electron microscopy (SEM). *E. coli* under control remained intact with smooth surfaces as shown in Figure 5.6, whereas copolymer-treated cells were significantly fragmented and damaged from the original morphology. A plausible mechanism is proposed for the action of spherical and rod-like aggregates onto the Gram-negative bacteria, which is shown in Figure 5.7. Sphere shaped nanoaggregates causes the significant perturbation on the bacterial membrane and penetrate the membrane leading to cell death. Treatment with C_CA3 especially showed significant fragmentation of bacterial cells (Figure 5.6). These rod-like shaped aggregates act possibly act as a knife severing the bacteria into small pieces (Figure 5.7). Nanoaggregates are showing potent antimicrobial activity due to their ability to carry higher charge density. These higher charge densities can easily attract by the outer cell membrane of Gram-negative bacteria and, eventually damage inner membranes.

5.4 Conclusions

In summary, we report the effect of the antimicrobial activity of different morphologies obtained from bile acid-based facially amphiphilic cationic copolymers. Three quaternary ammonium charge (QAC) containing cholic acid-based copolymers self-assembled into spheres, rods, and vesicles exhibited strong antimicrobial activity. All copolymer nanoaggregates exhibit strong antimicrobial activity against Gram-negative bacteria. These novel macromolecular structures and their self-assembly behavior may open a new avenue toward next-generation antimicrobial agents to treat multidrug-resistant Gram-negative bacteria.

5.5 Experimental Section

Bacteria Cell Culture. *Escherichia coli* (*E. coli*, ATCC-11775), *Pseudomonas aeruginosa* (*P. aeruginosa*, ATCC-10145), *Escherichia coli* (*E. coli*, ATCC- BAA-197), and *Staphylococcus aureus* (*S. aureus*, ATCC-33591) were purchased from ATCC. For these bacteria, a single colony was inoculated in 30 mL Tryptic Soy broth (TSB) at 37 °C for 24 h, shaking at 190 rpm/min. All bacteria were grown to an optical density of about l.00 (OD_{600} = 1.00) for further use.

Minimum Inhibitory Concentration (MIC) Measurements. The MIC of cationic bile acid-containing copolymers were determined using a broth microdilution method.[3-4] 100 μL of a water solution of copolymers with different concentrations was placed into each well of a 96-well plate. Then, 100 μL of bacterial TSB solution (OD_{600} = 1.00) was added into each well-containing polymer solutions. The bacterial TSB solution without polymers or compounds was used as the control. The 96-well plate was incubated at 37 °C under

constant shaking of 100 rpm for 18 h. Bacterial growth was detected at OD_{600}, and was compared to controls of bacterial TSB solution without polymers. All analyses were carried out in triplicates in the same assay plate. Optical density was plotted against polymer concentration, and linear regression analysis was used to determine the lowest concentration at which the optical density reading becomes zero. The MIC was taken as the concentration of bile acid-based polymers and compounds at which no microbial growth was observed.

Drug Resistance Study. A drug resistance study was performed against *E. coli* for two copolymers named as C_CA1 and C_CA3. Initially, the MIC of the polymer was measured as described above. The 10 μL bacterial solution was taken from the well that contains 2-fold serial diluted polymer solution of MIC and incubated for overnight at 37 ^{o}C. Then, using this newly grown bacterial solution previously exposed to the polymer sample, the new MIC was determined. This assay was repeated for ten passes, and MIC values were determined each time. Development of drug resistance was analyzed by observing the change in MIC after every pass. A polymer showing the same MIC in each successive passage indicates the bacteria did not develop resistance to the polymer.

Hemolysis Evaluation. Blood was collected from mice in heparinized tubes and diluted by mixing 800 μL of blood with 1000 μL of PBS. Polymer samples were prepared in PBS at concentrations of 0.5, 1, 2 4, 16,31, 62, 125, 250, 500, and 1000 μg/mL, and 60 μL of the diluted blood samples was added to 3 mL of polymers, PBS, or 0.1% Triton-X100 in PBS. The samples were incubated for 1 h at 37 °C followed by centrifugation for 10 min at 1500 rpm. Supernatants were collected, and OD was measured at 545 nm to calculate hemolysis rate by using the equation, HR = (AS – AN)/(AP – AN), where AS, AN, and

AP are OD values of the supernatants from test samples, negative control (PBS), and positive control (0.1% Triton-X100), respectively.

LIVE/DEAD Bacterial Viability Assays. Confocal laser scanning microscopy (CLSM) analysis was used to study the bacterial membrane permeability after polymer treatment. The bacterial strains were inoculated at 37 °C together with polymer C_CA1 and C_CA3 at two times the MIC value following the same procedure for MIC determination. An untreated bacterial solution was used as controls. After 18 h incubation at 37 °C, 1 μL of LIVE/DEAD BacLight (Bacterial Viability Kit; Invitrogen Inc.) was added to 5 μL incubated solution and incubated for 15 min. The LIVE/DEAD BacLight bacterial viability kit consists of propidium iodide (PI), and FITC-labeled SYTO 9 dye used to stain nucleic acid (DNA). Green-fluorescing SYTO 9 can enter all cells, live or dead, whereas red fluorescing PI can only stain the DNA of damaged cytoplasmic membranes of dead or dying cells. Cells were imaged under a Leica TCS SP5 CLSM with a 63× oil immersion lens. When excited at 488 nm with argon and helium/neon lasers, bacteria with intact membranes display green fluorescence (emission = 500 nm), and bacteria with disrupted membranes fluoresce red (emission = 635 nm).

Bacterial Morphology Assays. The scanning electron microscopy (SEM) was used to investigate the morphologies of different bacteria with a similar procedure reported earlier. In general, 10 μL of bacterial cell solution was grown on one glass slide in a 12-well plate containing 1 mL of TSB medium at 37 °C overnight. Cell suspensions were diluted to OD_{600} = 1.0. The polymer at twice the MIC was added to the 1 mL bacteria stock solution and incubated at 37 °C overnight. A bacterial solution without any polymers was used as the control. The samples were then fixed in cacodylate buffer with 2.5% glutaraldehyde

solution (pH = 7.2) for 2–3 h at 4 °C and post-fixed with 1% osmium tetraoxide at 4 °C for 1 h. The samples were dried at a critical point, then coated with gold using a Denton Dest II Sputter Coater for 120 s, and observed by FE-SEM. An untreated cell suspension was used as the control.

5.6 References

1. Hurdle, J. G.; O'Neill, A. J.; Chopra, I.; Lee, R. E., Targeting bacterial membrane function: an underexploited mechanism for treating persistent infections. *Nature Reviews Microbiology* **2010,** *9*, 62.
2. Takahashi, H.; Caputo, G. A.; Vemparala, S.; Kuroda, K., Synthetic Random Copolymers as a Molecular Platform To Mimic Host-Defense Antimicrobial Peptides. *Bioconjugate Chemistry* **2017,** *28* (5), 1340-1350.
3. Qiao, Y.; Yang, C.; Coady, D. J.; Ong, Z. Y.; Hedrick, J. L.; Yang, Y.-Y., Highly dynamic biodegradable micelles capable of lysing Gram-positive and Gram-negative bacterial membrane. *Biomaterials* **2012,** *33* (4), 1146-1153.
4. Lam, S. J.; O'Brien-Simpson, N. M.; Pantarat, N.; Sulistio, A.; Wong, E. H. H.; Chen, Y.-Y.; Lenzo, J. C.; Holden, J. A.; Blencowe, A.; Reynolds, E. C.; Qiao, G. G., Combating multidrug-resistant Gram-negative bacteria with structurally nanoengineered antimicrobial peptide polymers. *Nature Microbiology* **2016,** *1*, 16162.
5. Brogden, K. A., Antimicrobial peptides: pore formers or metabolic inhibitors in bacteria? *Nature Reviews Microbiology* **2005,** *3*, 238.
6. Kohanski, M. A.; Dwyer, D. J.; Collins, J. J., How antibiotics kill bacteria: from targets to networks. *Nature Reviews Microbiology* **2010,** *8*, 423.
7. Ling, L. L.; Schneider, T.; Peoples, A. J.; Spoering, A. L.; Engels, I.; Conlon, B. P.;

Mueller, A.; Schäberle, T. F.; Hughes, D. E.; Epstein, S.; Jones, M.; Lazarides, L.; Steadman, V. A.; Cohen, D. R.; Felix, C. R.; Fetterman, K. A.; Millett, W. P.; Nitti, A. G.; Zullo, A. M.; Chen, C.; Lewis, K., A new antibiotic kills pathogens without detectable resistance. *Nature* **2015,** *517*, 455.

8. Shi, Y.; Teng, P.; Sang, P.; She, F.; Wei, L.; Cai, J., γ-AApeptides: Design, Structure, and Applications. *Accounts of Chemical Research* **2016,** *49* (3), 428-441.
9. Radzishevsky, I. S.; Rotem, S.; Bourdetsky, D.; Navon-Venezia, S.; Carmeli, Y.; Mor, A., Improved antimicrobial peptides based on acyl-lysine oligomers. *Nature Biotechnology* **2007,** *25*, 657.
10. Xiong, M.; Han, Z.; Song, Z.; Yu, J.; Ying, H.; Yin, L.; Cheng, J., Bacteria-Assisted Activation of Antimicrobial Polypeptides by a Random-Coil to Helix Transition. *Angewandte Chemie International Edition* **2017,** *56* (36), 10826-10829.
11. Zasloff, M., Antimicrobial peptides of multicellular organisms. *Nature* **2002,** *415*, 389.
12. Tew, G. N.; Scott, R. W.; Klein, M. L.; DeGrado, W. F., De Novo Design of Antimicrobial Polymers, Foldamers, and Small Molecules: From Discovery to Practical Applications. *Accounts of Chemical Research* **2010,** *43* (1), 30-39.
13. Mowery, B. P.; Lee, S. E.; Kissounko, D. A.; Epand, R. F.; Epand, R. M.; Weisblum, B.; Stahl, S. S.; Gellman, S. H., Mimicry of Antimicrobial Host-Defense Peptides by Random Copolymers. *Journal of the American Chemical Society* **2007,** *129* (50), 15474-15476.
14. Ilker, M. F.; Nüsslein, K.; Tew, G. N.; Coughlin, E. B., Tuning the Hemolytic and Antibacterial Activities of Amphiphilic Polynorbornene Derivatives. *Journal of the American Chemical Society* **2004,** *126* (48), 15870-15875.

15. Lienkamp, K.; Madkour, A. E.; Musante, A.; Nelson, C. F.; Nüsslein, K.; Tew, G. N., Antimicrobial Polymers Prepared by ROMP with Unprecedented Selectivity: A Molecular Construction Kit Approach. *Journal of the American Chemical Society* **2008,** *130* (30), 9836-9843.
16. Palermo, E. F.; Kuroda, K., Chemical Structure of Cationic Groups in Amphiphilic Polymethacrylates Modulates the Antimicrobial and Hemolytic Activities. *Biomacromolecules* **2009,** *10* (6), 1416-1428.
17. Palermo, E. F.; Sovadinova, I.; Kuroda, K., Structural Determinants of Antimicrobial Activity and Biocompatibility in Membrane-Disrupting Methacrylamide Random Copolymers. *Biomacromolecules* **2009,** *10* (11), 3098-3107.
18. Nederberg, F.; Zhang, Y.; Tan, J. P. K.; Xu, K.; Wang, H.; Yang, C.; Gao, S.; Guo, X. D.; Fukushima, K.; Li, L.; Hedrick, J. L.; Yang, Y.-Y., Biodegradable nanostructures with selective lysis of microbial membranes. *Nature Chemistry* **2011,** *3*, 409.
19. Chin, W.; Zhong, G.; Pu, Q.; Yang, C.; Lou, W.; De Sessions, P. F.; Periaswamy, B.; Lee, A.; Liang, Z. C.; Ding, X.; Gao, S.; Chu, C. W.; Bianco, S.; Bao, C.; Tong, Y. W.; Fan, W.; Wu, M.; Hedrick, J. L.; Yang, Y. Y., A macromolecular approach to eradicate multidrug resistant bacterial infections while mitigating drug resistance onset. *Nature Communications* **2018,** *9* (1), 917.
20. Liu, S.; Ono, R. J.; Wu, H.; Teo, J. Y.; Liang, Z. C.; Xu, K.; Zhang, M.; Zhong, G.; Tan, J. P. K.; Ng, M.; Yang, C.; Chan, J.; Ji, Z.; Bao, C.; Kumar, K.; Gao, S.; Lee, A.; Fevre, M.; Dong, H.; Ying, J. Y.; Li, L.; Fan, W.; Hedrick, J. L.; Yang, Y. Y., Highly potent antimicrobial polyionenes with rapid killing kinetics, skin biocompatibility and in vivo bactericidal activity. *Biomaterials* **2017,** *127*, 36-48.

21. Rahman, M. A.; Bam, M.; Luat, E.; Jui, M. S.; Ganewatta, M. S.; Shokfai, T.; Nagarkatti, M.; Decho, A. W.; Tang, C., Macromolecular-clustered facial amphiphilic antimicrobials. *Nature Communications* **2018,** *9* (1), 5231.

22. Nguyen, T.-K.; Lam, S. J.; Ho, K. K. K.; Kumar, N.; Qiao, G. G.; Egan, S.; Boyer, C.; Wong, E. H. H., Rational Design of Single-Chain Polymeric Nanoparticles That Kill Planktonic and Biofilm Bacteria. *ACS Infectious Diseases* **2017,** *3* (3), 237-248.

23. Wong, E. H. H.; Khin, M. M.; Ravikumar, V.; Si, Z.; Rice, S. A.; Chan-Park, M. B., Modulating Antimicrobial Activity and Mammalian Cell Biocompatibility with Glucosamine-Functionalized Star Polymers. *Biomacromolecules* **2016,** *17* (3), 1170-1178.

24. Yang, C.; Krishnamurthy, S.; Liu, J.; Liu, S.; Lu, X.; Coady, D. J.; Cheng, W.; De Libero, G.; Singhal, A.; Hedrick, J. L.; Yang, Y. Y., Broad-Spectrum Antimicrobial Star Polycarbonates Functionalized with Mannose for Targeting Bacteria Residing inside Immune Cells. *Advanced Healthcare Materials* **2016,** *5* (11), 1272-1281.

25. Yuan, W.; Wei, J.; Lu, H.; Fan, L.; Du, J., Water-dispersible and biodegradable polymer micelles with good antibacterial efficacy. *Chemical Communications* **2012,** *48* (54), 6857-6859.

26. di Gregorio, M. C.; Travaglini, L.; Del Giudice, A.; Cautela, J.; Pavel, N. V.; Galantini, L., Bile Salts: Natural Surfactants and Precursors of a Broad Family of Complex Amphiphiles. *Langmuir* **2018**.

27. Patil, S.; Patil, S.; Gawali, S.; Shende, S.; Jadhav, S.; Basu, S., Novel self-assembled lithocholic acid nanoparticles for drug delivery in cancer. *RSC Advances* **2013,** *3* (43), 19760-19764.

28. Zhang, K.; Jia, Y.-G.; Tsai, I. H.; Strandman, S.; Ren, L.; Hong, L.; Zhang, G.; Guan, Y.; Zhang, Y.; Zhu, X. X., "Bitter-Sweet" Polymeric Micelles Formed by Block Copolymers from Glucosamine and Cholic Acid. *Biomacromolecules* **2017,** *18* (3), 778-786.

29. Khatri, V. K.; Chahar, M.; Pavani, K.; Pandey, P. S., Bile Acid-Based Cyclic Bisbenzimidazolium Receptors for Anion Recognition: Highly Improved Receptors for Fluoride and Chloride Ions. *The Journal of Organic Chemistry* **2007,** *72* (26), 10224-10226.

30. Pal, A.; Basit, H.; Sen, S.; Aswal, V. K.; Bhattacharya, S., Structure and properties of two component hydrogels comprising lithocholic acid and organic amines. *Journal of Materials Chemistry* **2009,** *19* (25), 4325-4334.

31. Zhang, M.; Strandman, S.; Waldron, K. C.; Zhu, X. X., Supramolecular hydrogelation with bile acid derivatives: structures, properties and applications. *Journal of Materials Chemistry B* **2016,** *4* (47), 7506-7520.

32. Ye, W.; Li, Y.; Zhou, Z.; Wang, X.; Yao, J.; Liu, J.; Wang, C., Synthesis and antibacterial activity of new long-chain-alkyl bile acid-based amphiphiles. *Bioorganic Chemistry* **2013,** *51*, 1-7.

33. Nascimento, P. G. G.; Lemos, T. L. G.; Almeida, M. C. S.; de Souza, J. M. O.; Bizerra, A. M. C.; Santiago, G. M. P.; da Costa, J. G. M.; Coutinho, H. D. M., Lithocholic acid and derivatives: Antibacterial activity. *Steroids* **2015,** *104*, 8-15.

34. Hofmann, A. F., Bile acids: Trying to understand their chemistry and biology with the hope of helping patients. *Hepatology* **2009,** *49* (5), 1403-1418.

CHAPTER 6

SUMMARY AND OUTLOOK

6.1 Dissertation Summary

In this dissertation work, three major research frontiers were explored. First, a new strategy was developed to innovate multicyclic natural product-based biomass-containing sustainable polymers with superior performance via control of macromolecular architectures. Our study demonstrated that bulky rosin-containing tri- and pentablock copolymers with low dispersity could be prepared by ROMP with one-pot sequential monomer addition. Rosin-based homopolymers below the chain entanglement molecular weight are brittle, whereas the tri- and pentablock copolymers are tough thermoplastic, even though their rosin-containing block has much lower molecular weight than M_e. Second, we designed novel antimicrobial polymers with repeat units possessing local facial amphiphilicity from multicyclic natural products, which could promote effective interactions of an entire macromolecule with bacterial cell membranes, circumventing the adoption of an energetically unfavorable global facial amphiphilicity. Among different derivatives of bile acids, cholic acid polymers were shown to be more efficient than their deoxycholic and lithocholic acid counterparts regarding both antimicrobial activity and selectivity. The macromolecular structure and conformation with a true facial amphiphilic structure derived from cholic acid derivatives showed potent activity against multidrug-resistant Gram-negative bacteria. Third, the facial amphiphilicity-induced self-assembly (FAISA) of gradient/blocky copolymers was developed. The facial amphiphilic moieties consist of large cross-sectional multicyclic hydrocarbons on one side, and multiple charged polar head groups on the other side dictate the self-assembled morphologies. The self-assembly of multicyclic natural product-based cationic homopolymer formed large vesicle while the gradient/blocky copolymers formed spheres, vesicles, and rod-like structures.

These natural product-derived cationic nanoaggregates exhibited excellent antimicrobial activity against Gram-negative bacteria.

6.2 Future Work

The sustainable development from renewable natural products has already gained incredible interest during the past decade. More researches still need to conduct in future in the field of sustainable development preparing functional polymers with improved performance from renewable biomass to replace fossil oil-based polymers or plastic materials. There are a variety of different multicyclic natural products or biomass available, which are cheap and abundant needs proper transformation to utilize in demanding applications. In this dissertation, block copolymer architecture was developed to enhance the physical and mechanical properties of multicyclic natural product-based plastic materials, where resin acid was used as an example. To further improve the mechanical properties of rosin acid-based polymers, random copolymer or dynamic crosslinking chemistry can be applied to overcome the high chain entanglement molecular weight problem. The development of antimicrobial biomaterial needs immediate attention to fight against multidrug-resistant bacteria as well as antibiotic resistance. The multicyclic natural products (Bile acid as an example) derived true facial amphiphilicity with cationic charges have been developed as a potent antimicrobial agent. New molecular biomass with true facial amphiphilicity can be explored in future that will selectively kill the bacteria and utterly biocompatible with no toxicity against mammalian cells. Facial amphiphilic molecules with different cationic groups such as phosphonium, sulfonium, and metallo-cations can be utilized to make different polymer architectures such as brush, star, and comb. Facial amphiphilic moieties can be functionalized by metallo-cation and conjugated

with antibiotics to make strong antimicrobial agent. Facial amphiphilicity induced nanoparticles were prepared for antimicrobial application from bile acid derivatives. More investigations can be carried out to establish the facial amphiphilicity induced self-assembly using other facial amphiphilic molecules or natural products.

APPENDIX A – PERMISSION TO REPRINT

Permission for Chapter 2

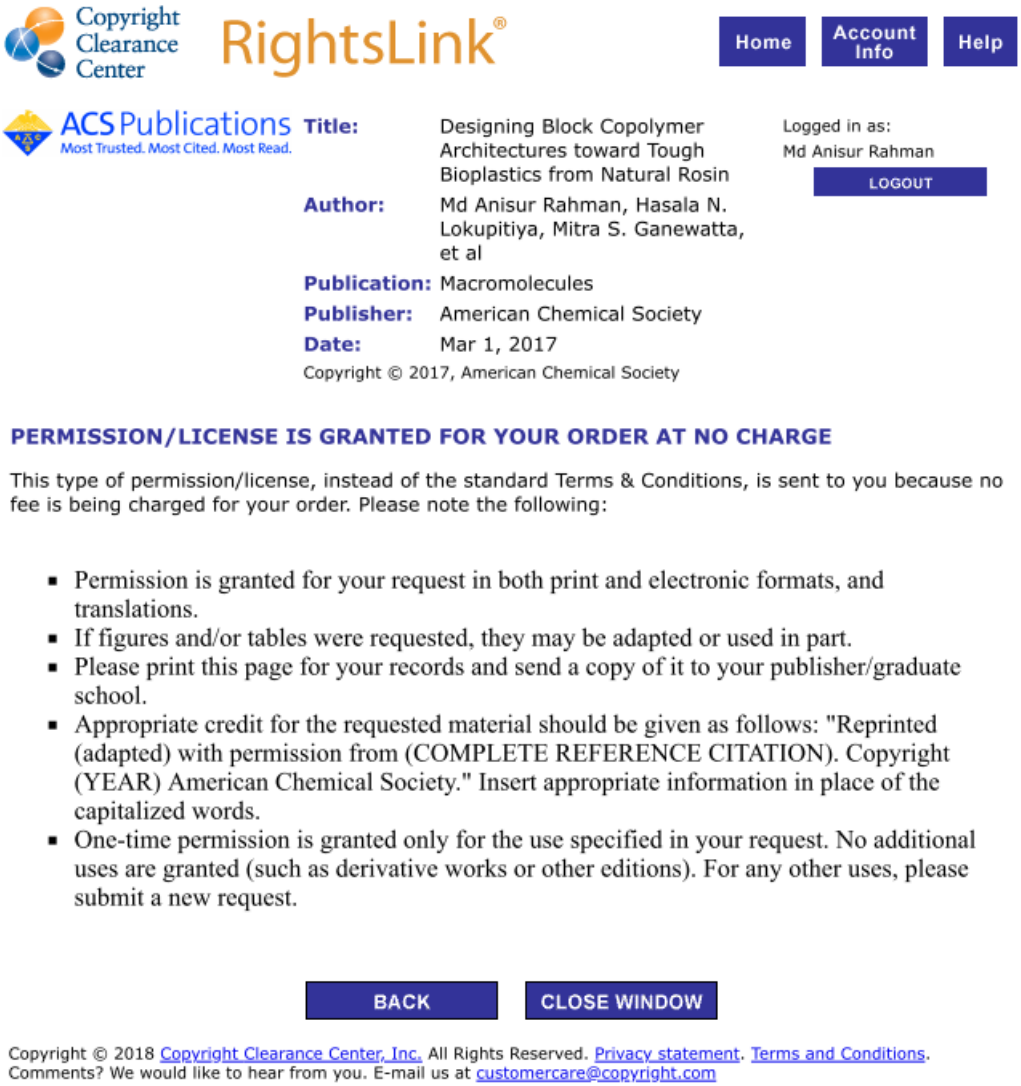

Copyright Clearance Center RightsLink®

Home | Account Info | Help

ACS Publications
Most Trusted. Most Cited. Most Read.

Logged in as:
Md Anisur Rahman
LOGOUT

Title: Designing Block Copolymer Architectures toward Tough Bioplastics from Natural Rosin

Author: Md Anisur Rahman, Hasala N. Lokupitiya, Mitra S. Ganewatta, et al

Publication: Macromolecules

Publisher: American Chemical Society

Date: Mar 1, 2017

Copyright © 2017, American Chemical Society

PERMISSION/LICENSE IS GRANTED FOR YOUR ORDER AT NO CHARGE

This type of permission/license, instead of the standard Terms & Conditions, is sent to you because no fee is being charged for your order. Please note the following:

- Permission is granted for your request in both print and electronic formats, and translations.
- If figures and/or tables were requested, they may be adapted or used in part.
- Please print this page for your records and send a copy of it to your publisher/graduate school.
- Appropriate credit for the requested material should be given as follows: "Reprinted (adapted) with permission from (COMPLETE REFERENCE CITATION). Copyright (YEAR) American Chemical Society." Insert appropriate information in place of the capitalized words.
- One-time permission is granted only for the use specified in your request. No additional uses are granted (such as derivative works or other editions). For any other uses, please submit a new request.

BACK | CLOSE WINDOW

Copyright © 2018 Copyright Clearance Center, Inc. All Rights Reserved. Privacy statement. Terms and Conditions.
Comments? We would like to hear from you. E-mail us at customercare@copyright.com

Permission for Chapter 3

To view the copyright policy please visit the following links.

https://www.nature.com/reprints/permission-requests.html

http://creativecommons.org/licenses/by/4.0/.

Permission requests from authors:

The author of articles published by SpringerNature do not usually need to seek permission for re-use of their material as long as the journal is credited with initial publication.

Ownership of copyright in in original research articles remains with the Author, and provided that, when reproducing the contribution or extracts from it or from the Supplementary Information, the Author acknowledges first and reference publication in the Journal, the Author retains the following non-exclusive rights:

To reproduce the contribution in whole or in part in any printed volume (book or thesis) of which they are the author(s).

The author and any academic institution where they work at the time may reproduce the contribution for the purpose of course teaching.

To reuse figures or tables created by the Author and contained in the Contribution in oral presentations and other works created by them.